



THE HONG KONG
POLYTECHNIC UNIVERSITY

香港理工大學

Pao Yue-kong Library

包玉剛圖書館

Copyright Undertaking

This thesis is protected by copyright, with all rights reserved.

By reading and using the thesis, the reader understands and agrees to the following terms:

1. The reader will abide by the rules and legal ordinances governing copyright regarding the use of the thesis.
2. The reader will use the thesis for the purpose of research or private study only and not for distribution or further reproduction or any other purpose.
3. The reader agrees to indemnify and hold the University harmless from and against any loss, damage, cost, liability or expenses arising from copyright infringement or unauthorized usage.

IMPORTANT

If you have reasons to believe that any materials in this thesis are deemed not suitable to be distributed in this form, or a copyright owner having difficulty with the material being included in our database, please contact lbsys@polyu.edu.hk providing details. The Library will look into your claim and consider taking remedial action upon receipt of the written requests.

**A HEURISTIC MODEL FOR MODE-
LOCKED FIBER LASERS**

ZHANG XIANTING

PhD

The Hong Kong Polytechnic University

2019

The Hong Kong Polytechnic University
Department of Electronic and Information Engineering

A HEURISTIC MODEL FOR MODE-
LOCKED FIBER LASERS

ZHANG XIANTING

A thesis submitted in partial fulfillment of the requirements for
The Degree of Doctor of Philosophy

May 2019

Certificate of Originality

I hereby declare that this thesis is my own work and that, to the best of my knowledge and belief, it reproduces no material previously published or written, nor material that has been accepted for the award of any other degree or diploma, except where due acknowledgement has been made in the text.

..... (Signed)

.....ZHANG Xianting (Name of student)

ABSTRACT

Offering the advantages of compact, portability, and low cost, fiber lasers have many applications. Mode-locked fiber laser is applied in many fields such as optical sensing, and super-continuum generation. Mode-locking requires balance of various effects such as gain, loss, dispersion and nonlinearity. An in depth understanding of how the various effects interact in a laser cavity would help the laser design.

Laser modeling can be used to analyze laser dynamics. With given parameters, a good laser model can give a prediction from simulation results which match the experimental observations and give the guidance on choosing the parameters of a laser. A good model does not always mean it contains all the effects in a laser system or it can give results close to experimental results. On the contrary, it can be a simple heuristic model. A heuristic model might not accurately match experiment data but helps to check whether one (or some) effect(s) is (are) responsible for an observed behavior in a laser cavity and give a good understanding on the working mechanism of lasers.

The theoretical works based on a simple heuristic model where only the most intrinsic factors, e.g. gain and loss, are contained have been proposed. The works point out that even only containing fundamental effects, various complex states, i.e. multi-pulse generation, chaos, still exist. One should note that in a heuristic model, the choice of physical effects to be included is crucial and not easy. In our former model, pulse shaping, i.e. dispersion and nonlinearity, was considered not influence

the pulse energy and it only contains gain and loss terms. However, such an assumption is not proper when a high peak pulse is lasing in the laser. Dispersion and nonlinearity have obvious impacts on the pulse, which further impacts the gain loss dynamics. In this thesis, we proposed an extension of our former model by taking into account the effects of pulse shaping. The model is applied to study the mode-locked fiber laser.

In this thesis, we investigate both single- and multi-channel mode-locked fiber lasers. Obtaining a high energy (high peak and narrow pulse width) pulse in single-channel mode-locking is attractive. But complex states such as multi-pulsing, periodic and chaotic states also exist in the laser. Mechanisms of multi-pulsing, periodic and chaotic states, which are thought to be factors that limit the pulse energy, are investigated and the guidance on obtaining high energy short pulse is given. Multi-channel mode-locking is also studied. The impacts of the devices in a laser cavity on the mode-locked pulse are studied. We found the energies of the mode-locked pulses in different channels can be different. The light interaction through pulse shaping and the impact of the spectral filter are found to be crucial roles for this phenomenon.

Publications Arising from the Thesis

Journal:

1. **Xianting Zhang**, Feng Li, K. Nakkeeran, Jinhui Yuan, Zhe Kang, J. Nathan Kutz and P. K. A. Wai, “Impact of spectral filtering on multi-pulsing instability in mode-locked fiber lasers.” IEEE Journal of Selected Topics in Quantum Electronics 24.3 (2018): 1-9.
2. **Xianting Zhang**, Shaokang Wang, Feng Li, Curtis R. Menyuk, and P. K. A. Wai, “Design of a dual-channel modelocked fiber laser that avoids multi-pulsing,” Optics Express, 27.10 (2019): 14173-14183.

Conference paper:

1. **Xianting Zhang**, Feng Li, Jinhui Yuan, Zhe Kang and P. K. A. Wai, “Spectral filtering induced multi-pulsing in mode-locked soliton lasers,” Photonics and Fiber Technology 2016, paper: JT4A. 7. (2016).
2. **Xianting Zhang**, Shaokang Wang, Feng Li, Curtis R. Menyuk, and P. K. A. Wai, “Design of a dual-channel modelocked fiber laser that avoids multi-pulsing,” Conference on Lasers and Electro-Optics (CLEO), paper: JTh2A.125. (2018).
3. **Xianting Zhang**, Feng Li, Jinhui Yuan, Zhe Kang and P. K. A. Wai, “Dynamics of dual-frequency mode-locked fiber lasers,” Pacific Rim Conference on Lasers and Electro-Optics, paper: 2978843. (2018).
4. **Xianting Zhang**, Feng Li, Zhe Kang, Zihao Cheng, Dongmei Huang, and P. K. A. Wai, “Energy discrimination in multi-channel simultaneously mode-locked fiber lasers,” OptoElectronics and Communications Conference/ International Conference on Photonics in Switching and Computing (OECC/PSC) , paper: WP4-C18. (2019).

Acknowledgements

I want to thank a number of people during my Ph.D. studies. First, I would like to express my deepest appreciation to my supervisor, Prof. P. K. A. Wai. He provided me the opportunity to join his group at The Hong Kong Polytechnic University and gave me patient guidance and continuous support on my research. Moreover, his noble personality has profoundly affected me. I am very grateful that I could be under the supervision of such an extraordinary advisor.

I am greatly indebted to Dr. Li Feng with whom I worked during my doctoral studies. I am very thankful for his generous help, valuable advice, and patiently supports. Without his contribution, the work in this thesis could not be fulfilled.

Especially, I want to thank Prof. J. Nathan Kutz, Prof. K. Nakkeeran, Prof. Jinhui Yuan, Dr. Zhe Kang, Dr. Shaokang Wang, Dr. Yin Xu, Mr. Chao Mei, Ms. Yazhi Luo, Ms. Dongmei Huang. They offered me many practical and constructive suggestions, which contributed much to my studies. My thanks are also extended to other colleagues at Photonics Research Centre and Department of Electronic and Information Engineering. I am also appreciative of the support from the staff of the Department and Research Office.

Finally, I would like to express my great gratitude to my family in China, especially my parents for their unconditional love, best wishes, and unwavering support. They always stand by me, whenever and wherever. Besides, I also want to thank Miss Ziyu Ning from the University of Hong Kong, who encourages me each time I am depressed.

Sep. 2019

Statement of Originality

The following contributions reported in this thesis are claimed to be original.

1. I extended a geometrical model developed in our research group by including pulse shaping effects, to investigate the laser dynamics and the mechanism of multi-pulsing instability.
2. The impact of spectral filter on the mode-locking dynamics and multi-pulsing generation was demonstrated with the extended model. The loss comes from the spectral filter is found responsible for generating multiple pulses.
3. By using the extended geometrical model, I found beside the gain loss dynamics, the pulse shaping effects in the fiber would also induce multi-pulsing instability when adding third order dispersion in the model.
4. Based on the extended model, mode-locking in dual-channel laser is studied. The frequency shift induced by the light interaction between the channels is found crucial on the laser dynamics, which even serves the unequal energy of the mode-locked pulses in two channels.
5. By modifying the proposed model, the mode-locked states in multiple channel mode-locked fiber lasers are studied. The reasons that cause the energy difference between channels are investigated.

Content

ABSTRACT	i
Publications Arising from the Thesis	iii
Acknowledgements.....	v
Statement of Originality	vii
Chapter 1 Introduction.....	1
1.1 Background	1
1.2 Mode-locking	3
1.2.1 Active mode-locking	4
1.2.2 Passive mode-locking	6
1.3 Modeling for mode-locked fiber lasers	10
1.3.1 Haus's master equation.....	11
1.3.2 cubic-quintic Ginzburg–Landau equation	12
1.3.3 Distributed models for multi-channel mode-locking.....	14
1.3.4 Discrete models	16
1.4 Outline of the thesis.....	17
Chapter 2 Multi-pulsing and Chaos in Single-channel Mode-locked Fiber Lasers	19
2.1 Theoretical model.....	20
2.1.1. Review of a heuristic model	20

2.1.2 An extended heuristic model.....	24
2.2 Pulse dynamics in a laser cavity	27
2.2.1 Multi-pulse generation	28
2.2.2 Chaos and high energy single pulse	32
2.2.3 Impact of third order dispersion.....	40
Summary	48
Chapter 3 Dual-channel Mode-locked Fiber Lasers	49
3.1 Introduction.....	50
3.2 Theoretical model	51
3.3 Nonlinear dynamics	55
3.3.1 Building up of a DSML state	55
3.3.2 Balances inside a DSML state.....	61
3.3.3 Energy discrimination in a DSML state.....	65
3.3.4 Independent mode-locking.....	74
Summary	76
Chapter 4 Multi-channel Mode-locked Fiber Laser and Its Nonlinear Dynamics	77
4.1 Theoretical model	78
4.2 Nonlinear dynamics	80
4.2.1 Different MSML states	80
4.2.2 Dynamics in the formation of MSML states.....	85
Summary	92

Chapter 5 Conclusions and Future Works	95
Appendix A: Acronyms	99
Appendix B: Split-step Fourier Method	101
Appendix C: Convergence of Split-step Fourier Method.....	103
Appendix D: Haus's Master Equation	105
Appendix E: Cubic-quintic Ginzburg-Landau Equation.....	107
Appendix F: Logistic Map.....	109
Appendix G: Chaos and Lyapunov Exponent.....	111
Appendix H: FWM Induced Frequency Detuning	115
Appendix I: Impact of SA on Energy Ratio	117
Appendix J: Accumulated Error in Simulations	119
Bibliography	121

Chapter 1

Introduction

1.1 Background

“Laser” is the acronym for “light amplification by stimulated emission of radiation”[1]. Different from other light sources, e.g. LED which emits light through spontaneous radiation [2], a laser emits light through the optical amplification based on the stimulated emission [3], and in principle it can produce a single color of light. Laser has been applied in many aspects of our lives. In industry, lasers are sources for optical communications [4-8]. In defense, it can be used to mark targets, or guide

munitions [9]. In medicine, lasers can be used for the treatment of cancer, since they can shrink or destroy tumors or precancerous growths [9]. Lasers are also useful in people's daily life, for example, in laser lighting displays of musical performance.

The history of lasers dates back to 1960, when the first laser was invented by Theodore Maiman in Hughes Research Institute [10]. In the first laser, a synthetic pink ruby crystal is used as a lasing gain medium, and the pump of this laser is a helical xenon flash lamp. A laser operating at 694.3 nm was obtained. Since then, lasers attract much attention and undergo drastic development. The first mode-locked laser was invented in 1964 [11]. In the cavity, an acousto-optic modulator (AOM), which was driven by an electrical signal, was used as a modulator to produce loss modulation in the He-Ne cavity. A 2.5 ns width pulse operating at 633 nm was obtained. Then the mode-locked laser becomes crucial in many applications.

Fiber lasers have the advantages of good compatibility, portability and low cost. The first fiber laser is invented by E. Snitzer in 1961. A Nd-doped fiber was used as an amplifier, and the laser operated at 1.06 μm [12]. However, fiber loss was high, approximately 1000dB/km at that time. Fiber lasers did not receive much attention then. In 1970, based on the work of Charles K. Kao [13], first low loss fiber that had a loss lower than 20 dB/km was made by Corning [14]. Now the loss of single mode fiber in communication band (C band 1525~1565 nm) is lower than 0.15 dB/km [15] which contributes to the fiber laser operating at communication band. All these techniques have led to rapid development of fiber lasers.

1.2 Mode-locking

Mode-locking technique allows a laser to emit pulses. Mode-locked lasers are essential scientific and industrial tools and attract lots of interests. They play an important role in many applications such as optical metrology [16-18], material processing [19], biomedical imaging [20], and supercontinuum spectrum generation [21-24].

The light, as the wave, would constructively and destructively interfere with itself during propagation in an optical cavity. Only the frequencies that lead to a standing wave in a given laser cavity are allowed to oscillate. Consequently, the light in a cavity has a discrete set of frequencies which are called longitudinal modes [25]. For a cavity with a length L , the frequency separation between the modes is given by $\Delta f = c/(nL)$, where c is the speed of light and n is the refractive index of the medium. Only the modes within the gain bandwidth medium survive, as shown in Fig. 1-1.

In general, the modes in a laser oscillate independently. The cavity modes interfere with each other, leading to fluctuations in intensity since the modes are without any fixed relationship. Mode-locking introduces a fixed phase relation to the cavity modes, thereby causing the lasers to emit pulses. There are both active and passive mode-locking techniques.

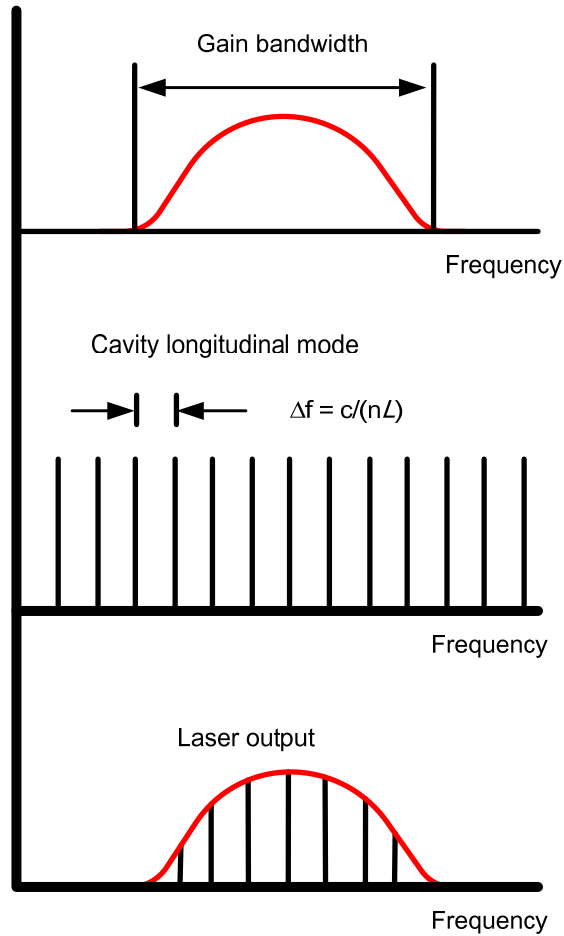


Fig. 1-1. Laser mode structure.

1.2.1 Active mode-locking

Active mode-locking can be achieved by adding a modulator in a laser cavity to modulate the amplitude or phase of light. We take active mode-locking via an amplitude modulator as an example as shown in Fig. 1-2. The laser cavity consists of a gain medium and a modulator. The modulator is driven by an electronic signal at frequency $\omega_m = 2\pi/T$, where T is the round-trip time of the cavity.

We assume that the interval of the cavity modes is Δf . For the cavity mode f_0 , the light field can be written as

$$E_0 = B\cos(2\pi f_0 t + \phi_0), \quad (1-1)$$

where B is the amplitude and ϕ_0 is the initial phase of the light field in the laser cavity.

The modulation signal $M(t)$ on the AOM can be written as

$$M(t) = 1 + A_m \cos(2\pi \Delta f t), \quad (1-2)$$

where A_m is the modulation depth and Δf is the interval of cavity modes. After the modulation, the light field becomes

$$\begin{aligned} E_0 M &= B\cos(2\pi f_0 t + \phi_0)[1 + A_m \cos(2\pi \Delta f t)] \\ &= B\cos(2\pi f_0 t + \phi_0) + \frac{A_m B}{2} \cos[2\pi(f_0 + \Delta f)t + \phi_0] \\ &\quad + \frac{A_m B}{2} \cos[2\pi(f_0 - \Delta f)t + \phi_0]. \end{aligned} \quad (1-3)$$

From Eq. (1-3), the neighbor cavity modes at $f_0 + \Delta f$ and $f_0 - \Delta f$ have the same initial phase ϕ_0 with their central cavity mode. Thus the phases of neighboring cavity modes are locked through the modulation. As a result, a mode-locked state is obtained and a pulse train can be observed in the time domain.

Active mode-locking can also be realized by using a phase modulator. A phase shift of light produces a frequency shift. When a phase modulator that is driven by an electrical signal $M(t)$ is placed in a laser cavity, the light in the cavity acquires a frequency shift (dM/dt) each time it passes through the modulator. The frequency shifts can make the frequency of light move away from gain bandwidth. However, if the light does not get frequency shift when it passes through the modulator, the light can survive. If the light is passing through the modulator at the time corresponding to the extreme points of the driven signal ($dM/dt=0$), the light will not get frequency shift. This results in a pulse output in the time domain.

The advantages of active mode-locking are that the repetition rate is determined by the driving signals of the modulators. Besides, the driving signals can be generated by the feedback signals that obtained by detecting the output pulse train of the laser cavity itself, leading to tunable pulse repetition rate and reduced timing jitter [26]. However, it is difficult to obtain short pulses below picoseconds by active mode-locking, because of the limited response speed of the electronic devices.

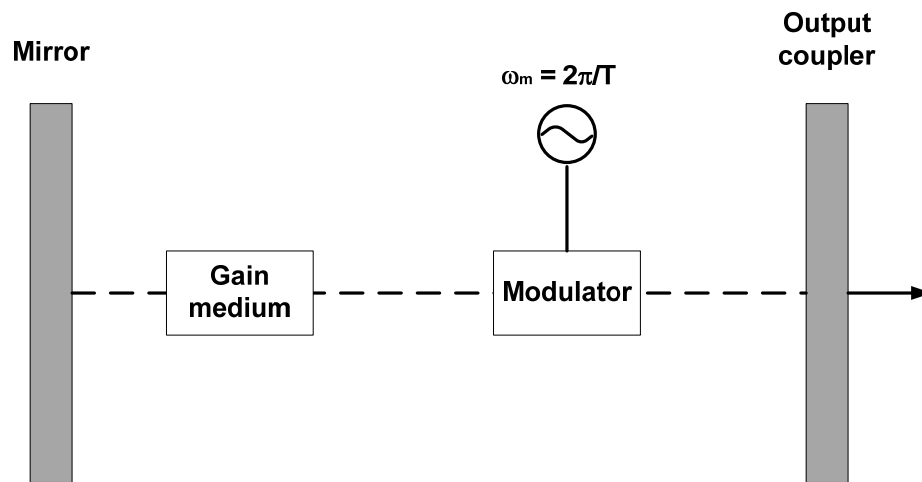


Fig. 1-2. Schematic of active mode-locking laser cavity. The modulation period equals to the roundtrip time of light in cavity.

1.2.2 Passive mode-locking

Recently, there is much interest in ultra-fast high power mode-locked pulse with a pulse width around hundreds of femtosecond or shorter, and the pulse energy larger than μJ . Such pulses can be achieved by passive mode-locking. In a passive mode-locking laser, the modulator is replaced by a saturable absorber (SA), which is an intensity dependent loss device. The loss is larger when the light intensity is weak

and the loss is smaller when the light intensity is strong. Thus high intensity light in the laser cavity can be amplified while the low intensity light is attenuated, leading to pulse generation.

There are many types of SAs. A typical SA in passive mode-locked lasers is the semiconductor saturable absorber mirror (SESAM) [27-30]. SESAM is a mirror structure with an incorporated saturable absorber and this structure requires expensive fabrication e.g. metal organic phase vapor epitaxy (MOPVE), metal organic chemical vapor deposition (MOCVD), or molecular beam epitaxy (MBE) [31]. An SA that based on the single-wall carbon nanotube (SWNT) had also been applied in a mode-locked laser. Its fabrication is comparatively simple, with only three steps, namely nanotube growth, dispersion, and deposition [32]. Graphene has also been proposed to serve as SA since the first demonstrations of graphene SAs in 2009 [33]. Graphene SAs are used to generate pulses at wavelength from 0.8 to 2.9 μm [34, 35], while the working bands of SESAM and SWNT are approximately 0.1 and 1 μm , respectively [36]. Other materials such as MoS_2 [37, 38] and black phosphorus [39, 40] have also been used as SAs for passive mode-locking.

In addition to the materials mentioned above, there are other kinds of SAs that are based on the Kerr nonlinearity. Kerr nonlinearity modifies the refractive index of a medium as $n = n_0 + n_2 I$, when the light is propagating in it. Here n_0 is the refractive index of the medium, n_2 is nonlinear refractive index coefficient, and I is optical intensity. Thus the nonlinear phase shift $\Delta\phi_{\text{NL}} = (2\pi/\lambda)n_2 IL$ is proportional to the light intensity, where L and λ are the medium length and light wavelength, respectively.

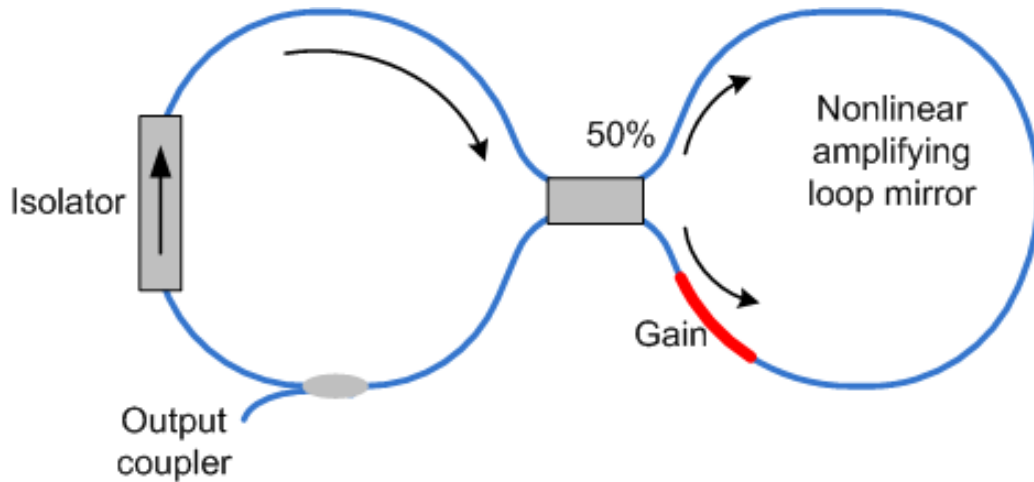


Fig. 1-3. Schematic of the Figure-eight mode locked fiber laser setup. A main resonator on the left-hand side, and a NALM as the mode-locker element on the right-hand side.

An figure-eight mode-locking fiber laser (F8L) utilizes Kerr nonlinearity to achieve mode-locking. The schematic of an F8L cavity is shown in Fig. 1-3. The ring on the right-hand side in the figure is a nonlinear amplifying loop mirror (NALM). The light splits into two counter-propagating components when it goes into NALM. In the NALM, the light that propagates in the anticlockwise direction first passes through the amplifier and then propagates in the fiber, while the light in the clockwise direction first passes the fiber and then gets amplified. As a result, the nonlinear phase shifts, which are proportional to the light intensity, are different among the light in two directions. When the combined light returns to the left loop in Fig. 1-3 through the coupler, the two light will interfere and the intensity dependent output is obtained. NALM was first used in mode-locked fiber in 1991 [41]. The author demonstrated the generation of 320 fs pulses at 1560 nm.

Nonlinear polarization rotation (NPR) as a mode-locking mechanism [42-48], was first used in a fiber laser in 1992 [46], where a 1.55 ps mode-locked pulse was

obtained. The schematic representation of the cavity is shown in Fig. 1-4(a). NPR mode-locking is based on both the nonlinearity and fiber birefringence. An optical fiber supports two orthogonally polarized modes of the light. Their refractive indices are n_x and n_y . In an ideal fiber, they are identical, but a real fiber exhibits some birefringence ($n_x \neq n_y$) because of the unintentional variations in the fiber core shape and anisotropic stress. There are two principal axes in a fiber with birefringence, which are the slow and fast axes. When light propagates in a fiber, the nonlinearity affects the light in both the fast and slow axes of the fiber. If the nonlinear phase shifts of the two components are different, the polarization of the light is changed. Since the nonlinear phase shift depends on the light intensity, the polarization of the light changes during the propagation in the fiber as shown in Fig. 1-4(b). If the light then passes a polarizer, intensity dependent output is obtained.

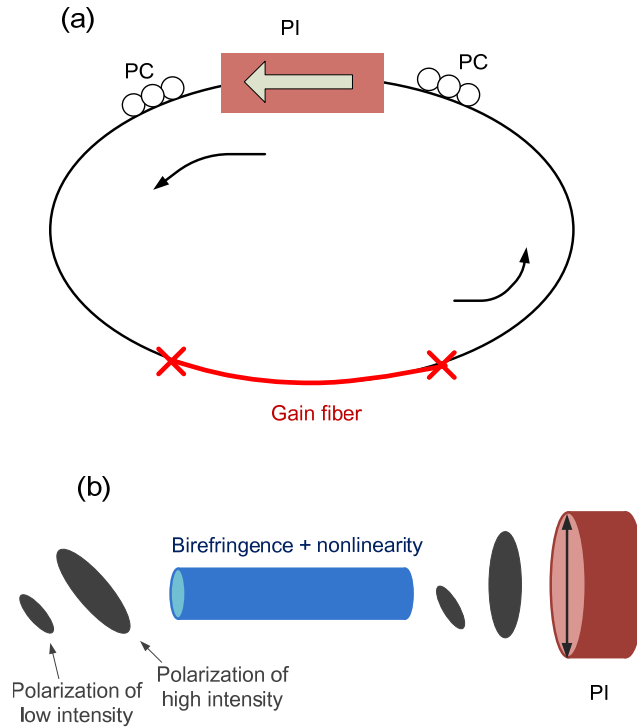


Fig. 1-4. (a) Schematic representation of the laser cavity. (b) the intensity depends on the transmission of NPR mode-locker. PI: polarization isolator, PC: polarization controller.

1.3 Modeling for mode-locked fiber lasers

A laser source that emits ultra-fast high power mode-locked pulse is attractive as mentioned above. Achieving such laser sources is not easy because as the pulse energy increases, multi-pulsing instability might occur [49].

A laser consists of different elements, e.g. gain fiber, SA and filter. The pulse in a laser cavity is modified by these optical components in each roundtrip. Thus intuitively, a model in which each optical component is modeled separately would better describe the pulse evolution in a laser cavity. However, if the laser pulses are not significantly modified by each element in a roundtrip, the effects of each

component on the light can be distributed throughout the laser cavity. Hence the light evolution inside the cavity can be approximated by a partial differential equation (PDE) which allows the use of analytical techniques to study the mode-locking [50-52]. In the following subsections, both distributed and discrete models are introduced.

1.3.1 Haus's master equation

The master equation proposed by H. A. Haus is one of most successful models for the mode-locked lasers [50-52]. Light evolution in the laser cavity is given by

$$iU_z + U_{tt} + \gamma|U|^2 U = i(g-l)U + ig\tau U_{tt} + i\mu|U|^2 U, \quad (1-4)$$

where U is the complex envelope of the electric field of light, β_2 is dispersion coefficient, γ is nonlinearity coefficient, τ is gain bandwidth, l is loss and μ is self-amplitude modulation (SAM) coefficient. Here g is the gain term. The gain medium in a laser amplifies the light through stimulated radiation which requires population inversion of the ions. If the light energy increases, amplifying the light consumes more excited ions, and the inversion level of ions is reduced. Hence the gain of an amplifier will be reduced [53]. This effect is known as gain saturation. The gain term that contains gain saturation is written as [50-52]

$$g = \frac{g_0}{1 + E/E_{\text{sat}}}, \quad (1-5)$$

where E_{sat} is the saturation energy and $E = \int |U|^2 dt$ is the light energy. From Eq. (1-5), the gain decreases when the pulse energy increases. The dispersion and Kerr nonlinearity are represented by the second and third term on left-hand side of Eq. (1-4). The second and third term on the right-hand side represents the action of a Gaussian filter and SA, respectively [see Appendix D].

The master equation has an analytical solution of the form [54, 55]

$$U(t) = x \operatorname{sech}^{1+iy}(t/T_0), \quad (1-6)$$

where x , y and T_0 are real constants. Such analytical solution allows one to calculate pulse duration, chirp, and spectral bandwidth as functions of the laser parameters.

The master equation captures the key characteristic of a mode-locked laser. However, it has been shown that Eq. (1-4) supports a stable mode-locked pulse in a relatively small parameter space only [55].

1.3.2 cubic-quintic Ginzburg–Landau equation

The action of SA in the master equation is modeled by the SAM term $\mu|U|^2U$ which assumes a monotonic increase of the SA transmission as the function of pulse intensity [see Appendix D]. Such an assumption is unrealistic. The SA transmission curve may decrease at high pulse intensity such as in NALM, NPR. Besides, because of the monotonic transmission of the SA in the master equation, the pulse intensity might quickly grow with the distance z as shown in Fig. 1-5 [55].

This can be solved by adding a high order term that prevents the transmission curve from monotonically increasing [see Appendix E]. Adding the quintic term in the master equation leads to the so-called cubic-quintic Ginzburg–Landau equation (CQGLE), which is written as

$$iU_z + U_{tt} + \gamma|U|^2U = i(g-l)U + ig\tau U_{tt} + i\mu|U|^2U - i\sigma|U|^4U. \quad (1-7)$$

The quintic term introduces saturation to the nonlinear growth of the mode-locked pulse [see Appendix E]. Fig. 1-6 shows one example of the pulse evolution in CQGLE. The parameters used in Fig. 1-6 are the same as that used in Fig. 1-5, but with $\sigma = 0.02$. Different to the case in Fig. 1-5 where the pulse dramatically grows up,

the pulse now does not blow-up as the propagation distance z increases, and here we give an example of $z = 20$.

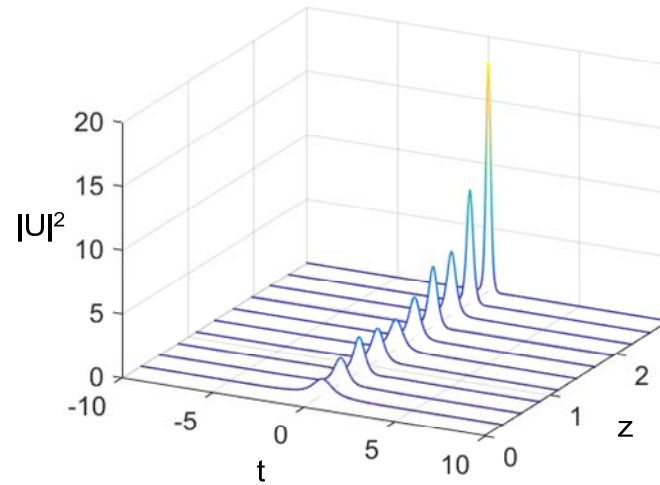


Fig. 1-5. The dynamics of the mode-locked pulse in the master equation. One example of the typical master mode-locking blow-up [55]. Other parameters: $\gamma = 4$, $l = 0.1$, $g_0 = 0.2$, $E_{\text{sat}} = 1$, $\tau = 0.1$ and $\mu = 0.1$.

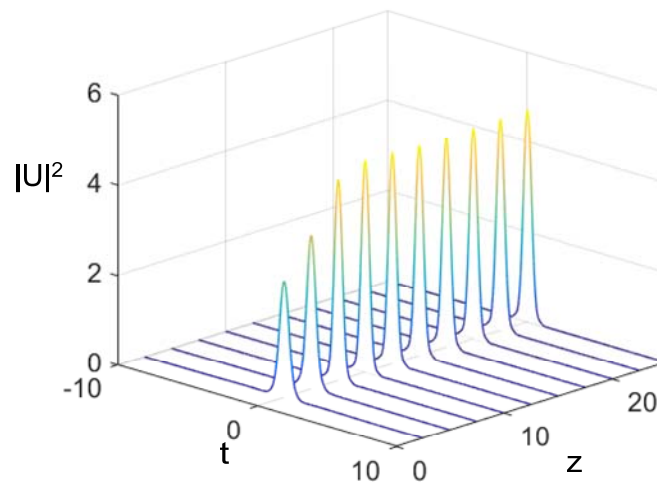


Fig. 1-6. The mode-locked pulse in the CQGLE. The parameters are the same as the case in Fig. 1-5 except the quantic term is added, $\sigma = 0.02$. The mode-locked pulse does not show the blow-up along the distance [55].

There are also mode-locked fiber lasers that produce mode-locked pulses at different central frequencies. They are called multi-channel mode-locked lasers [56, 57], which are attractive for applications in terahertz generation and optical sensors [56, 58-61]. Such a laser can also be modeled by distributed models.

1.3.3 Distributed models for multi-channel mode-locking

The Swift-Hohenberg equation (SHE) describes mode-locked lasers with a dual-channel filter. In both the master equation and CQGLE, the action of spectral filter is modeled by the second order differential terms $ig\tau U_{tt}$ (for details, please read Appendix D). In SHE, a higher order differential term is added such that the filter profile now has more than one maximum [62].

The SHE is written as

$$iU_z + U_{tt} + \gamma|U|^2 U = i(g-l)U + i\alpha_2 U_{tt} + i\alpha_4 U_{tttt} + i\mu|U|^2 U - i\sigma|U|^4 U. \quad (1-8)$$

The parameters α_2 , and α_4 are the coefficients of second and fourth order terms on the right-hand side of Eq. (1-8) which give the bandwidth and the distance between the two channels in the spectral response. In SHE, the filter is given by

$$U_z = \alpha_2 U_{tt} + \alpha_4 U_{tttt}, \quad (1-9)$$

where the filter function is $F(\omega) = \exp(-\alpha_2 \omega^2 - \alpha_4 \omega^4)$. If the fourth order differential term is removed, the filter profile (for instance, $\alpha_2 = -10$, $\alpha_4 = 0$ in a CQGLE) is reduced to that of a single channel filter, as shown in Fig. 1-7(a). A dual-channel filter is modeled with a nonzero value of α_4 , as shown in Fig. 1-7(b) (for instance, $\alpha_2 = 10$, $\alpha_4 = -5$).

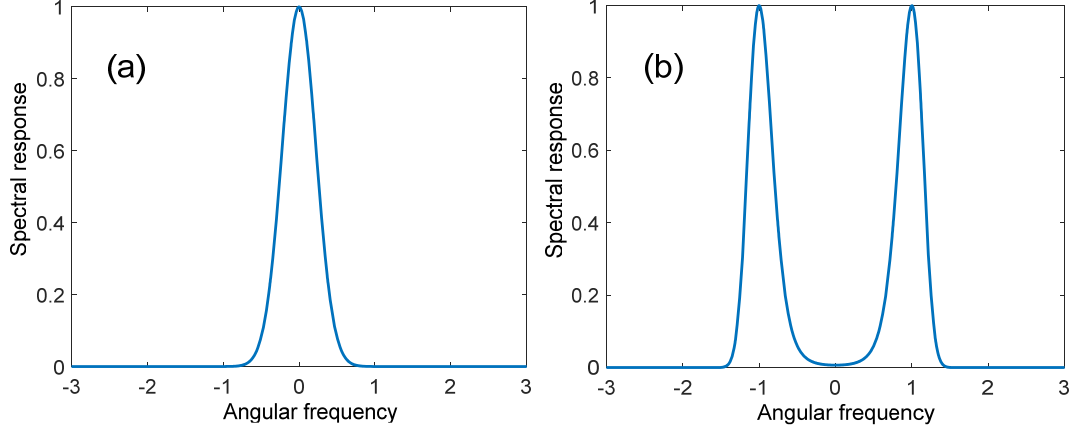


Fig. 1-7. The filter response curve in (a) CQGLE, where $l = 0$, $\alpha_2 = -10$, $\alpha_4 = 0$, (b) SHE where $l = -10$, $\alpha_2 = 10$, $\alpha_4 = -5$.

In addition to the model for dual-channel mode-locking, we can also easily model multi-channel mode-locking. Coupled equations can be used to study the mode-locking in the multi-channel laser. In these coupled equations, each channel is modeled by a single equation. The coupled equations are written as [63, 64]

$$\begin{aligned}
 & i \frac{\partial U_n}{\partial z} + i \delta_n \frac{\partial U_n}{\partial t} + \frac{1}{2} \frac{\partial^2 U_n}{\partial t^2} + (1 - i \mu_n) |U_n|^2 U_n - i g_n \left(1 + \tau \frac{\partial^2}{\partial t^2} \right) U_n, \\
 & + 2 \left(|U_{n-1}|^2 + |U_{n+1}|^2 \right) U_n + i \sigma_n |U_n|^4 U_n = 0
 \end{aligned} \tag{1-10}$$

where U_n is the light field in n -th channel ($n = 1, 2, \dots, N$). N is the total number of channels. g_n is the gain term to the light in n -th channel and τ represents the gain bandwidth. Due to the group-velocity dispersion (GVD), the light in different channels has different group velocity. The parameter δ_n is used to model the walk-off of the pulses in different channels. The coefficients μ_n and σ_n are used to model the SA for generating mode-locking.

With the help of coupled equations, multi-channel mode-locking can be modeled. Coupled equation requires multiple equations for the model, not as easy as SHE where only one equation is used. However, to this model, it is easier to model a laser cavity with a multiple channel filter. The reason is to SHE, we should adding more higher order terms along with α_2 and α_4 to describe the profile of a multi-channel filter.

1.3.4 Discrete models

In the models discussed so far, the effects of the discrete laser devices on the circulating light are distributed throughout the whole cavity. Such models allow the use of analytical techniques to investigate the mode-locking. Modeling on ultra-fast high power mode-locked laser sources is attractive, since such laser sources are powerful tools for the research in nonlinear optics and biomedicine as mentioned above. To an ultra-fast high power mode-locked laser, its duration might be as short as 100 fs and its spectrum might be around 20 nm. The pulse spectrum is comparable or even wider than the gain bandwidth (around 10 nm homogeneous gain bandwidth for EDFA [65]). The laser pulse undergoes significant evolution in each roundtrip in the cavity. Thus the distributed model cannot adequately describe the evolution of light in such a laser cavity. Instead, the action of each element on the light should be modeled separately. Although we cannot use the analytical tools as we did in distributed models, discrete models give a more realistic description of a laser cavity.

1.4 Outline of the thesis

The main objective of laser modeling is to provide insight of the mode-locking mechanism, rather than a quantitative description of the laser output in one special laser cavity. Recently, a discrete laser model with only the effect of gain and loss is shown to contain complex laser dynamics, including chaos and multi-pulsing.

The pulse shaping effect such as dispersion and Kerr nonlinearity were not included in the model because they are assumed not to affect the gain and loss. However, Kerr nonlinearity and spectral filtering, or dispersion and SA, give rise to energy dependent loss. Thus a full description of laser dynamics should contain the pulse shaping effects.

Chapter 1 of this thesis gives the background of mode-locked fiber lasers and laser models. Chapter 2 discusses a heuristic model and its extension to study the mode-locking mechanism in a fiber laser. Both the multi-pulsing and chaos can be observed with the model, and the guidance to obtain high energy pulse is given. In Chapter 3, a simpler case, dual-channel mode-locking is studied. The phases of the mode-locked pulses in the two channels can be either locked or unlocked. When the channels are locked, the impacts of different elements in a laser cavity are investigated. The gain loss dynamics is found to be different to the single-channel filter cavity. In Chapter 4, a comb filter is used in the laser cavity. The mode-locking states and the gain loss dynamics in such multi-channel mode-locking laser are investigated. Chapter 5 gives the conclusion and discusses the prospected works.

Chapter 2

Multi-pulsing and Chaos in Single-channel Mode-locked Fiber Lasers

2.1 Theoretical model

2.1.1. Review of a heuristic model

Achieving a high energy ultra-fast mode-locked pulse from a laser is attractive. However, when pump power increases, other phenomena such as multi-pulsing and chaos can happen, which prevents the energy of the pulse from increasing. Multi-pulsing and chaos have been investigated both theoretically and experimentally [49, 66-73]. Li et al. proposed a geometrical heuristic model which includes only the gain and loss but can successfully describe and study the laser output, e.g. onset of multi-pulsing and chaos [49, 71, 74]. Here “geometrical” refers to the fact that solution and the nature of the solution of the theoretic model can be determined through graphic methods, in a manner similar to determining the solutions of the logistic map in nonlinear dynamics [see Appendix F]. In the model, a laser is divided to gain and loss parts as shown in Fig. 2-1(a). The energy at point A is the input energy of the gain part E_{in}^{gain} and is also the output energy of the loss part E_{out}^{loss} . The energy at point B is the input energy of loss part E_{in}^{loss} and also output energy of gain part E_{out}^{gain} . Since pulse shaping effects are not included, the gain only depends on the total energy in the laser cavity. So the saturated gain is calculated as

$$g(z) = \frac{g_0}{1 + E_{tol}(z)/E_s}, \quad (2-1)$$

where g_0 is the small signal gain coefficient. E_s is saturation energy and z is the propagating distance in the gain fiber. In a mode-locked laser, both the pulse and the small signal (or noise) are included in E_{tol} to estimate the total energy of the light in

the cavity. Indicating from Eq. (2-1), we know that the small signal and pulse share the same strength of gain.

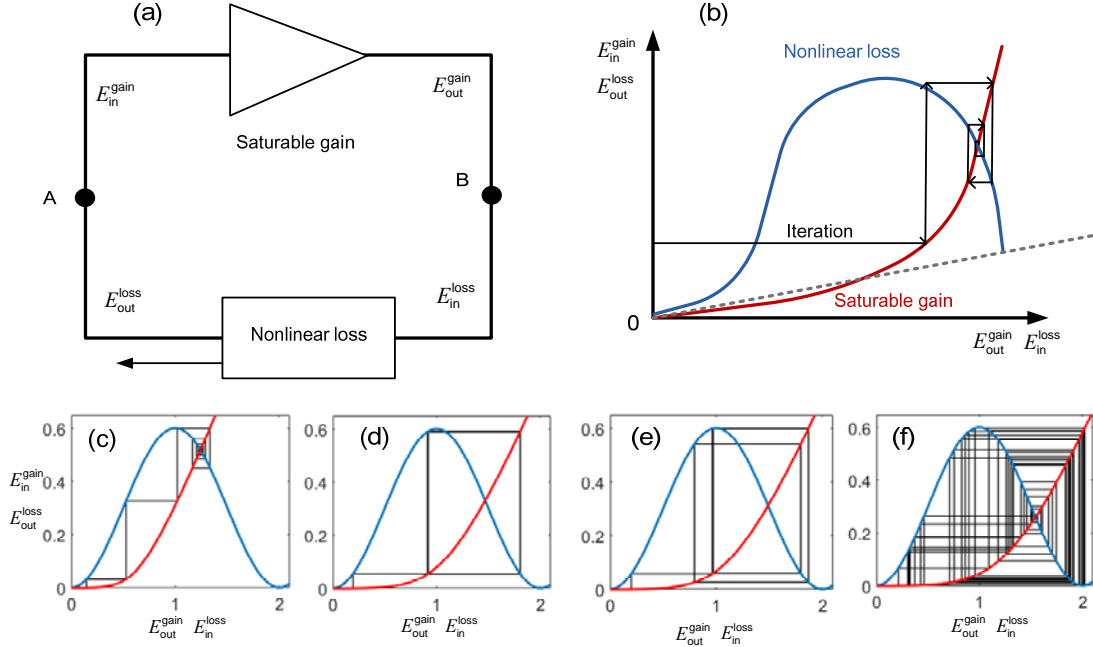


Fig. 2-1. (a) Schematics of the cavity configuration in the geometrical model which consists of a saturable gain element and a nonlinear loss element. (b) A typical gain and nonlinear loss curves. When the nonlinear loss term is modeled as a sinusoidal function as $E_{out}^{loss} = 0.3 - 0.3\cos(E_{in}^{loss}\pi)$, we observe (c) stable steady state, (d) period-2 state and (e) period-4, state and (f) chaotic states for increasing values of E_{sat} .

To simplify the system, the nonlinear loss term is considered as an explicit function of the pulse energy without including the pulse shaping. Such qualitative modeling of the nonlinear loss will allow us to model the gain loss dynamics in a very simple way and provide intuitive understanding of the mechanism without considering the realistic situation of laser cavities. In different experiments, the transmission function could vary significantly for different nonlinear loss elements.

For example, for mode-locking using NPR, the transmission of the nonlinear loss term varies periodically along the increase of input energy, e.g. a sinusoidal function [49]. In such case the transmission can first increase and then decrease when the pulse energy increases, as shown in Fig. 2-1(b).

The intersection point of gain and loss curve in Fig. 2-1(b) represents gain equal to lose in one roundtrip. Hence the intersection point represents an equilibrium solution in the cavity. Similar to the logistic map, we can determine the stability of the mode-locked solution as shown in Fig. 2-1(b). To an equilibrium solution, when there is a perturbation on the energy of the solution, the geometrical procedure shows the stability of the solution. Fig. 2-1(b) shows an example of a stable solution. In the following, we discussed the results of the geometrical model. In Figs. 2-1(c)-(f), the nonlinear loss term is modeled as a sinusoidal function in the form $E_{\text{out}}^{\text{loss}} = 0.3 - 0.3\cos(E_{\text{in}}^{\text{loss}} \pi)$, which can be considered as an NPR based mode-locker, for example. We note that as the pump increases, the gain curve moves towards the right-hand side. The steady state solution, i.e. the mode-locked state, is given by the intersection of the nonlinear loss curves and the gain curves. Theoretically, the laser will operate at the steady state solution if the laser is started there. However, if the laser is initiated away from the steady state solution in the parameter space, it might or might not converge to the steady state solution. The nature of the steady solutions can be determined graphically as shown in Figs. 2-1(c)-(f). For example, when $E_{\text{sat}} = 0.13$, the output energy $E_{\text{out}}^{\text{loss}}$ converges to the intersection point. As the pump increases, the output energy may settle in a periodic state, e.g. period-2 state in Fig. 2-1(d), and period-4 state in Fig. 2-1(e). When the pump is further increased, e.g. $E_{\text{sat}} =$

0.25, the output energy varies from roundtrip to roundtrip. In this state, the output data is sensitive to the initial input and it can be shown that the laser operates in a chaotic state [see Appendix G].

The model also helps to explain the multi-pulsing in a laser cavity. In a laser cavity, the pulse and the small signal share the same strength of gain, but they receive different strength of loss. To a pulse, its loss equals to the cavity gain. The loss value depends on the pulse energy because the SA in the model gives a light transmission that depends on the pulse energy. To small signal, its loss is a constant. The loss depends on the cavity linear loss, e.g. output coupler. In the gain loss map in Fig. 2-1(b), the loss seen by the small signal is given by the initial part of the loss curve, which is represented by the tangent to the initial point of the loss curve (dashed line) to describe the loss seen by the small signal in the cavity. In the region above (below) this tangent, gain seen by the noise is smaller (larger) than its loss, and hence the noise cannot (can) increase. If the nonlinear loss curve hits the threshold line, the noise receives a gain equal to its loss. Further increase of gain will make the noise grow up. In such a case, the additional pump gives the energy to the growing up noise, rather than making the original pulse to grow up.

The heuristic model successfully describes the mechanisms that prevent the increase on the energy of the mode-locked pulse. It shows that multi-pulsing and chaos can be avoided by engineering the transmission curve of the SA. However, the heuristic model is oversimplified as it assumes that the pulse shape does not affect the gain and loss in a cavity. The equations of both the gain and the nonlinear loss therefore depend on the light energy only. However, as mentioned in Chapter 1, for

high power ultra-fast lasers, the pulse shaping effects have obvious impacts on the gain and loss in the cavity. The nonlinearity broadens the pulse bandwidth and the newly created higher frequency components face higher loss induced by the filter. Furthermore, the dispersion changes the pulse shape in the time domain and hence SA will induce a different loss. The shape of the pulse is hence believed to affect the gain loss dynamics. Thus the heuristic model should be extended by including the pulse shaping effects, so as to study the dynamics of a high power pulsed laser cavity. The details of the extended model are given in the next subsection.

2.1.2 An extended heuristic model

Fig. 2-2 shows the schematic of a mode-locked fiber laser cavity. The cavity gain is provided by the gain fiber. The effects of dispersion and nonlinearity are also included. The SA provides the mode-locking mechanism and the spectral filter controls the pulse's bandwidth. An output coupler is placed after the spectral filter. The output points of the gain fiber, spectral filter (and output coupler) and SA are marked as A, B, and C, respectively in Fig. 2-2.

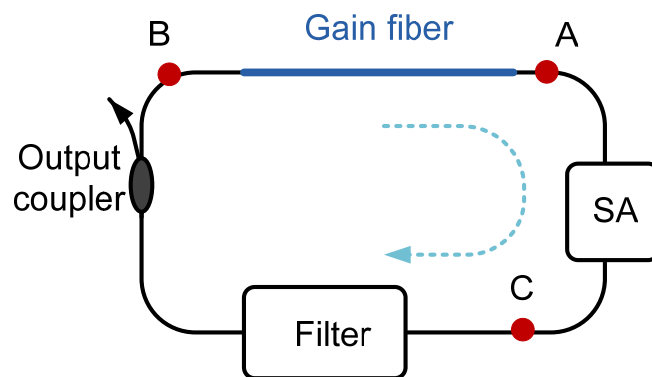


Fig. 2-2. Schematic of a typical mode-locked fiber laser cavity that consists of a section of gain fiber, an SA, a spectral filter and an output coupler.

Pulse evolution in the gain fiber is modeled by the nonlinear Schrödinger equation (NLS) with gain as [70],

$$\frac{\partial A}{\partial z} = \frac{1}{2}g(z)A - \frac{i}{2}\beta_2 \frac{\partial^2 A}{\partial t^2} + \frac{\beta_3}{6} \frac{\partial^3 A}{\partial t^3} + i\gamma|A|^2 A, \quad (2-2)$$

where A is the slowly varying envelope of the electric field, t is the time, z is the distance in the fiber, β_2 , β_3 and γ are the second order dispersion, third order dispersion, and nonlinear coefficients, respectively. The effect of dispersion and nonlinearity are added in the model in order to take into account the impact of the pulse shaping effects. The gain coefficient $g(z)$ is given by

$$g(z) = \frac{g_0}{1 + \int |A(z,t)|^2 dt / E_s}, \quad (2-3)$$

where g_0 is the small signal gain coefficient. E_s is saturation energy. A flat gain profile is adopted here for $g(z)$ as the effective gain profile is the combined effect of gain and the spectral filter. We assume a homogeneous gain, thus the gain depends on the total energy in the cavity, as shown in Eq. (2-3).

The SA is modeled by a power dependent transmittance function [70, 73, 75]

$$T_{SA}(t) = 1 - \frac{l_0}{1 + |A(t)|^2 / P_{sat}}, \quad (2-4)$$

where P_{sat} is the saturation power and l_0 is the unsaturated loss of the SA. One can note the unsaturated loss l_0 determines the transmission seen by the small signal. The transmission of the small signal can be obtained by setting $|A(t)|^2 \sim 0$ and then the transmission of SA on the small signal is $T_{SA} = 1 - l_0$.

The spectral filter is assumed to be a Gaussian bandpass filter [70]

$$H_f(\omega) = H_0 \exp \left[-\frac{1}{2} \left(\frac{\omega}{\omega_{band}} \right)^2 \right], \quad (2-5)$$

where ω_{band} is the filter bandwidth and H_0 is the maximum of transmission of the spectral filter. Both the linear loss in the cavity loss and the output coupler are included in H_0 . Hence in the revised geometrical model, the loss term, i.e. SA and filter, are functions of the pulse shapes in the time and frequency domain, respectively.

We normalize Eq. (2-2) as

$$\frac{\partial U}{\partial \xi} = \frac{i}{2} \frac{\partial^2 U}{\partial \tau^2} + D_3 \frac{\partial^3 U}{\partial \tau^3} + i|U|^2 U + \frac{g_n}{2} U, \quad (2-6)$$

where the normalized variables are

$$\begin{aligned} U &= A/\sqrt{P_{\text{sat}}}, \\ \xi &= z/L_N, L_N = 1/(\gamma P_{\text{sat}}), \\ \tau &= t \times |\beta_2 L_N|^{-1/2}, \\ D_3 &= \frac{1}{6} \beta_3 |\beta_2^3 L_N|^{-1/2}, \\ g_n &= \frac{g_0 L_N}{1 + \int |U|^2 d\tau / E_{\text{sat}}}, \\ E_{\text{sat}} &= E_s P_{\text{sat}}^{-1} |\beta_2 L_N|^{-1/2}. \end{aligned} \quad (2-7)$$

The transfer functions of SA and filter are normalized to

$$T_{\text{SA,n}} = 1 - \frac{l_0}{1 + P(\tau)}, \quad (2-8)$$

and

$$H(\Omega) = H_0 \exp \left[-\frac{1}{2} \left(\frac{\Omega}{\Omega_{\text{band}}} \right)^2 \right], \quad (2-9)$$

where $\Omega = \omega \times |\beta_2 / \gamma P_{\text{sat}}|^{1/2}$ is the normalized angular frequency and $\Omega_{\text{band}} = 2\pi \delta_f$ is the normalized filter bandwidth.

Equations (2-6), (2-8) and (2-9) together describe the action of each component in the cavity on the light field. In the simulation, the action of increasing pump power

is modeled by varying E_{sat} . The actions of gain fiber, SA and filter are modeled iteratively. Here Eq. (2-6) is solved numerically with the split-step Fourier method [76]. The white Gaussian noise is added after the gain fiber which can model the amplifier noise. The noise has a zero mean and a variance of $\sim 10^{-7}$ to 10^{-9} , which is within the range of typical noise level in a fiber laser [58, 61, 77]. The pulse after the gain fiber is subsequently multiplied by the point functions of SA and filter in the simulation. The simulation is stopped when the solution converges (generally, about 3000 roundtrips is enough), which means the differences of pulse profiles between roundtrips are nearly unchanged (at the level of noise, e.g. 10^{-9} in our case, as we added amplifier noise after gain fiber) in both time and frequency domain. Otherwise, the simulation is stopped after 20,000 roundtrips. We started with white Gaussian noise (a zero mean and a variance $\sim 10^{-9}$) and a mode-locked pulse is obtained with a relatively small value of E_{sat} (i.e. ~ 0.01). The output at this value of E_{sat} is used as the seed for next E_{sat} . This action corresponds to the realistic changing of the pump power of the laser in experiments.

2.2 Pulse dynamics in a laser cavity

In the original heuristic model, the laser dynamics is determined by the gain and loss curve only. In the extended heuristic model, the laser dynamics will be more complex. As the loss now depends on the profiles of the pulses in both the time and frequency domain, a deterministic loss curve does not exist. It is not possible to determine the equilibrium solution by a simple geometrical method. The final states have to be determined by simulations. Due to the frequency dependent loss, the spectral filter induces a dynamical loss to the pulse, which has an obvious impact on the laser

dynamics. In the following sections, the impact of spectral filtering on the laser dynamics is investigated with different filter bandwidths δ_f and cavity energy E_{sat} .

2.2.1 Multi-pulse generation

We study the pulse dynamics as the filter bandwidth is varied. We first set the filter bandwidth to 0.08 as an example. Other values of bandwidth will be studied later. For typical values in fiber laser cavity, e.g. $\gamma = 1/\text{W}/\text{km}$, $\beta_2 = -20 \text{ ps}^2/\text{km}$ and $P_{\text{sat}} = 200 \text{ W}$, this filter bandwidth (0.08) corresponds to $\sim 250 \text{ GHz}$ which is a typical value used in fiber lasers [78]. In the simulations, the small signal gain is chosen to be 30 dB. For SA and filter, $l_0=0.85$, $H_0 = \sqrt{0.9}$ and the length of gain fiber is 3. Simulation starts from Gaussian white noise with a zero mean and a variance $\sim 10^{-9}$. The parameters chosen here are typical parameters as referred to the study on mode-locked fiber lasers in Ref. [49, 70-72, 79, 80]. Third order dispersion D_3 is first set to 0, and its impact will be studied in Section 2.2.3.

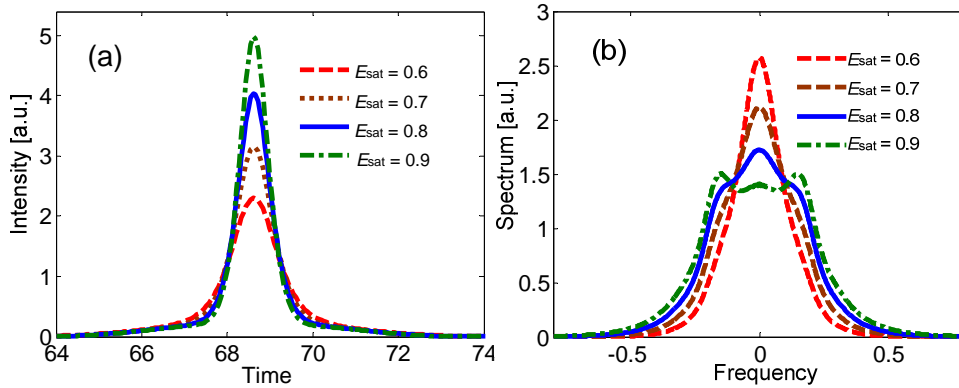


Fig. 2-3. (a) The pulse temporal profiles and (b) spectra after the gain fiber when the E_{sat} is gradually increased from 0.6 to 0.9 with $\delta_f = 0.08$. The pulse spectrum is broadened by the nonlinearity in gain fiber. Other parameters: $l_0 = 0.85$, $\delta_f = 0.08$, $D_3 = 0$.

Fig. 2-3 shows the pulse temporal and spectral profiles at point A of Fig. 2-2 when E_{sat} varies from 0.6 to 0.9 in step of 0.1. As we start with noise, the pulse temporal center can locate at any temporal position in our time window. To the obtained mode-locked pulses with different values of E_{sat} , the pulse shape varies in the both time and frequency domain as shown in Fig. 2-3(a). The peak pulse intensity increases from 2.30 to 4.97 and the full width at half maximum (FWHM) decreases from 1.31 to 0.79 when E_{sat} increases from 0.6 to 0.9. The variations of the pulse spectra are shown in Fig. 2-3(b). The pulse bandwidth increases as E_{sat} increases. From Fig. 2-3, it might appear that the pulse peak intensity can be increased by increasing E_{sat} . However, as E_{sat} increases, the pulse does not continuously absorb energy. Other states such as multi-pulsing and chaos will be found which prevent us from obtaining a high energy ultra-fast pulse.

Now we try to determine the mechanisms of multi-pulsing and chaos. As the loss curve is not fixed, we cannot analyze the laser dynamics by the geometric method as in the original heuristic model. However, the energies of the mode-locked pulses with different values of E_{sat} can be obtained by the simulations. We can put the final states on the gain loss map, e.g. in Fig. 2-1(b), by monitoring the energies at point A and point B in the laser cavity shown in Fig. 2-2.

The energies at point A and B in final states for different E_{sat} are shown in Fig. 2-4. Each black dot in Fig 2-4 corresponds to a mode-locked state with their corresponding value of E_{sat} . We cannot link these points and treat them as the loss curve. To each black dot, the corresponding mode-locked pulse experiences a loss equal to its gain. Hence the black dots also locate on a corresponding gain curve. For

example, the black dot obtained with $E_{\text{sat}} = 0.6$ is also on its gain curve [see Fig. 2-4]. As a flat gain profile is used, the gain remains dependent on the total energy in the cavity only and we can get the gain curve by solving the gain model in Eq. (2-7) with $E_{\text{sat}} = 0.6$.

As shown in Fig. 2-4, the pulse energy at first increases when E_{sat} increases. Inferred from Fig. 2-3(b), the pulse bandwidth increases when E_{sat} increases. When the pulse bandwidth increases, the filter loss increases. As a result, the pulse energy then decreases as E_{sat} is further increased. The black dots then decreases as E_{sat} increases as shown in Fig. 2-4. The black dots reach the gray dashed line when the E_{sat} increases to of $E_{\text{sat}} = 0.91$. From the previous heuristic model, we know now the small signal gets a gain equal to its loss. If E_{sat} is further increased, the small signal will grow and an example of multi-pulsing transition is shown in Fig. 2-5 where the E_{sat} is increased to 0.92. We find the small signal is increased and two identical pulses are circulating in the cavity.

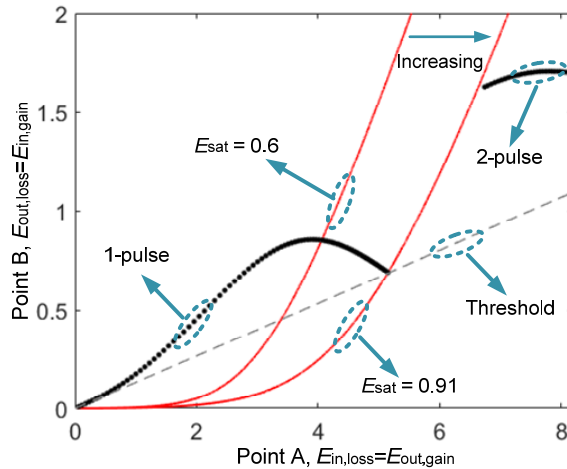


Fig. 2-4. The gain and loss map in the laser cavity for $\delta_f = 0.08$. The red solid curves are the gain curves with $E_{\text{sat}}=0.6$ and 0.91 respectively. The black solid points are the working points of combined nonlinear loss. The gray dashed line is the multi-pulsing threshold.

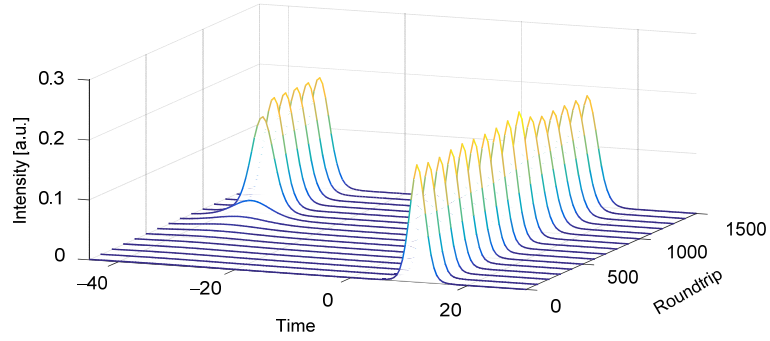


Fig. 2-5 Evolution from 1-pulse to 2-pulse by increasing the pump. Small signal is amplified to be another pulse. Other parameters: $l_0 = 0.85$, $E_{\text{sat}} = 0.93$, $\delta_f = 0.08$, $D_3 = 0$.

Such a multi-pulsing transition which a new pulse grows up from the background noise qualitatively agrees with the original heuristic model [49, 71]. The difference is that in the extended model the loss is not only caused by SA, but also from spectral filtering. In the original heuristic model, the loss curve is only determined by SA transmission. The authors suggested to engineer an SA with transmission far from the multi-pulsing threshold as the pump increases, e.g. a monotonic SA transmission, to avoid multi-pulsing [49, 71]. When pulse shaping is taken into account, even with an SA with a monotonic transmission, the filter induced loss can trigger the multi-pulsing. The results are consistent with the experiments in [69, 81, 82] where a SESAM was used in the laser cavity. A SESAM has a monotonic transmission. From the former model, multi-pulsing should not occur as the loss response would not reach the multi-pulsing threshold. However, multi-pulse state was still observed, indicating that effects other than gain and loss play a role in multi-pulsing.

Multi-pulsing has also been observed in distributed models [68, 69, 83]. These are distributed models and they contain many physical effects, such as the relaxation

time of gain and SA, all of them will affect the pulse profiles. The authors pointed out that a new pulse could grow from the background noise if its gain larger than loss. Our model shows that multi-pulsing is an intrinsic property of a laser cavity, it will occur even if only the most intrinsic effects, gain and loss, are included in the model.

2.2.2 Chaos and high energy single pulse

From the previous section, multi-pulsing is observed as the pump increases. Thus the occurrence of multi-pulsing has to be delayed in order to obtain higher energy single pulses. We observe that the filter loss contributes for multi-pulsing. Intuitively, a wider filter bandwidth might delay off multi-pulsing. However, other nonlinear dynamical phenomena such as periodic and chaotic states might occur as shown in the previous heuristic model. In the following section, we will study whether a higher energy pulse can be obtained with a wider filter bandwidth.

Fig. 2-6(a) shows one example of gain and loss of the mode-locked pulse when $\delta_f = 0.11$. Other values of the bandwidth δ_f will be studied later. Before the black dots reach the multi-pulsing threshold, we observe that as the pump increases a mode-locked pulse could not be formed. In the original heuristic model, a solution is determined by the intersection of the gain and loss curve, although the solution might not be stable. In the extended model, we determine the solutions with simulation. Therefore we can no longer find a solution that is not stable. To study the states that do not converge, we keep the last 100 values of the pulse energy in the last 100 roundtrips if the pulse does not converge. The pulse energy as a function of E_{sat} is shown in Fig. 2-6(b), and if the pulse does not converge, we plot the last 100 values for the corresponding E_{sat} . Periodic state is found when E_{sat} is increased to 0.803. We

observe that the pulse energy is switching between two values until the E_{sat} is increased to 0.816, where the pulse experiences a chaotic state as positive Lyapunov exponents are found [see Appendix G]. After the periodic and chaotic regions when E_{sat} varies from 0.803 to 0.959, a high energy single pulse is found.

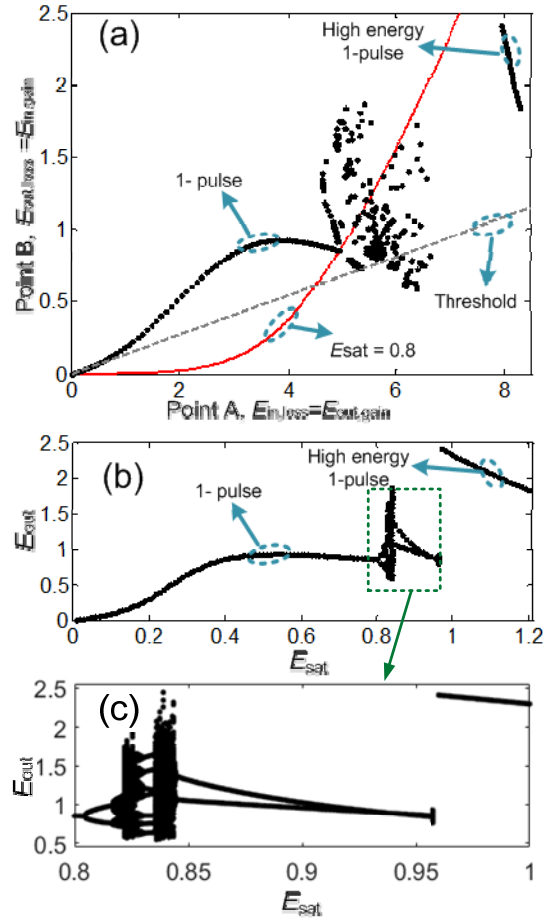


Fig. 2-6. (a) The gain and loss map in the laser cavity for $\delta_f = 0.11$. (b) The output energy of the filter E_{out} versus E_{sat} . (c) Details of the periodic and chaotic region in (b). The higher energy single pulse is obtained after periodic and chaos states.

Hence in our model, different states such as periodic states, chaotic states, and high energy single pulse state can be observed. Periodic and chaotic states are common phenomena in a nonlinear dynamical system like a mode-locked laser. We

note that the high energy single pulse state is obtained without any special designed SA transmission, as suggested in [49, 71].

We first discuss the periodic and chaotic states. We have observed that it is likely the multi-pulsing threshold is higher than the periodic and chaotic threshold in most cases in the previous heuristic model [49, 71]. Here in our extended heuristic model, although it is not possible to predict the threshold of chaos and periodic states without simulation, we can change or delay the multi-pulsing threshold to see its impact on the chaos or periodic states.

The multi-pulsing threshold is determined by the small signal loss. The transmission seen by the small signal is determined by the linear cavity loss, e.g. output coupler, and unsaturated loss l_0 of SA. From Eq. 2-8, we can estimate the transmission seen by the small signal from SA by setting $P(\tau) \sim 0$. Then $T_{SA} \approx (1-l_0)$. The total transmission seen by the small signal is $T_{loss} \times (1-l_0)$, where T_{loss} is the transmission of the linear loss in the cavity on the small signal.

Thus, if we vary the value of l_0 , the small signal loss will vary and the multi-pulsing threshold will also be changed. Fig. 2-7(a) shows the gain and loss of the laser cavity when $\delta_f = 0.08$ while the unsaturated loss l_0 is increased to 0.96 from its original value of 0.85 in Fig. 2-4. Comparing with Fig. 2-4, we find that as multi-pulsing is put off, the periodic and chaotic states are found before the black dots hit the gray dashed line. Another comparison can also be done by decreasing the unsaturated value of SA. Fig. 2-7(b) shows the gain and loss in a cavity when $\delta_f = 0.11$ while the unsaturated loss l_0 is decreased to 0.7 from 0.85. This time, the multi-pulsing threshold can be reached earlier. Instead of periodic and chaotic states in Fig.

2-6, we observed multi-pulsing generation as the pump is increased. Inferred from Fig. 2-7, periodic and chaotic states and multi-pulsing are all theoretically exist in laser systems. Which effect will occur first when the pump power increase depends of the respective thresholds. Starting from a single pulse state, if the thresholds of periodic and chaotic are smaller than that of multi-pulsing, periodic and chaotic states would be observed when the pump is increased [84, 85]. However, there are also laser systems in which the multi-pulsing state is reached without going through the periodic and chaotic states [81-83].

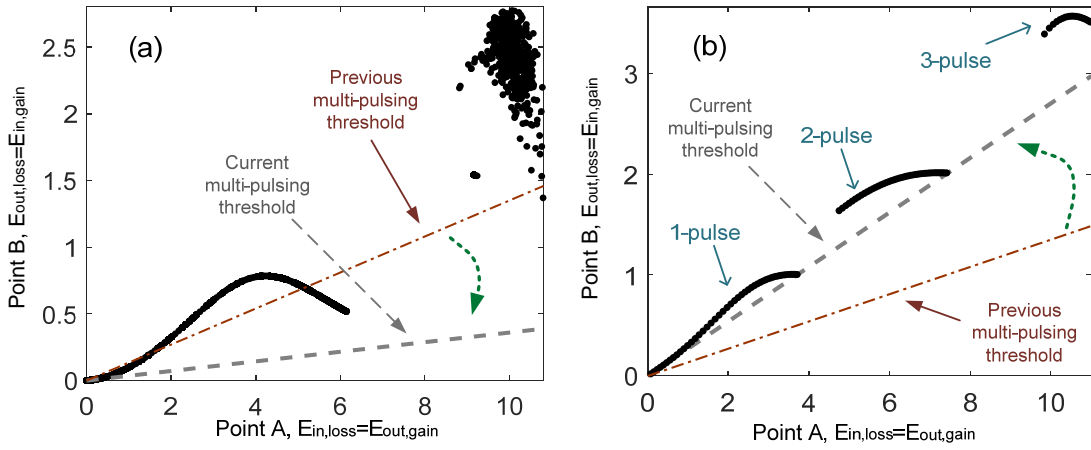


Fig. 2-7. The gain and loss map in the laser cavity for (a) $\delta_f = 0.08$ and $l_0 = 0.96$, (b) $\delta_f = 0.11$ and $l_0 = 0.7$. Gray dashed line represents the current multi-pulsing threshold, while the brown dash-dot line represents the previous multi-pulsing threshold. Other parameters are same.

Next, we will study the high energy single pulse state. As pulse shaping effects are included, we monitor the pulse profiles in both the time and frequency domain in the whole cavity. We compare the pulse evolution inside the laser cavity of both the lower and higher energy single pulse. Figs. 2-8(a) and (b) show the evolutions of the lower energy pulse in the laser cavity when $E_{sat} = 0.8$ in the time and frequency

domain, respectively. Fig. 2-8(a) shows the peak power of the pulse increases monotonically in the gain fiber, and Fig. 2-9(a) shows that the pulse bandwidth increases monotonically in the gain fiber as well. The pulse bandwidth is decreased after passing through SA and filter. Figs. 2-8(c) and (d) show the evolution of a high energy single pulse in the cavity when $E_{\text{sat}} = 1$. We observed that the pulse spectrum in the gain fiber evolves to its maximum bandwidth and subsequently begins to narrow as shown in Fig. 2-8(d) and in Fig. 2-9(b). The pulse bandwidth at the output of gain fiber is 1.03. To the lower energy pulse, its bandwidth at the output of gain fiber is 4.15. Hence the pulse evolution in the gain fiber can produce a much narrower pulse bandwidth, and significantly decrease the filter loss. Consequently, the pulse evolution contributes to a high energy single pulse.

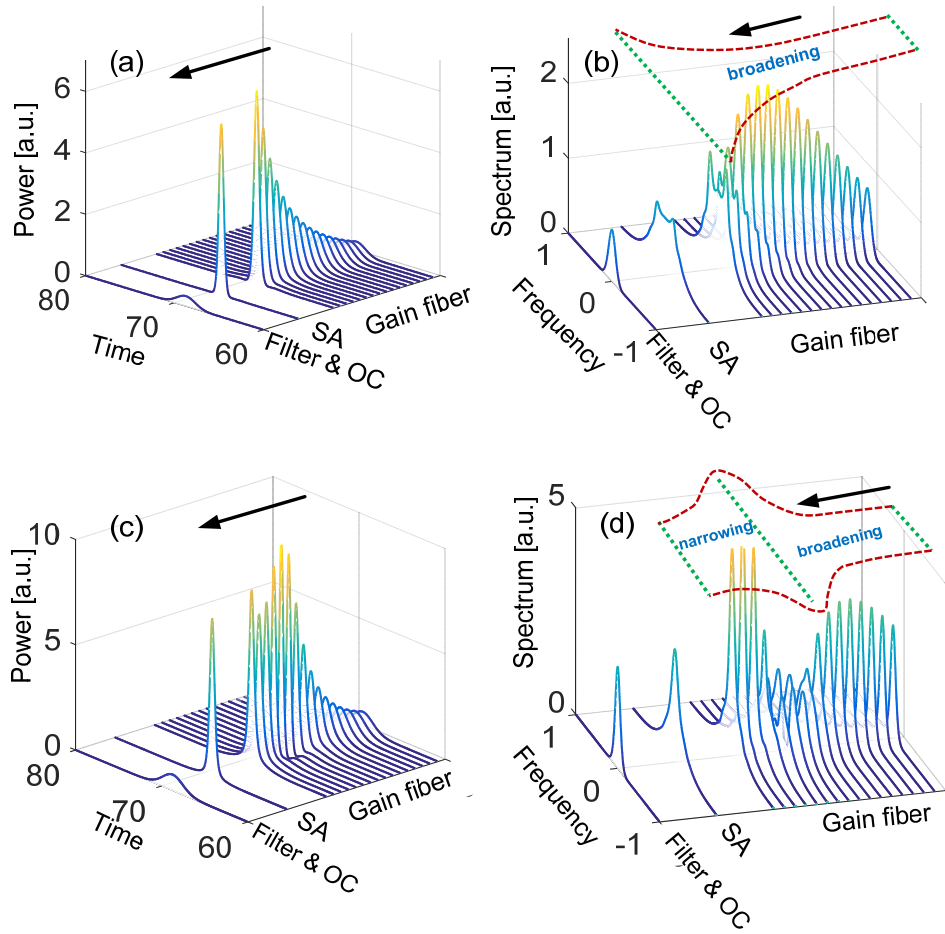


Fig. 2-8. The evolutions of (a), (c) pulse temporal and (b), (d) spectral waveforms in the laser cavity with (a), (b) $E_{\text{sat}} = 0.8$, and (c), (d) $E_{\text{sat}} = 1.0$, where $\delta_f = 0.11$. The black arrows show the direction of pulse propagation.

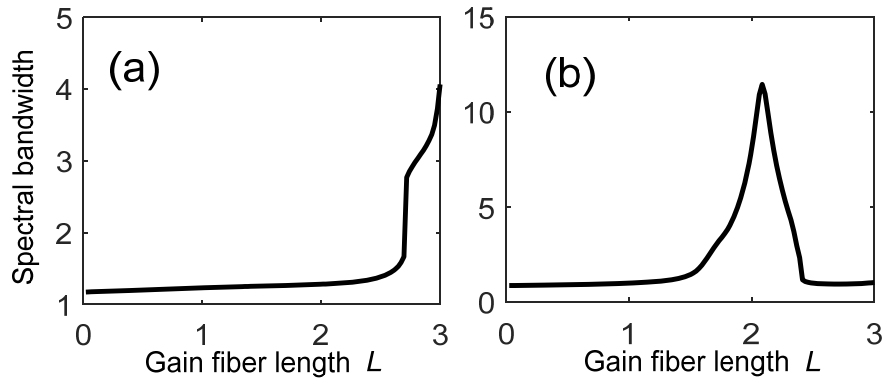


Fig. 2-9. The evolutions of the pulse spectral bandwidth in the gain fiber when (a) $E_{\text{sat}} = 0.8$, and (b) $E_{\text{sat}} = 1.0$, where $\delta\gamma=0.11$.

Then the question arises on the reason of pulse evolution in the gain fiber. Based on the theoretical works on the nonlinear Schrodinger equation with gain term, the pulse evolution is significantly influenced by the strength of the gain [86-88]. As E_{sat} increases, the increase in energy will create a new pulse within the existing pulse in the time domain [87, 88], as shown in Fig. 2-10. The newly created pulse and the existing pulse have different phases during the propagation. Hence the two pulses interfere and the overall pulse profile varies, leading to the evolution with both spectral broadening and narrowing in the gain fiber [87, 88].

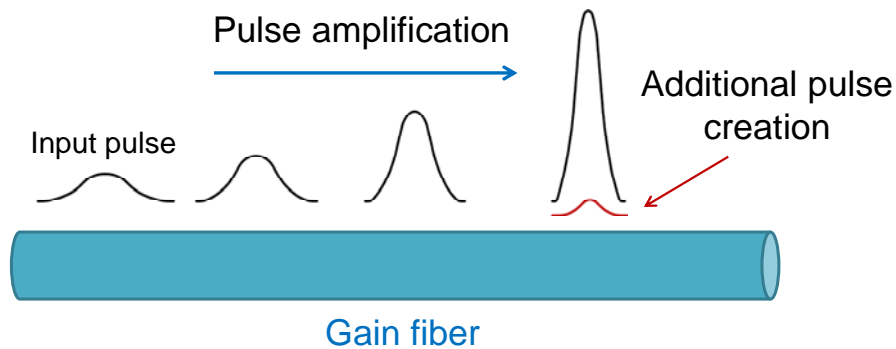


Fig. 2-10. Additional pulse creation during the pulse amplification in the gain fiber.

We define the length that a pulse performs a complete spectral broadening and narrowing process as the breathing period, as showed in Fig. 2-8 (d). If the length of a gain fiber is much shorter than the pulse's breathing period, we will only observe spectral broadening, as showed in Fig. 2-8 (b). As the pump increases, the peak of the pulse increases and the pulse width decreases and hence the breathing period of the pulse decreases [87, 88]. If the breathing period is shorter than, or comparable to, the length of a gain fiber, the pulse spectrum will evolve to its maximum bandwidth and then become narrow, as we showed in Figs. 2-8(c) and (d).

Fig. 2-11 shows the output state of the fiber laser as a function of filter bandwidth and E_{sat} . When a smaller pump is used, only one pulse is output from the cavity, shown as Region I, (black inverted triangles). When the filter bandwidth is narrow, i.e. $\delta_f < 0.09$, multi-pulsing (red stars, Region II) will occur when the pump is increased. In these cases, we did not observe periodic and chaotic states as before. If the filter bandwidth δ_f is increased, $\delta_f \geq 0.09$, periodic and chaotic states occur as shown in Region III (red solid circles) when E_{sat} is increased. If E_{sat} is further increased, a high-energy single pulse is observed. From Fig. 2-11, with a narrow bandwidth filter, we found the laser dynamics is dominantly controlled by the gain loss dynamics in the cavity which causes multi-pulsing. Different nonlinear dynamics are observed if the bandwidth of the filter is large. In such a case, the pulse evolution in the gain fiber plays an important role and we know the laser cavity can attain a high-energy single pulse output.

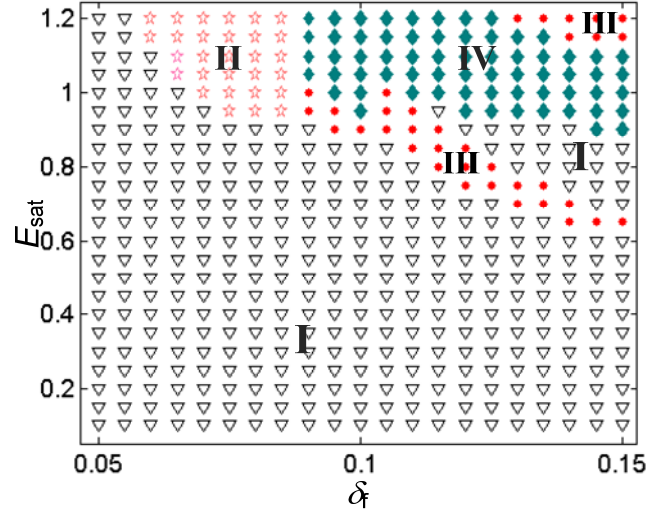


Fig. 2-11. Output states of the fiber laser as the function of filter bandwidth. Region I: single pulse (black triangle); Region II: 2-pulse state (red star); Region III: periodic and chaotic states (red dot); Region IV: high energy single pulse state (blue diamond)

On first glance, the high energy single pulse state may be utilized to obtain a high power ultra-fast laser source. However, in the following section, we will show that the high energy single pulse is unstable in the presence of high order dispersion.

2.2.3 Impact of third order dispersion

Recall that the high energy single pulse is obtained because of a new pulse is created in the gain fiber as mentioned above. In other words, multi-pulsing has occurred but the new pulse grows up within the existing pulse during the propagation in gain fiber. Apparently, the two pulses move with the same speed [87, 88], thus one does not recognize that it is a multi-pulsing state. Guided from the theoretical works in Refs. [87-89], we know the constituent pulses in the high energy single pulse do not have to move with the same speed. Higher order dispersion, e.g. third order dispersion (TOD) can induce different speeds in the constituent pulses and cause the

higher energy single pulse to split. Hence TOD might also be one of the factors of multi-pulsing and prevents the formation of a high energy ultra-fast pulse. In this section, we will study the impact of TOD.

We first study whether the higher energy single pulse is consisted of multiple pulses. To do this, we perform artificial simulations to investigate the nature of the high energy single pulse. We use the high energy pulse obtained without TOD as the initial condition and artificially turn on the TOD by setting $D_3 = 0.05$. The evolutions of the pulse temporal and spectral profiles in the first roundtrip are shown in Figs. 2-12(a) and (b), respectively. We observe that the pulse initially undergoes a temporal compression and spectral broadening. One can note a resonated narrow band exists at normal dispersion region as shown in Fig. 2-12(b). The resonance sideband is induced by the phase matching between the solitary wave, i.e. the high energy pulse, and the dispersive wave [89-91]. When the solitary pulse circulates in the cavity, it will shed energy, also called dispersive wave, soliton pulse shaping in the cavity [89]. To the dispersion relation $\approx \frac{\beta_2 \omega^2}{2} + \frac{\beta_3 \omega^3}{6}$, where k is the wave number, we know for a nonzero β_3 , there exists a frequency $\omega_r = -3\beta_2/\beta_3$ near which $k(\omega_r) = k(0) \approx 0$, i.e. the phase matching condition is satisfied [89-91]. In the time domain, a radiation is found near the main pulse (high energy pulse) as shown in Fig. 2-12(a). The initial emission of dispersive radiation is primarily from the high energy single pulse that possesses its broadest bandwidth during the propagation in the gain fiber ($L \sim 2.25$) and thus has the maximum overlap with the resonated band.

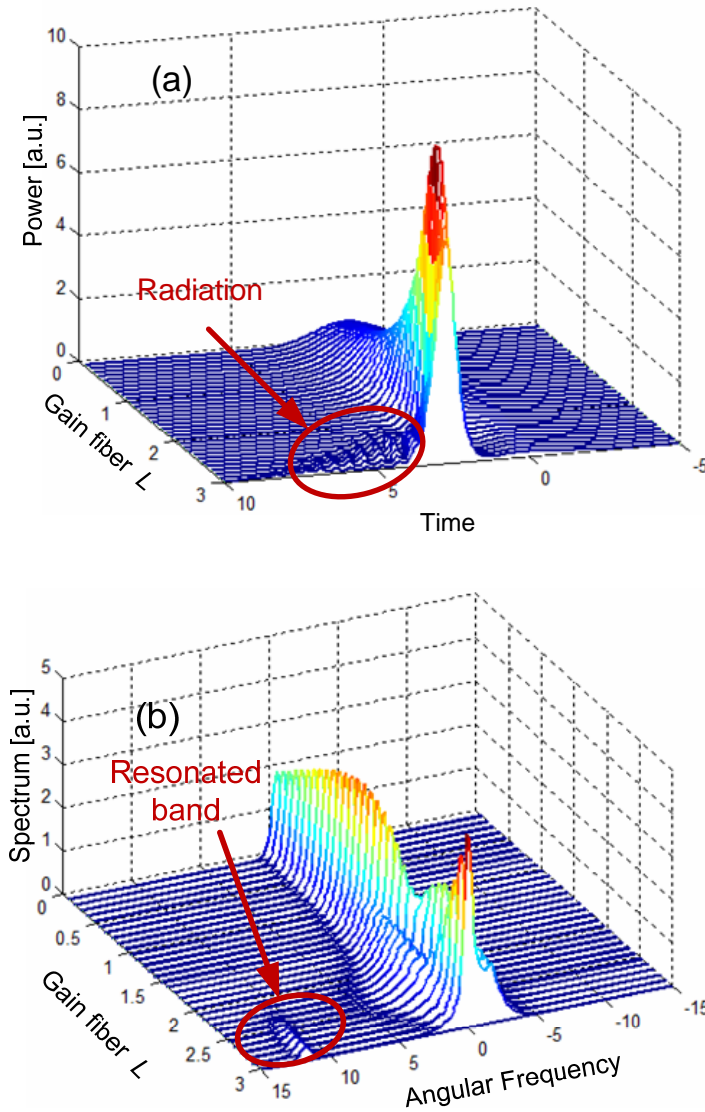


Fig. 2-12. The temporal (a) and spectral (b) evolution in the gain fiber of the high-energy single pulse, when TOD is turned on.

We also give the details of the pulse evolution at different distances L in the gain fiber, and in order to observe the time and frequency characters of these pulses simultaneously, the spectrograms are shown in Fig. 2-13. After the propagation in the gain fiber ($L = 3$), we observe a smaller amplitude temporal pedestal (at a temporal position of $\tau \sim 7.3$) which corresponds to the radiation caused by TOD, since its

central frequency locates at the resonated sideband as shown in Fig. 2-13(d). It shows that the radiation is emitted during the propagation in the gain fiber, and it separates from the main pulse in the positive time direction. The lower amplitude pulse at the edge of the main pulse is also observed.

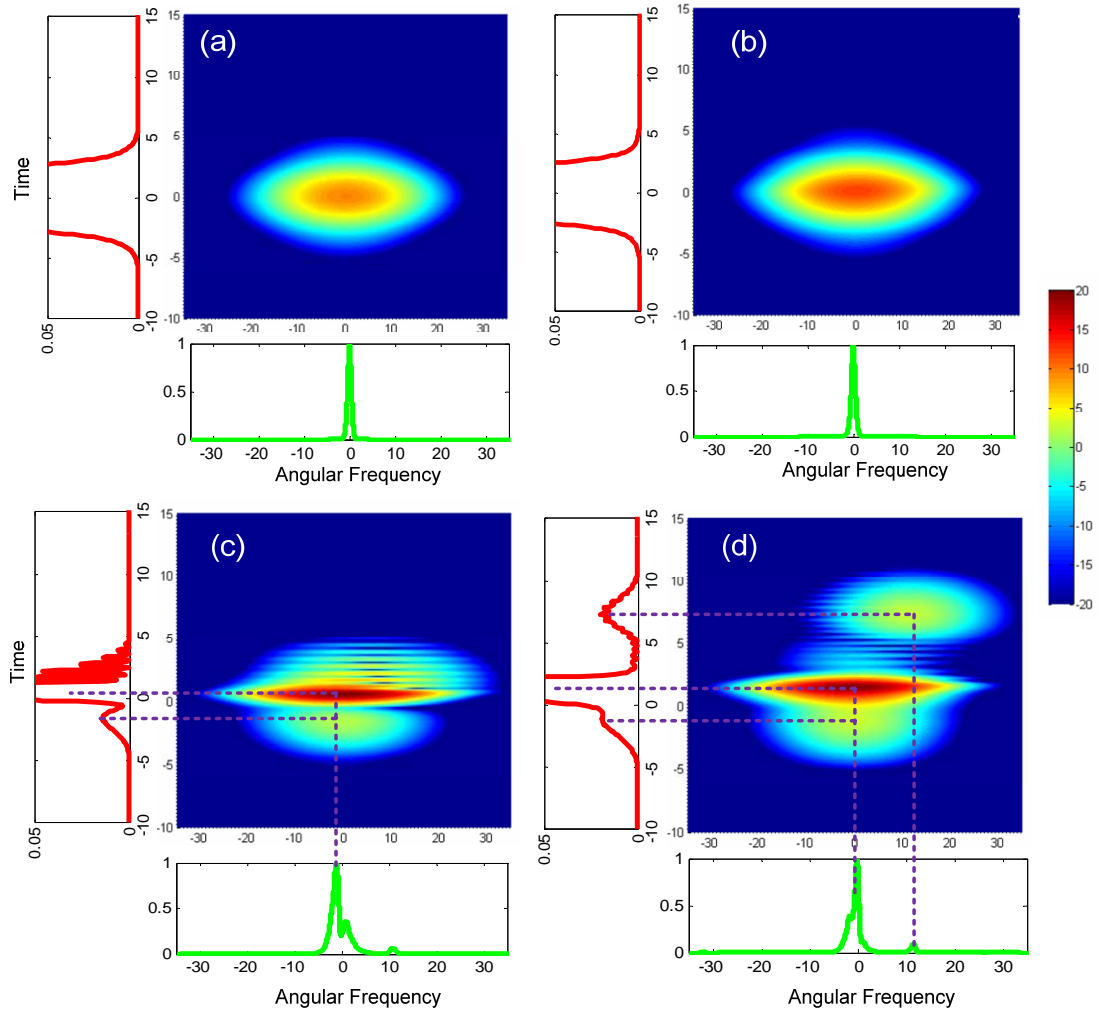


Fig. 2-13. Spectrogram of the pulse in gain fiber at (a) $L = 0$, (b) $L = 0.75$, (c) $L = 2.25$ and (d) $L = 3$.

Theoretical work [89] shows that the TOD induces different speeds to the constituent pulses resulting in pulse splitting. The time delays between the constituent pulses increases as the value of TOD increases. We believe this phenomenon also hold in the laser cavity. Hence we also compare the impact of different values of TOD on the high energy single pulse seed. The pulse profiles at the output of gain fiber, SA and filter are shown in Fig. 2-14. Fig. 2-14(a) shows the pulse profiles when TOD equals to 0.01. The third order dispersion length T_0^3/D_3 is more than 100 times longer than the length of the gain fiber, where T_0 is the pulse width of the mode-locked pulse that is going into the gain fiber. In such a case, the impact of TOD is not obvious as shown in Fig. 2-14(a). We cannot see an obvious radiation and the delay between the constituent pulses. For a higher value of TOD such as D_3 equals 0.03, 0.05 and 0.07, the TOD length is around 40, 30 and 20 times of the gain fiber length, respectively. The impact of TOD is more obvious. Fig. 2-14(b) shows that when $D_3 = 0.03$, a stronger radiation can be seen after the gain fiber, and we can also note there is a smaller pulse trying to move away from the main pulse. If the value of TOD is further increased, a split pulse can be observed after the gain fiber as shown in Figs. 2-14(c) and (d). The time delay between the pulses is larger if a higher value of TOD is used.

As a smaller value of TOD induces a smaller time delay between the two constituent pulses, only a small portion of the smaller pulse is separated from the larger pulse after the propagation in gain fiber [see Fig. 2-14(b)]. After the gain fiber, the SA will attenuate the separated part of the smaller pulse as shown by the green dash-dotted line in Fig. 2-14(b) which hinders the separation between the two pulses.

However, from Figs. 2-14(c) and (d), the hindrance from SA will not be sufficient to prevent pulse separation if the two pulses have been largely or almost completely separated after the propagation in gain fiber. After the spectral filter, the pulse spectrum is decreased and the pulse width increase. The filter attenuates the resonated sideband since it locates far from the central frequency of the pulse, and hence the radiation (at $\sim \tau = 7$) becomes weak.

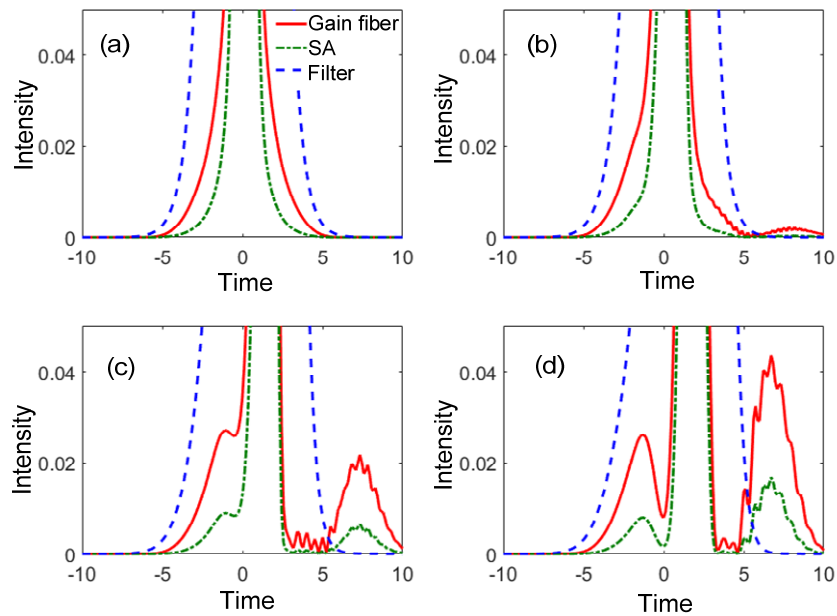


Fig. 2-14. Pulse characters after gain fiber, SA and spectral filter in the first roundtrip when TOD is (a) $D_3 = 0.01$, (b) $D_3 = 0.03$, (c) $D_3 = 0.05$ and (d) $D_3 = 0.07$.

From the study of the pulse evolution in the first roundtrip we learnt that a small value of TOD induces a weak walk-off between the constituent pulses, and the SA might even hinder the pulse splitting for weak TOD effect. Thus, in subsequent roundtrips we might not see multiple pulses lasing in the cavity. Fig. 2-15 shows the pulse profiles as the function roundtrip for different values of TOD. For small TOD values, e.g. $D_3 = 0.01$ or 0.03 , only one pulse is observed in the cavity. Figs. 2-15(c)

and (d) show the pulse profiles when D_3 is increased to 0.05 and 0.07, respectively. At first, the pulse shows both the radiation and a small pulse splitting from the main pulse. After several roundtrips, the radiation is attenuated by the filter, while the small pulse splits from the main pulse is amplified to be a second pulse. Finally, two identical pulses are mode-locked in the cavity.

Based on the results in Figs. 2-11 to 2-15, we confirmed that the high energy single pulse actually consists of two pulses. Tuning on sufficiently large TOD in the laser cavity will split the high energy mode-locked pulse into its two constituent pulses.

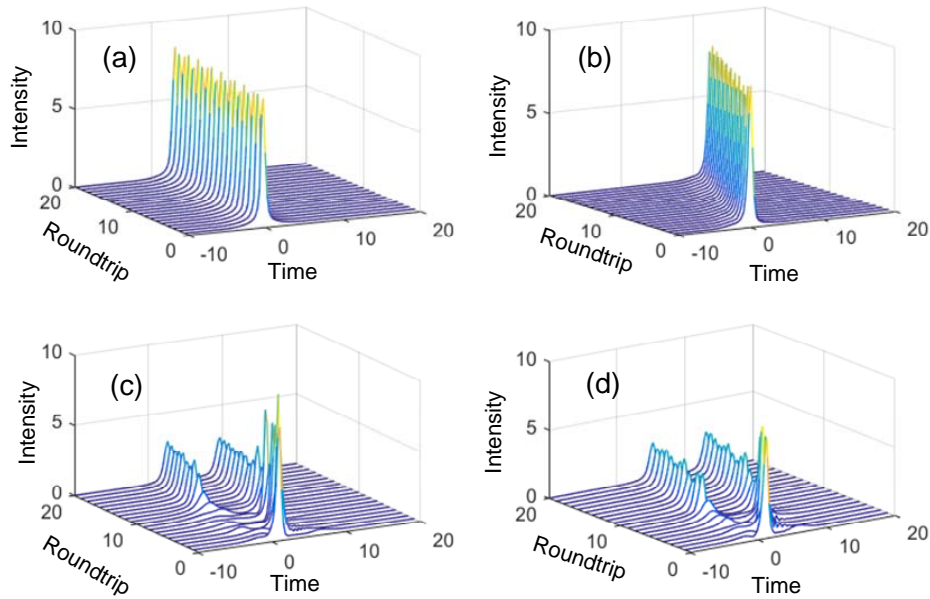


Fig. 2-15. Pulse profiles after gain fiber as the function of roundtrip when TOD is (a) $D_3 = 0.01$, (b) $D_3 = 0.03$, (c) $D_3 = 0.05$ and (d) $D_3 = 0.07$.

To study the impact of TOD in the laser dynamics, we also repeated the simulations in Fig. 2-6 with nonzero values of TOD. Figs. 2-16(a) and (b) show the E_{out} as the function of E_{sat} with $D_3 = 0.005$ and 0.05, respectively. For $D_3 = 0.005$, a

high-energy single pulse could be obtained, but for $D_3 = 0.05$, two pulses are observed. We would like to emphasize that, comparing with the previous heuristic model, a new mechanism of multi-pulsing is found. The new pulse is obtained from the existing high energy pulse during the amplification in the gain fiber. Higher order effects such as TOD can produce multiple pulses in the cavity through pulse splitting. Since this mechanism of multi-pulsing comes from the pulse shaping effects, it cannot be observed in the original heuristic model. In the former model, multi-pulsing is induced from the growth of the background noise. In the extended model, besides the growth of background noise, a new pulse can be created by the soliton mechanism inherent in the interaction of anomalous dispersion and self-phase modulation (SPM). The additional pulse split by higher order effects such as TOD will be observed.

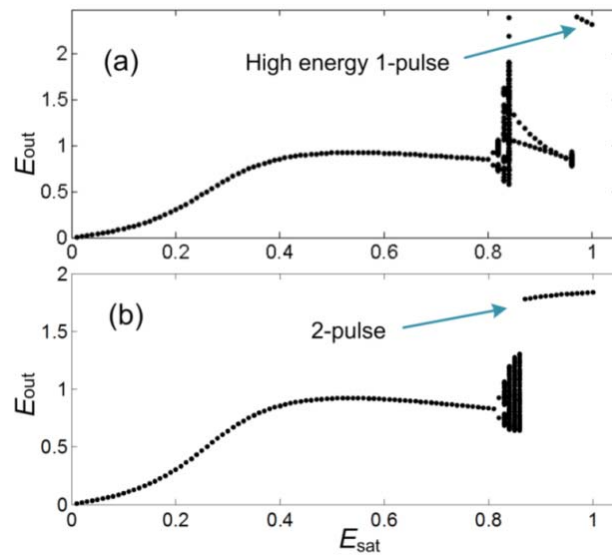


Fig. 2-16. The impact of TOD on the laser dynamics. $E_{loss,out}$ as the function of E_{sat} when (a) $D_3 = 0.005$, and (b) $D_3 = 0.05$.

Up to now, various nonlinear dynamical states such as periodic, chaotic, multi-

pulsing, and high energy single pulse states are observed in our model. The high energy single pulse state is attractive in applications. However, the presence of pulse splitting due to higher order effects such as TOD have to be suppressed. Otherwise, the splitting of multiple pulses in the cavity prevents the formation of a high energy single pulse. From the extended heuristic model we show that the spectral filter has a significant impact on the mode-locking dynamics of a fiber laser. We conclude that a wider filter bandwidth and a smaller value of TOD will help to produce higher energy single pulse output.

Summary

We extended a heuristic geometrical model by including the pulse shaping effects. Based on the extended model, we investigated the impact of spectral filtering in a laser cavity. The pulse shaping effects include dispersion, SPM, and spectral filtering. The spectral filter introduces frequency dependent loss, thus multi-pulsing will be triggered even if a monotonic transmission of SA is used.

Both the occurrence of the multi-pulsing and periodic and chaotic states prevents the formation of high energy single pulse laser source. We observed that a new pulse grown from noise is more likely to occur if the filter bandwidth is narrow. On these cases, periodic and chaotic states will not be observed as the pump power increases.

A high energy single pulse state was also observed and its formation is dominated by the interaction of anomalous dispersion and SPM. The high energy single pulse is potential to offer an ultra-fast laser source, but it should be noted that TOD could induce the splitting of high energy single pulse.

Chapter 3

Dual-channel Mode- locked Fiber Lasers

In Chapter 2, the proposed heuristic model is used to investigate the mode-locking in a single-channel laser cavity. There are also laser sources that emit mode-locked pulses with different central frequencies simultaneously in one laser cavity. They are called multi-channel mode-locked lasers, and are attractive for the applications on terahertz generation and optical sensors. Multi-channel mode-locked lasers exhibit rich dynamics. In this Chapter, we apply the proposed heuristic model to investigate

the mode-locking in a multi-channel laser cavity. We start with the simplest case, which is a dual-channel mode-locking cavity.

3.1 Introduction

Dual-channel output can be realized by inserting a dual-channel filter in the cavity to select the lasing wavelength as observed in the experiments [56, 57]. Such a laser source can output various mode-locked states which are determined by the profile of a dual-channel filter. When the pump is weak, one mode-locked pulse is obtained in either of the two channels, while the light in the other channel is at the noise level. As the pump power increases, different cases can happen. For a given filter (channel) bandwidth, if the two channels locate near to each other in the frequency domain, a dual-channel simultaneously mode-locked (DSML) state can be obtained [59, 61-64, 92-94]. Such an output is believed to be potential laser sources for terahertz generation and optical sensors [56, 58-61].

A DSML state means each channel achieves mode-locked and the phases of the pulses in different channels are also locked. In such a state, when observing at one position in the laser cavity, e.g. output coupler, the pulses in different channels are combined in the time domain, despite their different central frequencies which should have caused the walk-off between the pulses [59, 61-64, 92-94]. The energies in different channels are not always identical in a DSML state [62, 63, 92-94]. For example, for given channel bandwidth, the energies in channels are different if the channel separation in the frequency domain is increased [92, 93].

If the two channels are located quite far away in the frequency domain, one may not get a DSML state. Instead, when there is a pulse in one channel, as the pump is

further increased multi-pulsing is triggered. The new pulse can grow up in either channel. If they are in the same channel, one can obtain a state that one channel has two pulses while the other channel is at the noise level. If the two pulses are in different channels, a dual-channel lasing is obtained but the pulses are lasing independently in their respective channel frequencies. The two pulses cannot see each other except the time that they cross over in the time domain, as they have different group velocities [61].

In this chapter, we will delineate the mode-locked states and the dynamics in a dual-channel laser cavity. We will study how the DSML state is built up. The balances inside the DSML state are also discussed. We would also investigate why no DSML is obtained if the channels locate quite far apart.

3.2 Theoretical model

Laser modeling is helpful for the understanding of the working mechanism of lasers. There are distributed models used to study the multi-(dual-) channel mode-locked fiber lasers. For example, the Swift-Hohenberg equation has been used to study the dual-channel mode-locking [62, 93, 94]. Edward D. Farnum et al. proposed a set of coupled equations, where each equation describes the light in one channel, to study multi-(dual-) channel laser cavity [59, 63, 64]. Different mode-locked states such as multi-(dual-) channel simultaneously or independently mode-locked state are observed in these models. These models showed which set of parameters can provide the corresponding mode-locked states.

In our work, we pay more attention to the laser dynamics, not just parameter sweeping. Thus we would like to know the interplay of various physical effects inside

a DSML state, and the discrete actions of different laser elements, e.g. SA and filter. The discrete actions are more easily studied with discrete models. As a result, a discrete heuristic model is preferred to be utilized in our work. The heuristic model that was used to study single-channel mode-locking can be adopted to study the multi-(dual-) channel cavity by modifying the single-channel filter model to a multi-(dual-) channel filter model. This can be done to either the previous or the extended heuristic model. Hence one question has to be asked is whether we should still keep the pulse shaping effects.

We observe that the pulse shaping effects are important to a multi-(dual-) channel laser cavity. As the pulses in different channels have different central frequencies, the group velocities are supposed to be different due to the dispersion. Throwing away the dispersion would lose the walk-off effect between the pulses in different channels. In addition, if a homogeneous gain medium, e.g. EDFA, is used, the gain competition might make one channel absorb all the cavity energy and thus prevent achieving a multi-(dual-) channel lasing [63]. The Kerr nonlinearity induces the four-wave mixing (FWM) process and helps to transfer energy to different channels. Thus the nonlinearity helps to overcome the gain competition and contribute to a multi-channel lasing. For these reasons, the pulse shaping effects are still retained in our model.

The schematic of the fiber laser cavity is shown in Fig. 3-1. The discrete gain is followed by a passive fiber that provides dispersion and nonlinearity in the cavity. The SA gives the intensity discrimination for mode-locking. The dual-channel filter

limits the spectral bandwidth of the light in each channel. An output coupler is located right after the spectral filter.

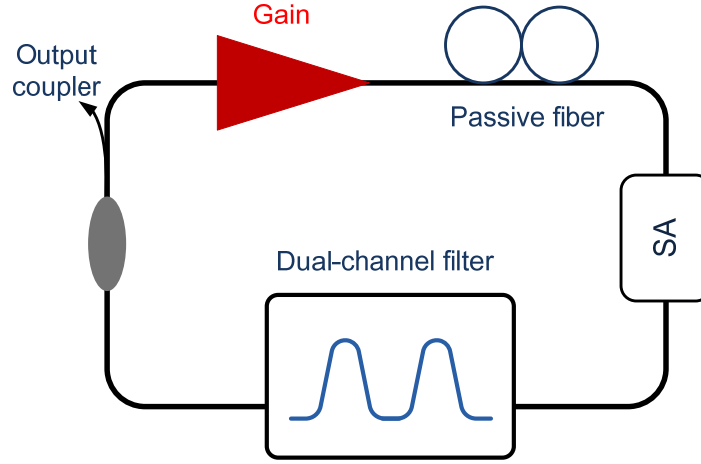


Fig. 3-1. Schematic of a dual-channel mode-locked fiber laser cavity.

The gain element which provides a saturating gain is modeled as

$$g(z) = \frac{g_0}{1 + \int |A(z,t)|^2 dt / E_s}, \quad (3-1)$$

where g_0 is the small signal gain coefficient and E_s is the saturation energy. The increase of cavity energy could be realized by increasing E_s . Similar as we did in the last Chapter, the white Gaussian noise (zero mean and a variance $\sim 10^{-9}$) is added after the gain element to model the amplifier noise.

For the pulse evolution in a fiber in a laser cavity, the pulse behavior is governed by the NLS

$$\frac{\partial A}{\partial z} = -\frac{i}{2}\beta_2 \frac{\partial^2 A}{\partial t^2} + i\gamma |A|^2 A, \quad (3-2)$$

where β_2 , and γ are second order dispersion and nonlinear coefficients, respectively.

The SA is modeled by a power transfer function

$$T_{SA}(t) = 1 - \frac{l_0}{1 + |A(t)|^2 / P_{\text{sat}}}. \quad (3-3)$$

In a dual-channel laser cavity, two filters are required. The central frequencies are $\pm \Omega_{\text{shift}}$, which corresponds to a separation of $2\Omega_{\text{shift}}$ in our system. The field transmittance of a dual-channel filter is modeled as

$$H_f(\Omega) = \exp\left[-\frac{1}{2} \frac{(\Omega + \Omega_{\text{shift}})^2}{\Omega_{\text{band}}^2}\right] + \exp\left[-\frac{1}{2} \frac{(\Omega - \Omega_{\text{shift}})^2}{\Omega_{\text{band}}^2}\right], \quad (3-4)$$

where Ω_{band} is the filter bandwidth. The amplitude is normalized by its maximums, $H_f(\Omega) = H_f(\Omega) / \text{Max}[H_f(\Omega)]$.

The equations above could be normalized by using the following transformation.

$$U = A / \sqrt{P_{\text{sat}}}, \quad \xi = z / L_{\text{cavity}}, \quad T = \frac{t}{\sqrt{|\beta_2|} L_{\text{cavity}}}. \quad (3-5)$$

Then the discrete gain becomes

$$g = \frac{g_0}{1 + \int |U(\xi, \tau)|^2 dT / E_{\text{sat}}}, \quad (3-6)$$

where $E_{\text{sat}} = E_s / [P_{\text{sat}} (|\beta_2| L_{\text{cavity}})^{0.5}]$. The equation for the passive fiber is

$$\frac{\partial U}{\partial \xi} = \frac{iD}{2} \frac{\partial^2 U}{\partial \tau^2} + i\Gamma |U|^2 U, \quad (3-7)$$

where $D = 1$ in anomalous dispersion region, and $\Gamma = \gamma P_{\text{sat}} L_{\text{cavity}}$, where L_{cavity} is the length of the total cavity.

For SA and filter, the equations are

$$T_{SA} = 1 - \frac{l_0}{1 + U^2}, \quad (3-8)$$

$$H(\omega) = \exp\left[-\frac{1}{2} \left(\frac{\omega + \omega_{\text{shift}}}{\omega_{\text{band}}}\right)^2\right] + \exp\left[-\frac{1}{2} \left(\frac{\omega - \omega_{\text{shift}}}{\omega_{\text{band}}}\right)^2\right], \quad (3-9)$$

where ω is the normalized angle frequency and the filter bandwidth $\omega_{\text{band}} = \Omega_{\text{band}}(|\beta_2|L_{\text{cavity}})^{0.5}$. The channel separation is $\omega_{\text{sep}} = 2\omega_{\text{shift}}$.

Eqs. (3-6), (3-7), (3-8) and (3-9) comprehensively describe a dual-channel mode-locking fiber laser cavity. We do the simulation as the way we did in last Chapter with these equations. Based on the models, the discrete actions of each element and the laser dynamics can be studied.

3.3 Nonlinear dynamics

A single-channel mode-locked state can be obtained in either channel of the cavity, and both channels can get mode-locked if the pump is further increased. On one hand, the pulses in different channels can affect each other through the saturable gain if a homogeneous gain medium is used. On the other hand, the pulses in different channels sometimes can even lock their phases and produce a DSML state. Different effects such as dispersion, SPM, cross-phase modulation (XPM) and FWM all exist in our system. Thus the pulse interactions among different channels are complex and may induce a different laser dynamics when compared to the dynamics in a single-channel laser. In the following, the laser dynamics are investigated.

3.3.1 Building up of a DSML state

Starting from noise, a pulse can grow up in either one of the channels if the pump is increased, as in the examples shown in Fig. 3-2 ($\omega_{\text{sep}} = 2$ and $E_{\text{sat}} = 0.1$). A DSML state might be achieved if the pump is further increased. The mode-locked state can be determined by the spectral profile of a dual-channel filter. For a given channel bandwidth, the mode-locking is determined by the channel separation. We first set the

channel bandwidth as $\omega_{\text{band}} = 0.2$ which corresponds to a realistic filter bandwidth of ~ 118 GHz if other parameters are $\gamma = 1/\text{W}/\text{km}$, $\beta_2 = -20 \text{ ps}^2/\text{km}$ and $P_{\text{sat}} = 100 \text{ W}$, which are all typical values for laser cavities [59, 61-64, 92-94]. Other values of channel bandwidth have also been used to the study in the following.

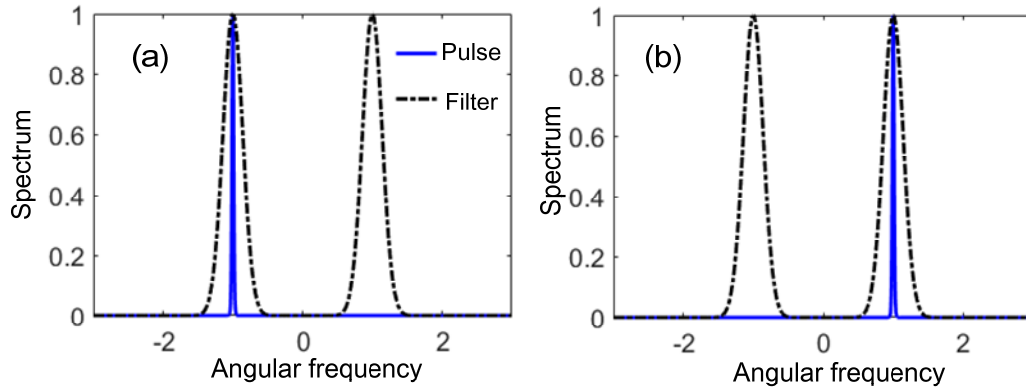


Fig. 3-2. The spectra of the mode-locked pulse in dual-channel mode-locking cavity when $E_{\text{sat}} = 0.1$. For a weak pump, only one channel achieves mode-locking. The mode-locked pulse could exist in either of the two channels.

To the single-channel mode-locked state in a dual-channel laser cavity, one may believe the pulse will absorb all the cavity energy as the pump is further increased since a homogeneous gain model is used in our laser system. However, as the pump is further increased, the light in the other channel is increased. The phases between the light in two channels might also be locked. This will be the case if the channel separation is small such that the cross-talk between channels is strong. The dual-channel filter can even be treated as a single-channel filter with two humps if the channel separation is too small. If that is the case, the pulse spectrum at one hump will easily leak to the other hump as the pump is increased. Both the energy and

phase relationships are transferred to the other channel (hump) and hence producing a DSML state. However, a DSML state can also be achieved if the channels are weakly overlapped, e.g. the filter in Fig. 3-2 where the power transmission of the filter is $\sim 10^{-11}$ around $\omega = 0$. Achieving a DSML state with this filter profile indicates that other effects help to produce the DSML state. In the following, the building up of a DSML state is studied.

In order to study the mechanisms that build up a DSML state, we use a single-channel mode-locked state (in left channel as an example) obtained with $E_{\text{sat}} = 0.5$ as the initial seed and increase the pump to $E_{\text{sat}} = 0.6$. We choose the filter in Fig. 3-2 ($\omega_{\text{band}} = 0.2$ and $\omega_{\text{sep}} = 2$) where the cross-talk of the two channels is weak. The transient from a single-channel mode-locked state to DSML state is shown in Fig. 3-3. Figs. 3-3(a) and (b) show the evolutions of the pulse profiles after the output coupler in the time domain during the transient in the right and left channel, respectively. Figs. 3-3(a), (b) and (c) show that a new pulse is growing in the right channel after ~ 500 roundtrips. Compared with Figs. 3-3(a) and (b), we note the temporal position of the growing pulse in the right channel is close to the temporal position of the original pulse in the left channel. Fig. 3-3(d) shows the combined temporal profiles of the pulses in the two channels during the transient. The combined pulse performs an obvious modulation on its temporal profile after ~ 500 roundtrips. The modulation depth increases as the energy of the pulse in the right channel is increased. Finally, a DSML state is observed as shown in Fig. 3-4.

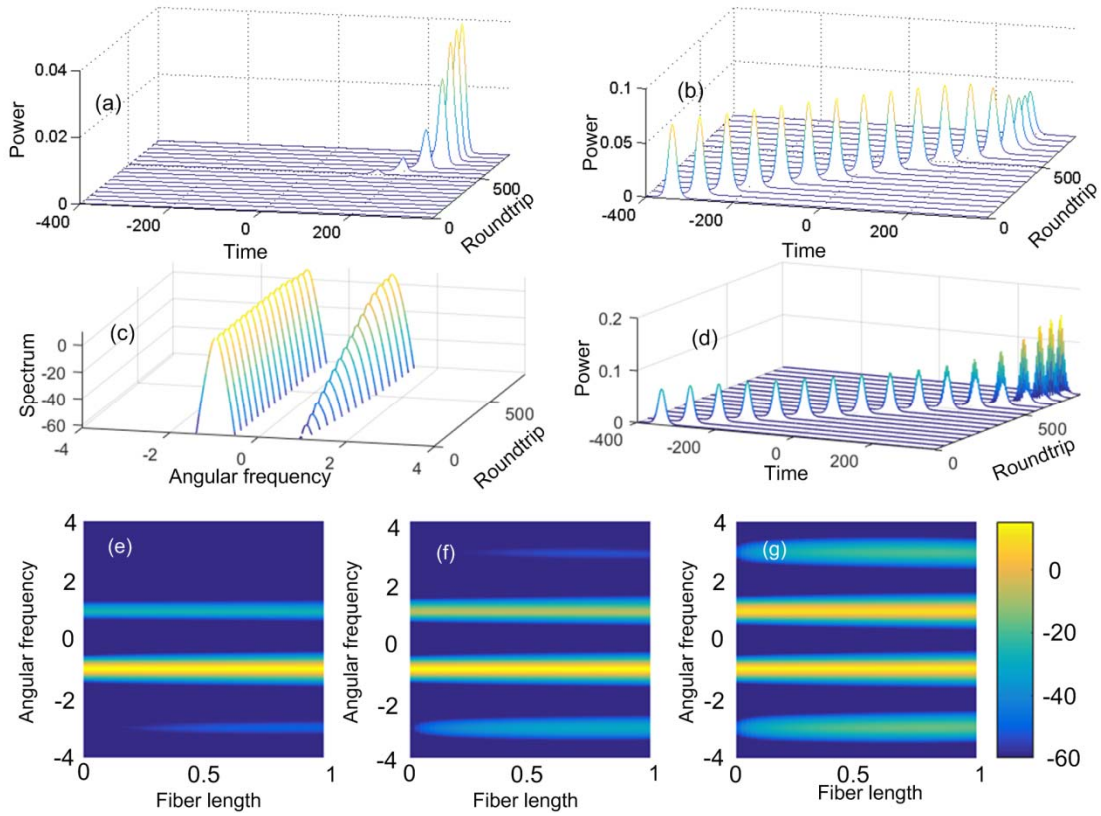


Fig. 3-3. The transient from a single-channel mode-locked state to a DSML state in a dual-channel laser cavity. The evolution of the pulse in the (a) right and (b) left channels in the time domain, and the evolution of combination of the two pulses in the (c) frequency and (d) time domain are given. The spectral evolution in the passive fiber at the (e) 300-th, (f) 500-th, and (g) 700-th roundtrip are shown.

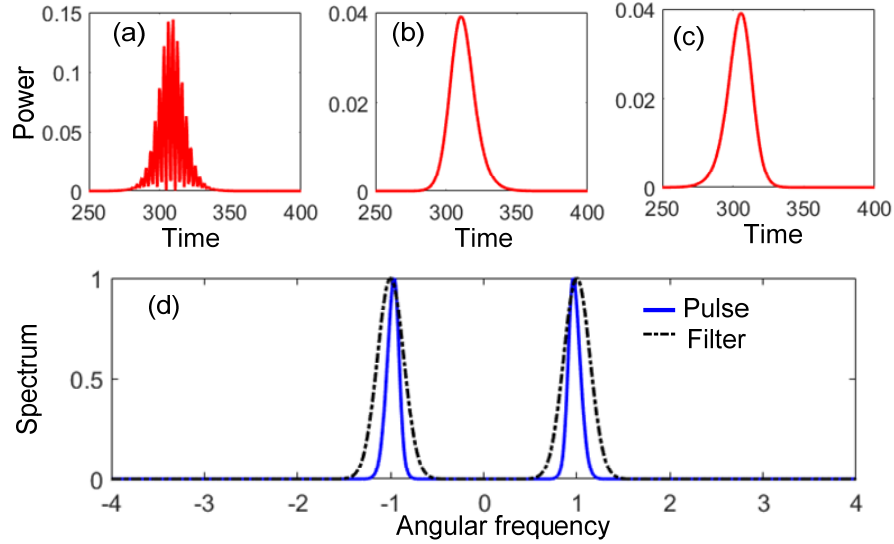


Fig. 3-4. (a) DSML pulse which consists of two mode locked pulses in (b) left and (c) right channel. (d) The spectrum after the filter of the mode-locked pulse. Both the spectrum and spectral filter are normalized by its maximum.

As the pulse shaping effects are included in the model, nonlinear processes such as SPM, XPM and FWM can all affect the pulses during the propagation in the passive fiber. Figs. 3-3(e), (f) and (g) show the examples of the spectral evolution in the passive fiber at the 300-th, 500-th and 700-th roundtrip. We observe that the FWM process exists in the system and the light energy can be transferred to different frequencies. In the passive fiber, to the light in different channels that are temporally overlapped, FWM and XPM can introduce a phase relation between them, and FWM can even transfer energy among them [76, 95]. Thus the new pulse in the right channel grows up at a temporal position near the original pulse in the left channel [see in Figs. 3-3(a) and (b)] and the phase relation between the two channels produces the temporal modulations on the combined pulse profiles [see in Fig. 3-3(d)].

The energy transfer through FWM can help to overcome gain competition.

Besides, we note SA can also help the built up of a DSML state. During the transient, when the combined pulse passes through the SA, it gives higher loss to the stronger pulse in the left channel and smaller loss to the weak pulse in the right channel. This equivalently enhances the weak pulse. The reason is the combined pulse performs a modulation on its temporal profile during the transient, as shown in Fig. 3-3(d). SA gives an intensity (pulse shape) dependent loss that is larger when the light intensity is weak and smaller when the light intensity is strong. Consequently, during the transient, the modulation depth on the combined pulse is enhanced when the combined pulse passes through the SA, as shown in Fig. 3-5. Such effect on the combined pulse during the transient can make the energies of the two channels closer.

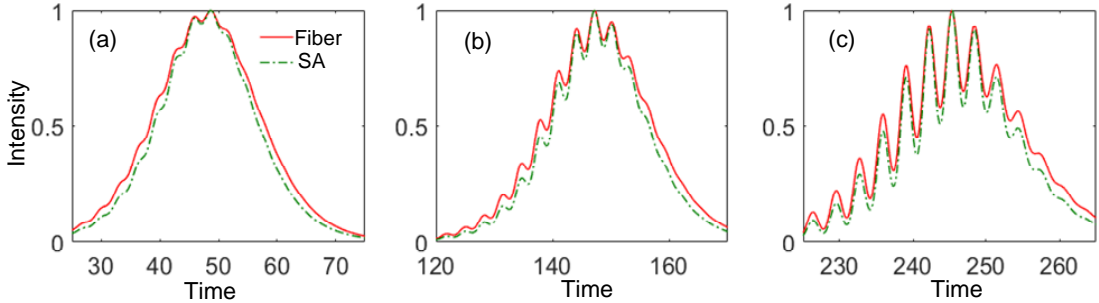


Fig. 3-5. The pulse profiles after the passive fiber (red solid line) and after SA (green dash-dotted line) during the transient at the (a) 400-th, (b) 500-th and (c) 600-th roundtrip. The pulse intensities are normalized by their maxima.

From Figs. 3-3 and 3-5, we found that the light interaction through Kerr nonlinearity, e.g. XPM and FWM, and the effect of SA are important for the buildup of a DSML state. The nonlinearity helps to produce the phase relation between channels during the propagation in the passive fiber. FWM transfers the energy from the original (stronger) pulse to other sidebands, and SA can also make the energies in

weak and strong channel closer so as to counterbalance the gain competition.

Like the mode-locking in a single-channel laser cavity, a DSML state requires the balances of different effects in a laser cavity. Intuitively, the balances and the laser dynamics in a DSML state should not be a simple extension of that of the single-channel mode-locked state. Hence after the building up of a DSML state, we will investigate the dynamics and the balance among different effects in it.

3.3.2 Balances inside a DSML state

Up till now, the balances inside the DSML state have not been delineated. For example, in such a state, the pulses in the two different channels have different group velocities due to the dispersion. However, the pulses in the two channels move together. Thus a different laser dynamics exists in the DSML state. In this section, both the laser dynamics and the balance of different physical effects in the DSML state are investigated.

We first observe the evolution of a DSML state in the whole cavity. Fig. 3-6 shows an example of the spectral evolution of a DSML state obtained with $\omega_{\text{sep}} = 2$ and $E_{\text{sat}} = 1$. The gain element amplifies the mode-locked pulse. In the passive fiber, the spectrum in each channel is broadened because of the nonlinearity. We note that the sidebands increases in the passive fiber (at $\omega = \pm 3$) because of the FWM process [76]. The SA and spectral filter act as loss elements in the cavity. The energy is reduced by SA. The sidebands generated in the passive fiber are obviously reduced by the spectral filter. From Fig. 3-6, we note the elements in the cavity induce an obvious evolution of the mode-locked pulse along the laser cavity. The distributed models that average all the effects of different elements [59, 62-64, 93, 94] obviously

cannot capture such intra-cavity evolution.

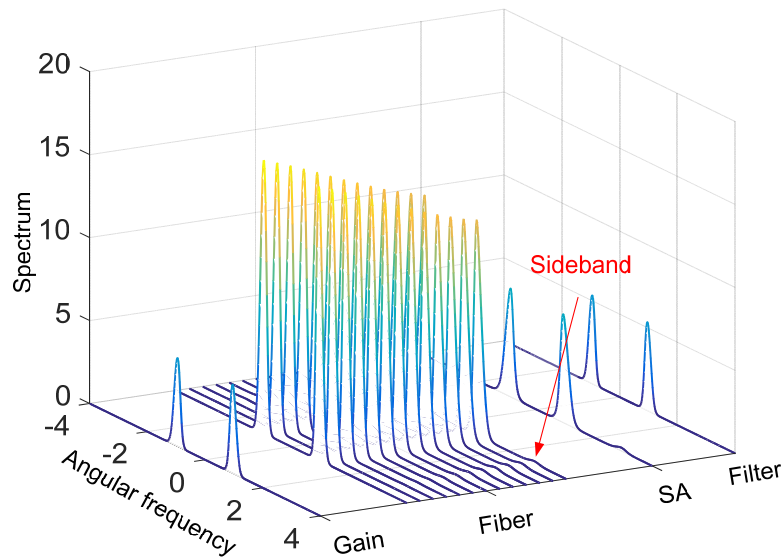


Fig. 3-6. Dynamics of the mode-locked pulse along the entire laser cavity in the frequency domain. The elements in the laser cavity induce an obvious evolution of the pulse.

More details can be seen by simultaneously observing the impact of laser elements on the pulses in both the time and frequency domain by using a time-frequency map (TFM), i.e. a spectrogram. We can determine the effect of each element by calculating the differential TFM (diff-TFM) which is the difference of the two TFMs before and after the element. The diff-TFM reveals the direction of the energy movement after passing through an element [54]. The diff-TFMs that tell the effects of passive fiber, SA and a dual-channel filter are shown in Figs. 3-7(a), (b) and (c). The warm colors indicate increase in energy while cool colors indicate decrease in energy.

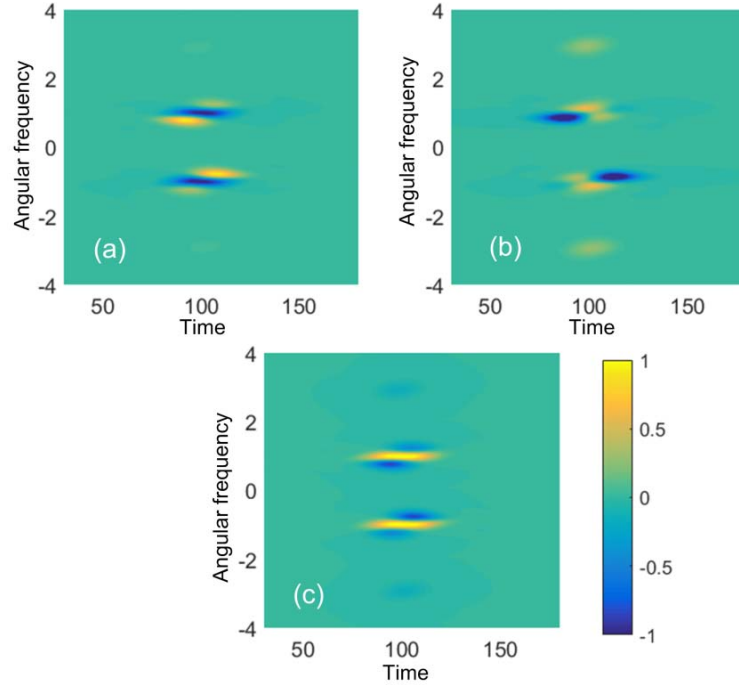


Fig. 3-7. The diff-TFMs of the mode-locked pulse along the cavity which show the impact of (a) passive fiber, (b) SA, and (c) spectral filter. Warm color side indicates the energy increase and cold color side indicates energy decrease.

The effect of passive fiber is shown in Fig. 3-7(a). From the time domain side of Fig. 3-7(a), the shorter wavelength channel signal (top pulse) travelled faster than the longer wavelength channel signal (bottom pulse) as indicated by the strong yellow color in the left side of the top pulse and right side of the bottom pulse of the respective channel signals in the diff-TFM. Thus, the pulses are temporally pulled apart by the dispersive effect of the passive fiber. As both channels are in the anomalous dispersive regime of the passive fiber, the mode-locked pulse of the longer wavelength channel (bottom pulse) travelled slower than the shorter wavelength channel pulse (top pulse). As seen from the frequency domain side of Fig. 3-7(a), for the pulses in both channels the blue color in the center of the spectra and warm

yellow color in either sides of the center of the spectra indicate spectral broadening. This spectral broadening is caused by the nonlinearity of the passive fiber. But the stronger yellow colors in the interior (interacting) sides for both the pulses compared to the weaker yellow color in the exterior sides indicates an asymmetrical spectral broadening of the individual pulses of both channels. The shorter wavelength channel pulse (top pulse) undergoes more spectral broadening in the longer wavelength side compared to the shorter wavelength side and vice-versa. This asymmetrically spectral broadening causes the spectral attraction between the two pulses, in other words, the pulse spectra in the two channels are moving towards each other in the passive fiber [92]. This is caused by the interaction of the two pulses in the two channels through XPM. The details will be clarified in the following sections.

Fig. 3-7(b) shows the effect of the SA. The exterior edges of the individual channel pulses undergo more intensity dependent loss as blue colored edges at the left side of the top pulse and right side of the bottom pulse. Thus the action of SA is to remove the walk-off parts of the pulses in both channels which are induced by the fiber. As a result, in a DSML state, the pulses would not move apart even the central frequencies are different. The dual-channel filter attenuates the spectra of the pulses in the two channels. The action broadens the pulse width in the time domain, as shown in Fig. 3-7(c). The spectral attraction between the pulses in the passive fiber is counter-acted by the dual-channel filter. The filtering action causes relatively higher loss for the longer wavelength side compared to the shorter wavelength side for the top pulse and vice-versa, as indicated by the relatively stronger blue colors in the interior edges of the pulses in Fig. 3-7(c).

From Fig. 3-7, in the time domain the pulses in the two channels are trying to move apart in the passive fiber due to the GVD. The SA chops the combined pulses in the time domain, such that the leading and trailing edges of the combined pulse get higher loss. This action suppresses the walk-off between the pulses in the two channels. In the frequency domain, the interaction among the pulses during the propagation in the passive fiber makes their spectra move towards each other. Such action is counter-balanced by the dual-channel filter. From Fig. 3-7, there are two set of balances in a DSML state. One is between the GVD and the SA on the walk-off of the two-channel pulses in the time domain. The other one is between the nonlinearity and the filter on the spectral detuning (attracting) in the frequency domain.

Thus the laser dynamics in a dual-channel cavity is not a simple extension from a single-channel mode-locked state. Interactions between the pulses in the two channels make the laser dynamics more complex. We would like to point out that the new laser dynamics can even render the energies in the two channels unequal. This is counter-intuitive because the light in both channels shares the same strength of gain, and the two channels in the dual-channel filter have the same profiles. The symmetry in our laser system is expected to produce identical energies in the two channels of a DSML state. In the next subsection, we will discuss the DSML state with unequal energy in the two channels.

3.3.3 Energy discrimination in a DSML state

Again, we assume that starting from noise a mode-locked pulse is achieved first in either one of the channels. If the channel separation is larger, when the pump increases, a DSML state with unequal energies between channels can be obtained.

Fig. 3-8 shows an example of such a state with channel separation $\omega_{\text{sep}} = 2.4$ and $E_{\text{sat}} = 1.8$. Both channels have a mode-locked pulse, and the modulation in temporal profile is still observed as shown in Fig. 3-8(a) showing that the pulses in the two channels are still phase-locked. The pulse in one channel is much weaker than the pulse in the other channel as shown in Figs. 3-8(b) and (c). The energies of the two channels are unequal all along the laser cavity as shown in Fig. 3-9.

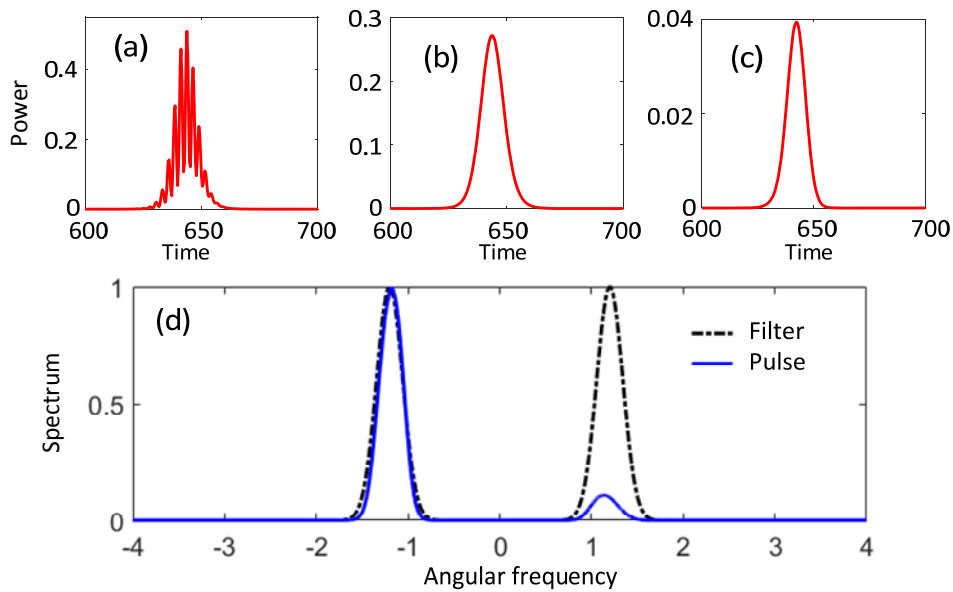


Fig. 3-8. (a) A DSML state with unequal energy. The mode locked pulse in (b) left and (c) right channel. (d) The spectrum after the output coupler. Both the spectrum and spectral filter are normalized by its maximum.

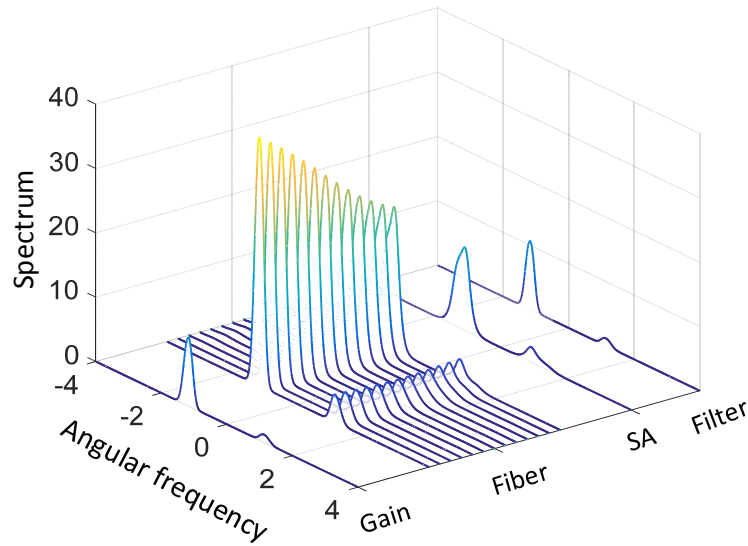


Fig. 3-9. Dynamics of the unequal energy DSML state along the entire laser cavity in frequency domain. The energies in two channels are not equal in the entire cavity.

The differences in energy in the mode-locked pulses from different channels have been observed experimentally [61]. The gain profile certainly contributes to the energy difference observed in experiments. However, our model shows that even when a flat gain profile is used, the peak powers of the mode-locked pulses in different channels are not the same. Similar energy differences between mode-locked states were also reported in [62, 94] using distributed models but the mechanism leading to the energy differences are been addressed. We use the proposed discrete heuristic model to investigate the dynamics of this state.

We start with the discrete actions of the laser elements in the cavity. The diff-TFMs obtained with the mode-locked state in Fig. 3-8 are shown in Fig. 3-10. From the frequency domain side of Fig. 3-10(a), the spectra of both pulses are broadened. Similarly, the stronger yellow colors in the interior (interacting) sides for both pulses

compared to the weak yellow color in the exterior sides indicates an asymmetrical spectral broadening of the individual pulses in both channels. Fig. 3-10(b) shows the effect of SA. The SA chops the pulse edges of the combined pulse. The effect of the filter is shown in Fig. 3-10(c). It shows the spectral filter chops the spectra of the pulses in the two channels and simultaneously broadens the pulse width in the time domain. Similarly, the filter causes an asymmetrical loss on the pulse spectrum. It causes a relatively higher loss for the longer wavelength side compared to the shorter wavelength side for the top pulse and vice-versa, as indicated by the relatively stronger blue colors in the interior edges of the pulses in Fig. 3-10(c).

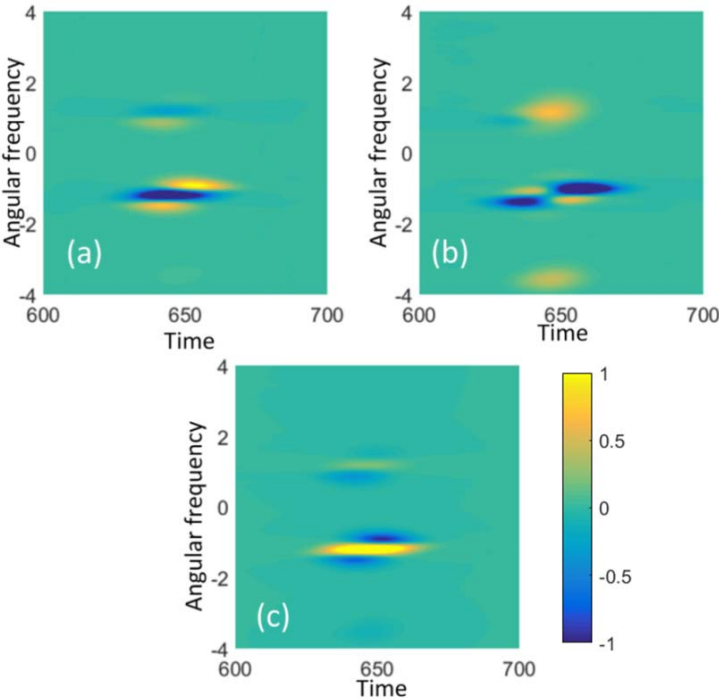


Fig. 3-10. The diff-TFMs of the mode-locked pulse along the cavity that showing the impact of (a) passive fiber, (b) SA and (c) spectral filter when the energies of the two pulses are unequal.

The impacts of the elements on the strong and weak pulse are different as depicted in Fig. 3-10. We note that the ratio of the energy of weak pulse to the energy of strong pulse in two channels appears to vary along the laser cavity. Fig. 3-11 shows the evolution of ratio of energy of weak pulse to that of the strong pulse along the laser cavity. The energy is transferred between channels, which is caused by the FWM process in the passive fiber [76]. The weak pulse is enhanced, and the energy ratio is increased from 0.121 to 0.145 in the passive fiber. In our model, we use a fast SA whose loss response depends on the instantaneous intensity of the light. As a result, the modulation depth of the combined pulse is enhanced by SA. Such an action makes the energies in the weak and strong channel closer [see Appendix I]. Hence the SA further increases the energy ratio to 0.183.

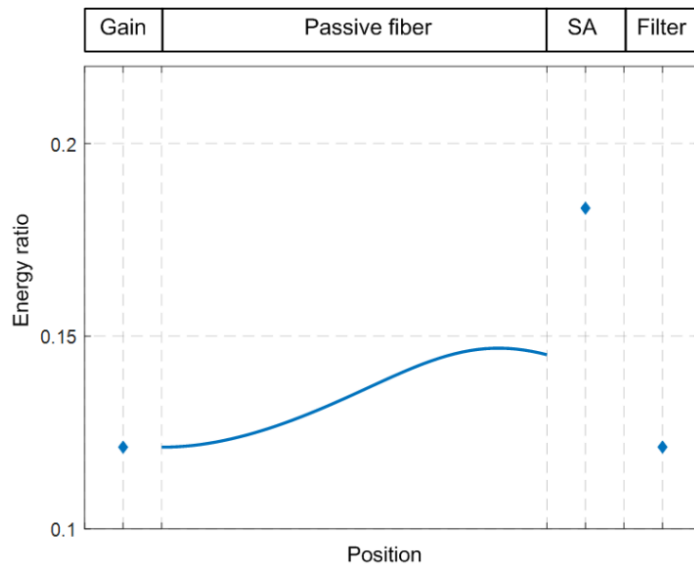


Fig. 3-11. The energy ratio between the pulses in weak and strong channels along the cavity.

The spectral filter decreases the energy ratio back to 0.121. Inferred from Fig. 3-11, the filter hinders the relative increase of the energy of the weaker pulse, thus

prevents the formation of a DSML state with identical energies in the two channels. We also note that the effect of filter here is different from that in the single-channel laser cavity. From Chapter 2, we found the filter gives a larger loss to a stronger pulse because the stronger pulse has a wider spectrum because of the SPM effect. Based on this understanding, the filter should have enhanced, rather than reduced, the energy ratio in Fig. 3-11. The different role played by the filter is due to the intrinsic frequency detuning of the pulses in the two channels in our DSML state.

From Figs. 3-4 and 3-8, the mode-locked pulses in both channels experience a slight frequency detune with respect to the central frequency of the spectral filter, which means the central frequencies of the pulses in these two channels are not equal to the respective central frequencies of the two channels. The frequency detuning is due to XPM and lead to additional filter loss to the mode-locked pulses in each channel. To investigate the frequency detuning, we monitor the central frequency ω_c of the pulses in two channels. The ω_c is calculated as $\omega_c = \int \omega |\mathcal{F}(\omega)|^2 d\omega / \int |\mathcal{F}(\omega)|^2 d\omega$, where $\mathcal{F}(\omega)$ is the spectrum of mode-locked pulse in the left or right channel. In the unequal mode-locking state as shown in Fig. 3-8, the evolution of ω_c along the laser cavity is shown in Fig. 3-12(a). From Fig. 3-12(a), the central frequencies of the two pulses move towards each other in the fiber. The detuning of the two channels is different as depicted in Fig. 3-12(a). After the fiber, the strong pulse is detuned by 0.03, while the weaker pulse is detuned by 0.17, which is almost six times larger than the strong pulse.

The action of the spectral filter is equivalent to pulling the central frequencies of the pulses back to their initial positions at the input point of the passive fiber. The

losses induced by the filter to the weak and strong pulses are hence different. As the weaker pulse experiences a larger frequency detune, it suffers a higher loss, about 1.5 times larger in the case, than that suffered by the stronger pulse when they pass through the spectral filter. Thus the energy ratio is decreased by the spectral filter.

For comparison, Fig. 3-12(b) shows the evolution of pulse central frequencies along the entire cavity in the case of DSML with identical energy in Fig. 3-6. We observed that the central frequency moves towards each other in the passive fiber. However, the amounts of the detuning in each channel are the same (which is 0.021). Thus, the two pulses suffer the same filter loss when they pass through the filter.

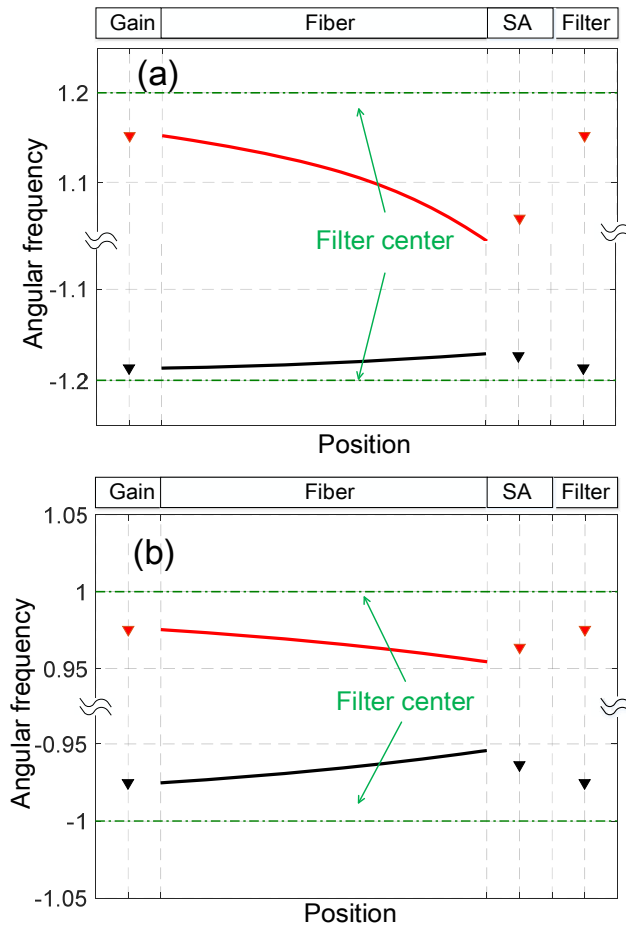


Fig. 3-12. The central frequency as the function of cavity position for (a) unequal energy mode-locked state in Fig. 3-8 and, (b) equal energy DSML state in Fig. 3-6.

The frequency detuning is observed in both identical and unequal energy states. Inferred from Fig. 3-12, we know the frequency detuning mainly comes from the propagation in the passive fiber. In the following, we will study the mechanisms that cause the detuning.

Both the GVD and the pulse interaction through XPM are responsible for the frequency detuning. These effects make the co-propagating pulses perform asymmetrical spectral broadening when they are temporally overlapped during the propagation in the fiber [76, 96]. We can use A and B to represent the complex field envelop of the pulses in left and right channel, respectively. The GVD causes the walk-off between A and B , and the pulse centers are different. In our case, B moves faster than A in anomalous dispersion region. In addition to the GVD, the nonlinear interaction, i.e. XPM, has an impact on A and B . Due to the temporal walk-off, B has more impact on the leading edge of A . The nonlinear phase shifts of leading and trailing edge of A are hence different. This induces an asymmetrical spectrum broadening of A [76], which induces a nonzero value of frequency detuning.

If the pulse in one channel is stronger than the pulse in the other channel, the strong pulse causes an obvious XPM effect on the weak pulse but gets little impact of XPM back from the weak pulse. Consequently, the weak pulse performs a more obvious asymmetrical spectral broadening. Its frequency detuning is hence larger than that of the strong pulse, which agrees well with the result in Fig. 3-12(a). If the intensities of the two pulses are identical, the strengths of XPM effects from the two pulses are also identical. Hence the frequency detuning of the two pulses will be the same, which still agrees with the results in Fig. 3-12(b).

To give a more general insight on DSML state, we study the effect of different filter parameters, e.g. channel separation ω_{sep} and channel bandwidth ω_{band} , on the mode-locked state. Starting with a single-channel mode-locked state in the dual-channel cavity, the threshold of pump E_{th} to build up a DSML state as the function of $\omega_{\text{sep}}/\omega_{\text{band}}$ is shown in Fig. 3-13. We can achieve the DSML states with identical (iden-ML) and unequal (uneq-ML) energies between channels. For a given channel bandwidth ω_{band} , the threshold increases with the channel separation. This is because the mode-locked pulse in one channel acts as a pump and enhances the light in the other channel through FWM. However, the effect of the FWM decreases when the channel separation increases. In the time domain, the walk-off between light in different channels is more obvious if the channel separation ω_{sep} increases. The nonlinear interactions, e.g. XPM and FWM which requires temporally overlapped of the light in two channels hence become weaker. As a result, when the channel separation increases, a higher value of pump is required to build up a DSML state as shown in Fig. 3-13. Starting from a single-channel mode-locked pulse, if the E_{th} is higher the peak power of the single-channel pulse is also higher. A stronger pulse induces a larger frequency detune on the weaker light in the other channel, leading to a higher filter loss. Hence we are more likely to obtain a uneq-ML state when the channel separation increases.

If the channels separation is increased further, a much higher pump might be required for achieving a DSML state. However, the pulse in one channel might first reach the multi-pulsing threshold before it starts to build up a DSML state. If the multi-pulsing makes a new pulse grow up in the other channel, we can also obtain a

dual-channel mode-locked state. However, the pulses in the two channels will not be phase locked and they have different group velocities. In the following subsection, we will study such state.

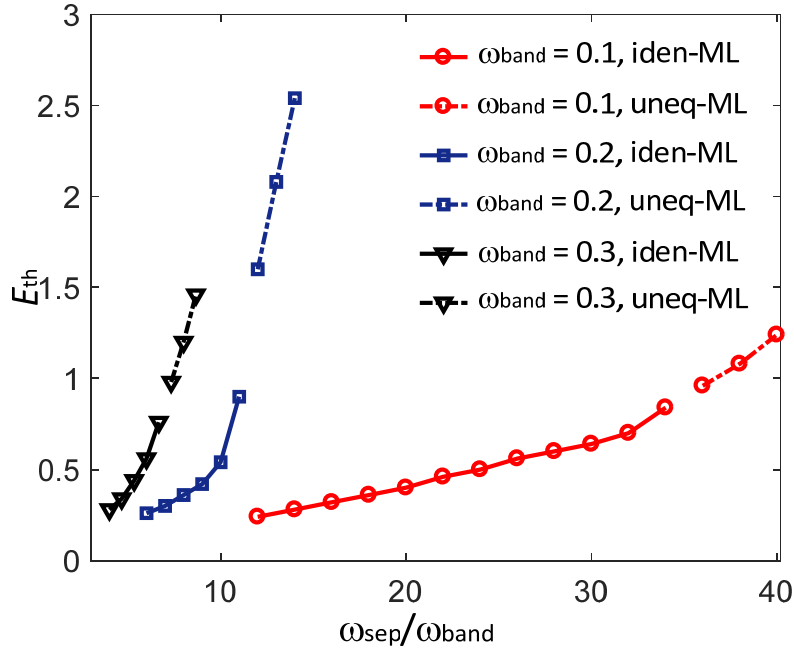


Fig. 3-13. Mode-locking state impacted by filter profiles. The pump threshold of achieving dual-channel simultaneously mode-locking as the function of $\omega_{\text{sep}}/\omega_{\text{band}}$ is given. The energies of the mode-locked pulses in the two channels can be either identical or unequal.

3.3.4 Independent mode-locking

We consider the channels of the dual-channel filter to be far apart from each other. In such a case a dual-channel mode-locked state can still be obtained, but the pulses are lasing independently in their respective channel frequencies. The two pulses do not interact with each other except the time that they cross over each other in the time domain [61]. Fig. 3-14(a) shows an example ($\omega_{\text{sep}} = 3$ and $\omega_{\text{band}} = 0.2$) of the evolution of dual-channel independent mode-locking as the function of roundtrips.

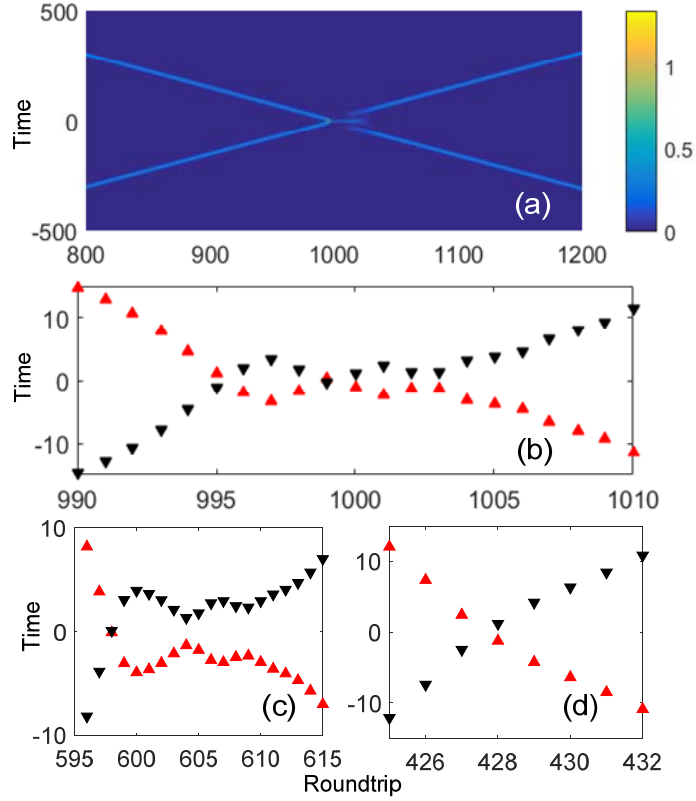


Fig. 3-14. (a) Contour of dual-channel intra-mode-locked pulses evolution the spectrum. Tracks of the centers of the two-channel pulses (b) $\omega_{\text{sep}} = 3$, (c) $\omega_{\text{sep}} = 5$ and (d) $\omega_{\text{sep}} = 7$.

Fig. 3-14(b) shows the location of the pulse centers (left channel black colored and right channel red colored) during the cross-over. The location of the pulse centers are calculated as $\tau_c = \int \tau |q(\tau)|^2 d\tau / \int |q(\tau)|^2 d\tau$ where $q(\tau)$ is the pulse electric-field envelope of either the left or right channel. We know in the dual-channel independent mode-locked state, most time the pulses in different channels cannot see each other. However, they can still affect each other at the time they are temporally crossing over. During the crossing over, based on the study above, we know other laser elements such as SA have a more obvious impact on the walk-off between the pulses. Since the channel separation that provides different group velocities of the two-channel pulses

is large enough, the dispersion effect of the fiber separates the two pulses finally. We also present the results (tracks of two-channel pulses centers) of two different large channel frequency separations, viz., $\omega_{\text{sep}} = 5$ [Fig. 3-14(c)] and $\omega_{\text{sep}} = 7$ [Fig. 3-14(d)]. When the channel frequency separations are increased, the dispersive effect of the fiber is more dominant hence the pulses will continuously cross over. The transition from a DSML to an independent mode-locked state has been observed in experiment in Ref. [61]. For a given channel separation, the authors found that the DSML state is achieved for small dispersion only. When the net dispersion increases, the pulses in the two channels will eventually circulate independently. The observation agrees with our results as the pulses in different channels will separate if the temporal walk-off caused by the group velocity difference between the pulses dominates.

Summary

Multi-channel mode-locked fiber laser has potential applications in many fields. In this chapter, we start with the simplest case, a dual-channel mode-locked laser. The pulses in the two channels can be either phase locked or not. The pulses in two channels would not move apart if their phases are locked. The building up of such a state was studied. The interaction between the light in different channels is important for its building up and exhibits a different laser dynamics when compared with that of a single-channel mode-locked state. The pulses in such a state do not move apart in the time domain because SA can balance the walk-off of the pulse caused by GVD.

Chapter 4

Multi-channel Mode-locked Fiber Laser and Its Nonlinear Dynamics

In Chapter 3, we investigated dual-channel mode-locking which is the simplest case of a multi-channel laser cavity. In this Chapter, we will investigate multi-channel mode-locking using the proposed heuristic model. We found that nonlinear phenomena such as FWM, XPM, frequency detuning and the filter loss continue to play a role in the laser dynamics.

4.1 Theoretical model

Multi-channel fiber lasers have attracted much research interest in past decades. It is possible to achieve multi-channel simultaneously mode-locked (MSML) state, in which each channel is mode-locked and the phases between the pulses from different channels are also locked [56]. Such output has potential applications in terahertz generation and optical sensors [56, 58-61].

The laser cavity is similar to that in Fig. 3-1, except that the dual-channel filter is replaced by a comb filter, as shown in Fig. 4-1(a). The models of the gain, passive fiber and SA are the same as that in Eqs. (3-6) (3-7) and (3-8), respectively. As we did in the previous Chapters, the white Gaussian noise (zero mean and a variance of $\sim 10^{-9}$) is added after the gain element to model the amplifier noise. The comb filter in the cavity is modelled as

$$H(\omega) = \sum_n \exp \left[- \left(\frac{\omega + n\omega_{\text{shift}}}{\omega_{\text{band}}} \right)^2 \right], \quad (4-1)$$

where n is the channel number, ω is the angular frequency, ω_{band} is the bandwidth of each channel and ω_{shift} is the channel separation between the channels.

In experiments, the peak powers of the pulses in different channels are different. The difference is attributed to the gain profile of the gain fiber. Obviously, the gain profile can modify the energies in different channels, but we believe the laser dynamics is also responsible for the difference in pulse peak power in different channels. Hence in our study, we assume a flat gain profile to remove the impact of the gain profile on the pulse energies in different channels.

The number of channels in a multi-channel laser cavity can be quite different between different cavities, e.g. 3- [58, 97], 6- and 8-channel [59, 63], and more than 50 channels lasing [98, 99] have been reported. We study the simplest non-trivial examples, i.e. 3-channel and 4-channel comb filter. In both cases, the comb filter is symmetric about $\omega = 0$ in the frequency domain as shown in Figs. 4-1(b) and (c). In a 3-channel laser cavity, the channels from left to right in the frequency domain are labelled as (-1)-th, 0-th and (+1)-th channel. In a 4-channel laser cavity, the four channels are named as (-2)-th, (-1)-th, (+1)-th and (+2)-th channel, respectively.

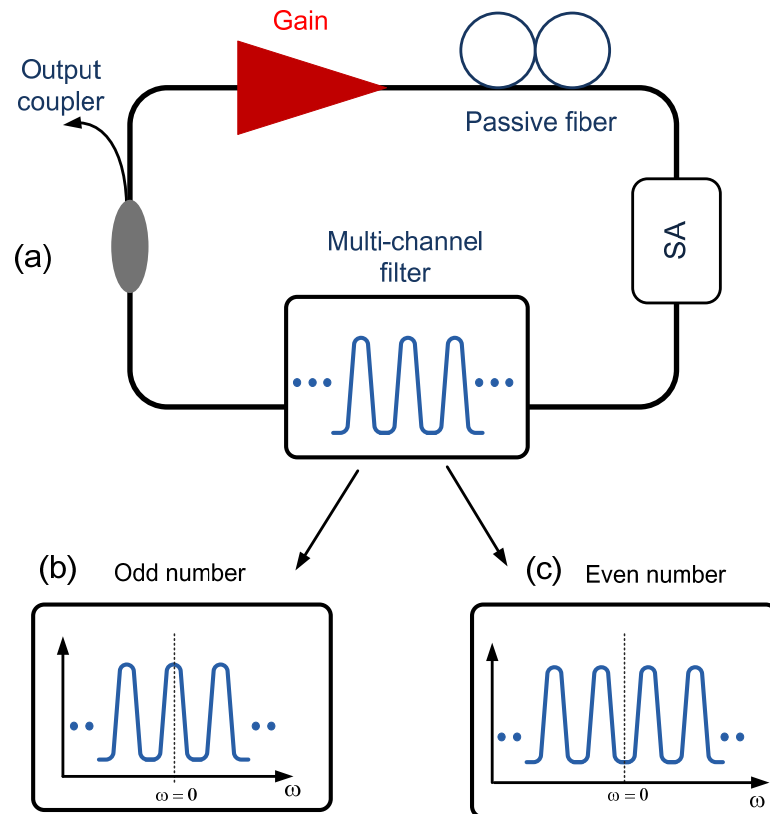


Fig. 4-1. (a) Schematic of a multi-channel mode-locked fiber laser cavity. The channel number can be (b) odd or (c) even but they are both symmetric about $\omega = 0$.

4.2 Nonlinear dynamics

Similar to a dual-channel cavity, when the pump power is increased from zero, one channel will first be mode-locked. It can be any channel of the comb filter as the simulation is started from noise and the gain profile is assumed to be flat. When the pump is further increased, we observe a variety of mode-locked states. The energies in the channels are not all identical. In some cases the spectra can even be asymmetric about the center of the spectrum although the comb filter is symmetric in the frequency domain.

4.2.1 Different MSML states

Figs. 4-2, 4-3 and 4-4 show examples of the different steady-state mode-locked outputs we observed with different pump powers in the 3-channel and 4-channel cavity. In a 3-channel cavity, if the pump is weak, e.g. $E_{\text{sat}} = 0.1$, it is possible that only one of the side channel has a mode-locked pulse as shown in Fig. 4-2(a). If the pump power is further increased, the pulse will not absorb all the cavity energy but transfer the energy to its adjacent channels through FWM [56]. Similar to the dual-channel case, the light in the adjacent channels will grow as shown in Figs. 4-2(b) and (c). These steady state outputs are not symmetric about $\omega = 0$. When the pump is further increased, the weak light at the (-1) -th channel increases and a symmetric state can be obtained as shown in Fig. 4-2(d).

Fig. 4-2(e) shows an example in which the 0-th channel is first mode-locked when the pump is weak. We note noise is able to break the symmetry and the light in the two side channels do not necessarily increase simultaneously when the pump is further increased (details are given later in this Chapter). Instead, as shown in Fig. 4-

2(f), only the light in the (+1)-th channel increases (it is also possible that the light in the (-1)-th channel increases, but not shown here). Similarly to Figs. 4-2(c) and (d), when the pump is further increased the light in the (-1)-th channel will grow as depicted in Fig. 4-2(g) and (h).

Figs. 4-3 and 4-4 show the different laser output observed in a 4-channel cavity (only the output in the right-hand side channels are shown because of symmetry). When the pump is weak, the single-channel pulse can locate at the (+2)-th channel as shown in Figs. 4-3(a). When the pump is increased, the light in other channels grow. The obtained steady states laser output can also be asymmetric about $\omega = 0$, as shown in Figs. 4-3(b) and (c). The light in the (-2)-th and (-1)-th channel are much weaker than the light in the (+1)-th and (+2)-th channel in these states. Further increase of the pump enhances the light in both the (-2)-th and (-1)-th channels and result in a symmetric state as shown in Fig. 4-3(d).

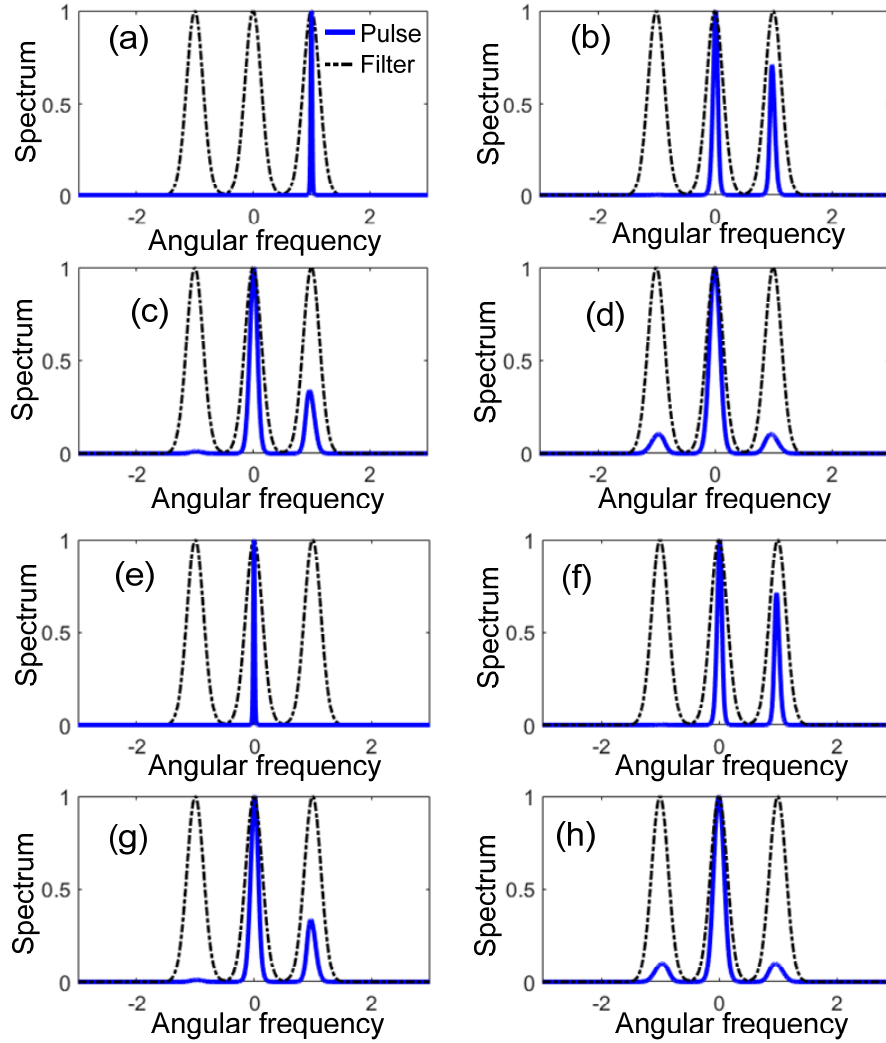


Fig. 4-2. Different steady state output of a multi-channel mode-locked laser. (a) Only the right-hand side channel is mode-locked for $E_{\text{sat}} = 0.1$ in a 3-channel cavity. From the mode-locked state in (a), the pump power is increased to (b) $E_{\text{sat}} = 0.3$, (c) $E_{\text{sat}} = 0.5$ and (d) $E_{\text{sat}} = 0.7$. (e) Only the central channel is mode-locked for $E_{\text{sat}} = 0.1$ in a 3-channel cavity. From the mode-locked state in (e), the pump power is increased to (f) $E_{\text{sat}} = 0.3$, (g) $E_{\text{sat}} = 0.5$ and (h) $E_{\text{sat}} = 0.7$. The spectra are normalized by their maxima and the channel bandwidth is 0.2 and they locate at $\omega = 0$ and ± 1 .

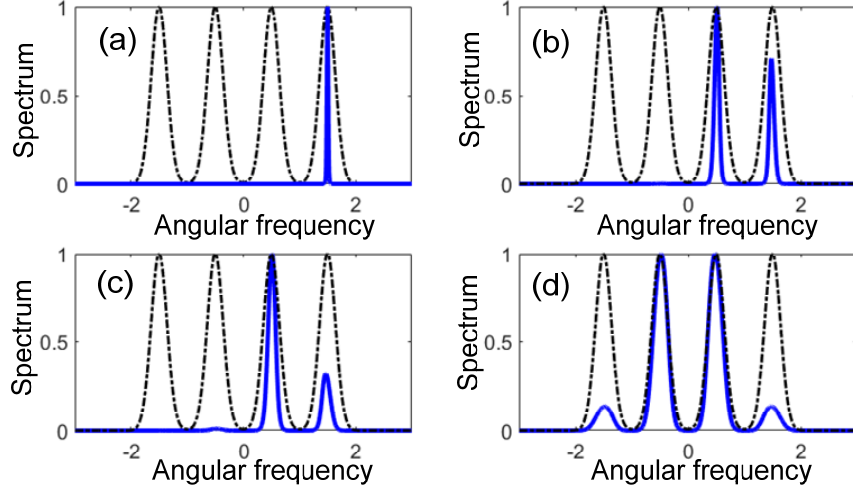


Fig. 4-3. (a) Single-channel mode-locked states when $E_{\text{sat}} = 0.1$ in (+2)-th channel in a 4-channel cavity. The obtained states from (a) by increasing the pump to (b) $E_{\text{sat}} = 0.3$, (c) $E_{\text{sat}} = 0.5$ and (d) $E_{\text{sat}} = 0.7$ are given. The spectra are normalized by their maxima and the channel bandwidth is 0.2 and they locate at $\omega = \pm 0.5$ and ± 1.5 .

Fig. 4-4(a) shows that the light at the (+1)-th channel is mode-locked first. When the pump is increased, the energy in either side of the (+1)-th channel can grow. The energy in the (+2)-th channel is increased as shown in Fig. 4-4(b). It is the same state as that shown in Fig. 4-3(b). Thus further increase in the pump power will render the laser to repeat the states observed in Figs. 4-3(c) and (d), as shown in Figs. 4-4(c) and (d). To the state in Fig. 4-4(a), if the light in the (-1)-th channel grows first when the pump is increased, we can obtain the state shown in Fig. 4-4(e). The energies in the (± 1)-th channel are identical and the energies in the (± 2)-th channel are also identical. The weak light in (± 2)-th channels are enhanced if the pump is further increased, as shown in Figs. 4-4(f) and (g).

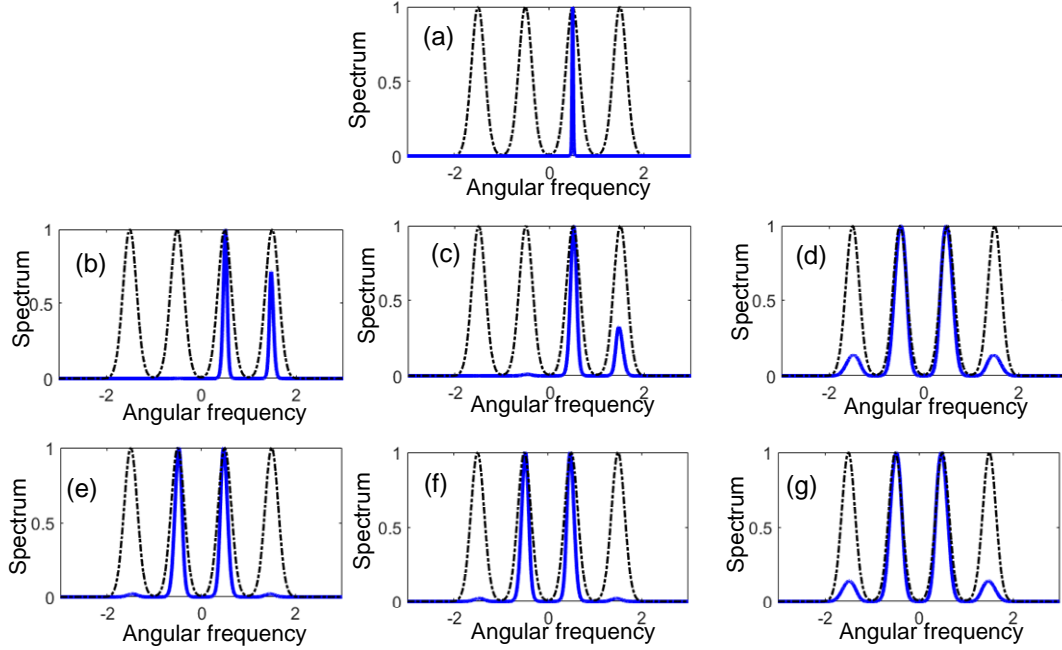


Fig. 4-4. (a) Single-channel mode-locked states when $E_{\text{sat}} = 0.1$ in the (+1)-th channel in a 4-channel cavity. The energy in the channel on either side of the (+1)-th channel might increase when pump is increased. (b) The (+2)-th channel might increase when the pump is $E_{\text{sat}} = 0.3$. The obtained states from (b) by increasing the pump to (c) $E_{\text{sat}} = 0.5$ and (d) $E_{\text{sat}} = 0.7$ are given. From (a), the (-1)-th channel might also increase when the pump is $E_{\text{sat}} = 0.3$ as shown in (e). The obtained states from (e) by increasing the pump to (f) $E_{\text{sat}} = 0.5$ and (g) $E_{\text{sat}} = 0.7$ are given. The spectra are normalized by their maxima and the channel bandwidth is 0.2 and they locate at $\omega = \pm 0.5$ and ± 1.5 .

Figs. 4-2, 4-3 and 4-4 show a rich variety of mode-locked states in a multi-channel laser cavity. In these states, we note that the energies in the channels are not all identical and some MSML spectra are asymmetric even though a symmetric comb filter is used. Up till now, we have not found an MSML state that emits identical energies in all channels even a flat gain profile is used. It indicates that, in addition to the gain profile, there are other effects that cause the energy difference among

channels. In the following, we discuss the laser dynamics that affect the channel energy.

4.2.2 Dynamics in the formation of MSML states

We begin by looking at the buildup of the MSML state from a single-channel mode-locked pulse. As an example, Fig. 4-5(a) shows the transient from Fig. 4-2(a) to 4-2(b). The (+1)-th channel is mode-locked first. The energy at other channels is increased through FWM as shown in Fig. 4-5(b). Figs. 4-5(c) and (d) show the spectral evolution in the passive fiber at the 200-th and 400-th roundtrip, respectively. Thus in the beginning, the energy in the 0-th channel is increased by the light in the (+1)-th channel through FWM as shown in Fig. 4-5(c). When both the light in 0-th and (+1)-th channel are sufficiently high, the light in these channels can transfer energy to other channels, i.e. (-1)-th and (+2)-th ($\omega = +2$) channel, through degenerated FWM process [76, 95] as shown in Fig. 4-5(d). The light at $\omega = +2$ is attenuated by the comb filter while the light at (-1)-th channel continuously increases. Finally, the MSML state shown in Fig. 4-2(b) is observed. Both FWM and XPM introduce a phase relation between the light that are temporally overlapped [76, 95]. The pulses in the MSML state also locate closely in the time domain, as shown in Figs. 4-5(e), (f) and (g). Interference among the pulses in different channels results in a temporal modulation of the combined pulse as shown in Fig. 4-5(h).

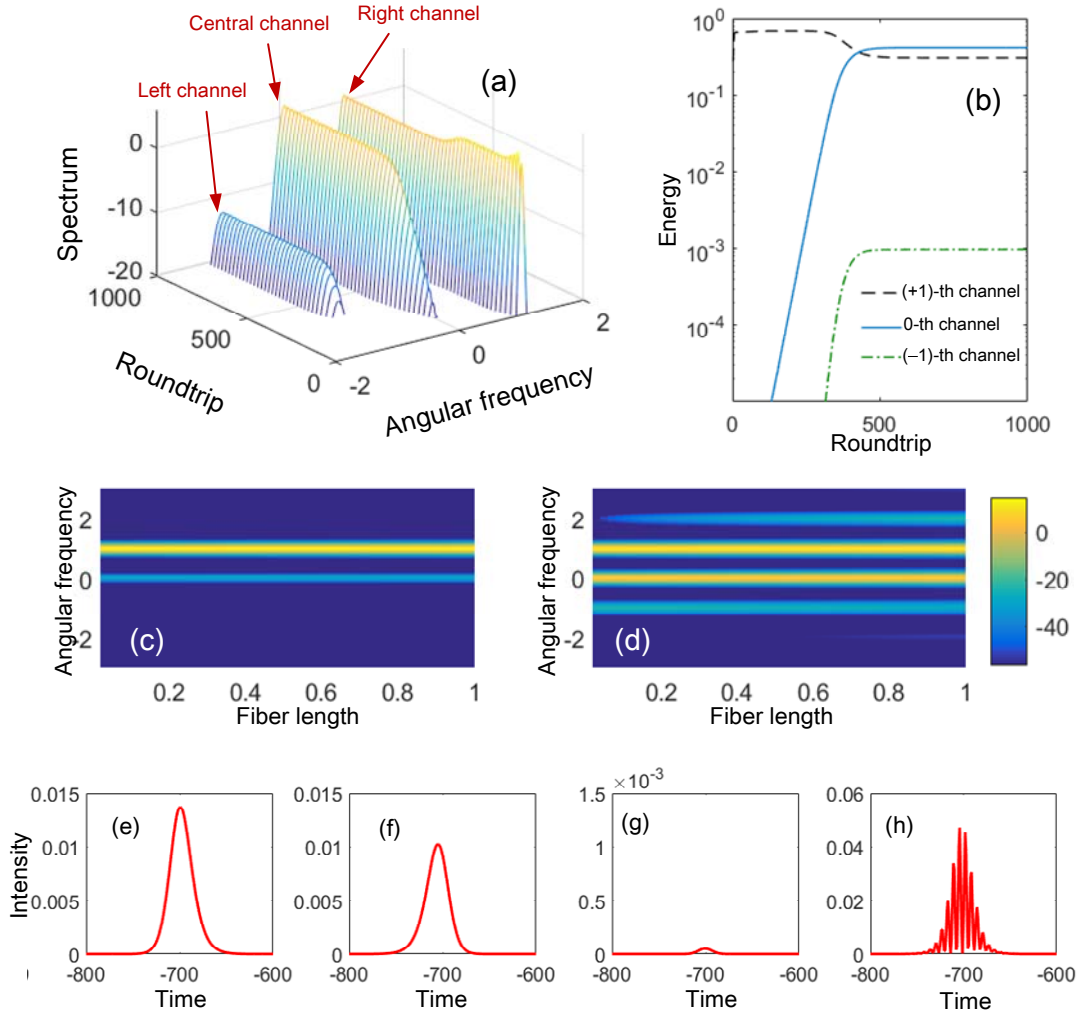


Fig. 4-5. (a) The transient of the spectra evolution after the output coupler from a single-channel mode-locked state in Fig. 4-2(a) to an MSML state in Fig. 4-2(b). (b) The energy evolution in different channels during the transient. The spectral evolution in the passive fiber at (c) 200-th and (d) 400-th roundtrip are shown. The temporal profiles of the final mode locked pulse in (e) the central, (f) the right and (g) the left channel. (h) Shows the combined pulse profile.

Fig. 4-5(b) shows that, during the transient, the energy in the (-1) -th channel first increases but stops before it grows to the same value as the energy in the $(+1)$ -th

channel. Further growth of the (-1) -th channel requires a higher pump power, as shown in Figs. 4-2(c) and (d). We believe that it is the laser dynamics in the multi-channel cavity that hinders further growth of the pulse in the (-1) -th channel. From the previous Chapter, the evolution of energy ratios between the light in different channels along the cavity reveals the laser dynamics. Figs. 4-6(a) and 4-6(b) show the energy ratios between the $(+1)$ -th and 0-th channel, and the energy ratio between the (-1) -th and 0-th channel, respectively. In the passive fiber, the light at different channels transfer the energy to other frequencies through the FWM process [76], hence the energy ratios vary along the passive fiber. The SA still increases the energy ratios for it enhances the modulation depth in the temporal profiles of the mode-locked pulses. The spectral filter decreases the energy ratio.

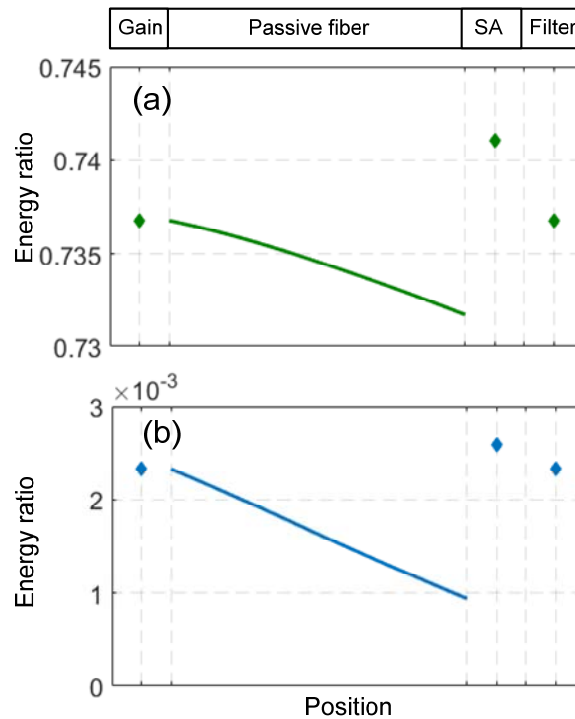


Fig. 4-6. The evolution of energy ratios of the state in Fig. 4-2(b). The ratios of the pulse energies between (a) the right and the central channel, (b) the left and the central channel.

From the last Chapter, the pulses in two channels induce frequency detuning to the central frequencies of each other. The detuning and the filter loss induce losses to the pulses in different channels, which could lead to the energy difference among channels in a DSML state. Similar action of the spectral filters in both dual-channel and multi-channel shown in Fig. 3-11 and Fig. 4-6 indicates that the filter loss and the frequency detuning play an important role in the dynamics of a multi-channel cavity. Thus, we monitored the central frequencies of the pulses in different channels.

Fig. 4-7 shows the evolution of the central frequencies of the pulses in different channels. The detuning of the pulse in the (+1)-th channel and the 0-th channel are 0.014 and 0.010, respectively. The detuning of the weak pulse in the (-1)-th channel is 0.035, which is two to three times of the detuning in the other two channels. Similar to dual-channel cavity, the stronger pulses experience a smaller detuning and vice versa. The central channel experiences the smallest frequency detuning.

The same is true for the symmetric spectra in both 3-channel and 4-channel cavity, e.g. the states in Figs. 4-2(d) and 4-3(d). Because of the symmetry of these states, we only calculate the energy ratio between the (+1)-th and 0-th channel in a 3-channel cavity, and that between the (+2)-th and (+1)-th channel in a 4-channel cavity. The evolution of the energy ratios in 3-channel and 4-channel cavity are shown in Figs. 4-8(a) and (b), respectively. Figs. 4-8(c) and (d) show that the weaker pulses in the side channel(s) in both the 3-channel and 4-channel experience a higher detune. Thus, the weaker pulse suffers a higher filter loss when compared to the stronger pulses in the cavity. Based on the results in Figs. 4-7 and 4-8, the FWM frequency

detune combined with the spectral filter lead to the energy difference among different channels even when a flat gain profile is assumed.

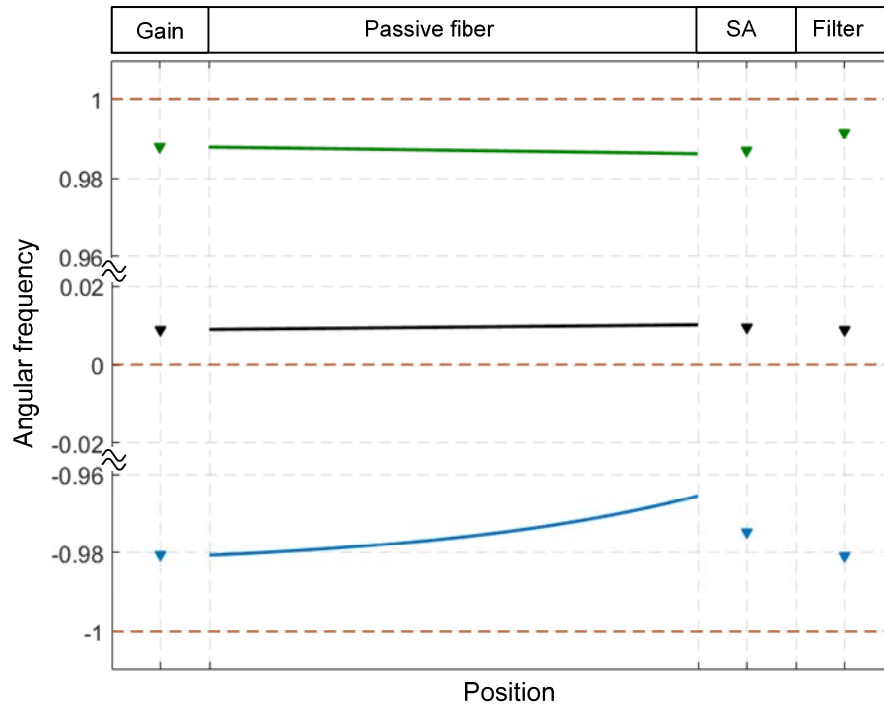


Fig. 4-7. The evolution of the central frequencies of the pulses of the state in Fig. 4-2(b) in different channels as the function of the cavity position.

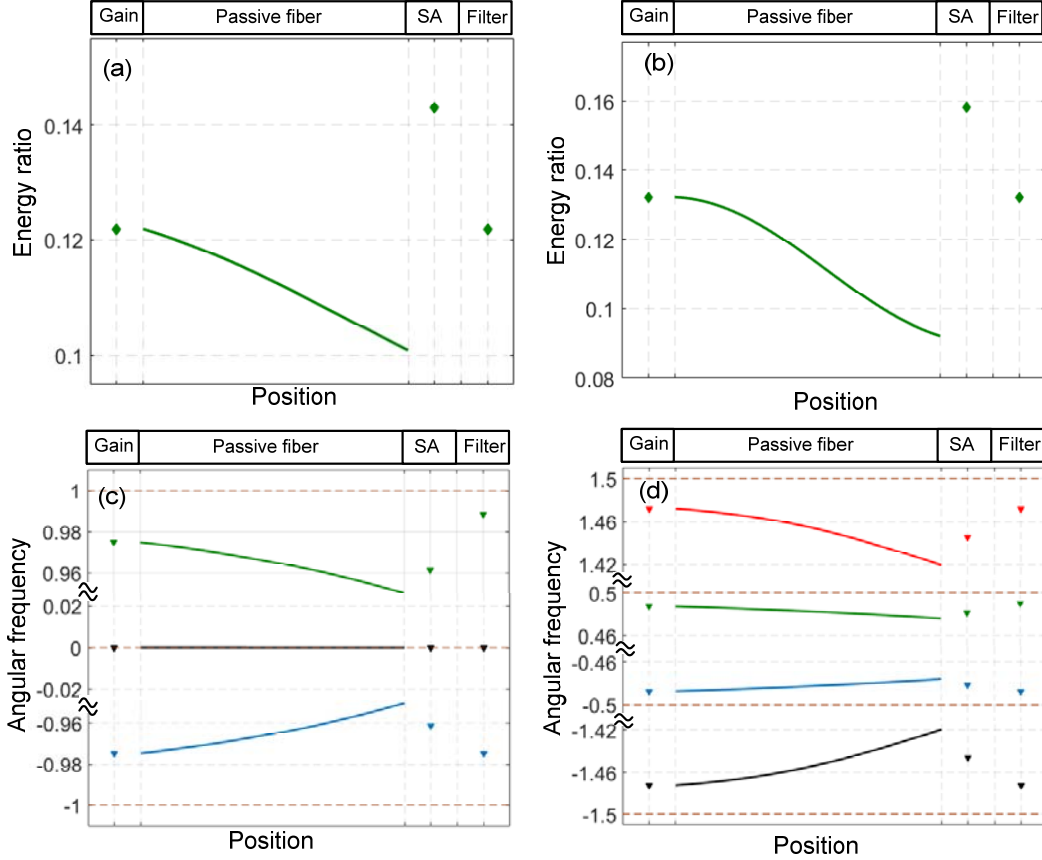


Fig. 4-8. The dynamics of the symmetric MSML states in the 3-channel [Fig. 4-2(d)] and 4-channel [Fig. 4-3(d)] cavity. (a) and (b) show the evolution of the energy ratios of the states in 3-channel and 4-channel, respectively. (c) and (d) show the central frequencies of the pulses in different channels as the function of cavity position in 3-channel and 4-channel cavity, respectively.

Up till now, we know both the asymmetric and symmetric MSML states can survive in the cavity. The filter profile is symmetric in the frequency domain, and one may believe that, due to the symmetry of the system, if the 0-th channel is first mode-locked, the (± 1)-th channels should always have identical energy when the pump is increased. However, we should note that there is noise and accumulated numerical error [100, 101], (see Appendix J) in our simulation. The symmetry of the system can

be easily broken and hence it is not impossible to produce an asymmetric MSML state, as the example we given in Fig. 4-9 which shows the evolution from the state in Fig. 4-2(e) to Fig. 4-2(f). We note that the light in both (± 1) -th channel are mode-locked from noise. Hence their energies are not identical during the evolution. In Fig. 4-9, the $(+1)$ -th or (-1) -th channel can have a higher energy depending on the noise. In Fig. 4-9, the $(+1)$ -th channel is higher and finally an asymmetric MSML state, i.e. Fig. 4-2(f), is obtained. Its evolution in one roundtrip is shown in Fig. 4-6.

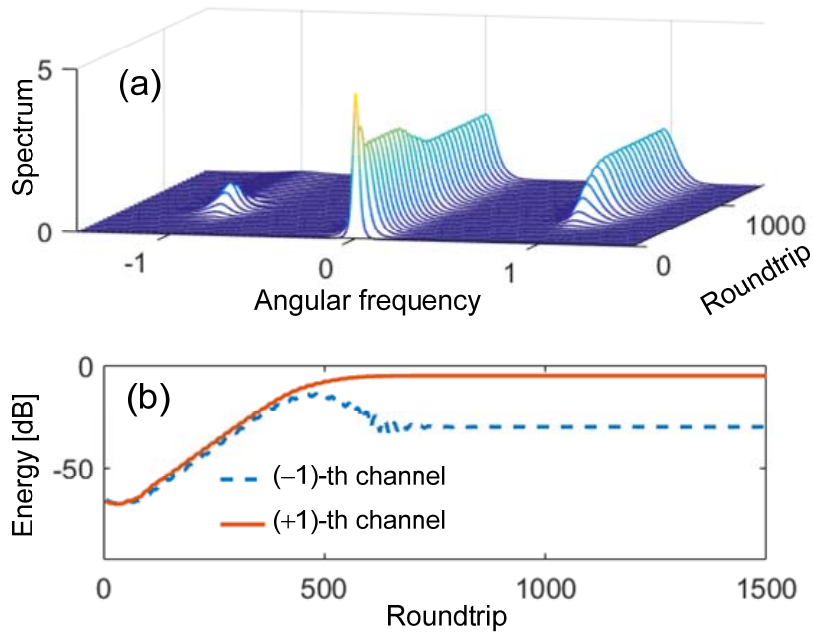


Fig. 4-9. (a) The transition from single-channel mode-locking to an MSML state in the frequency domain. (b) The energy evolutions in the $(+1)$ -th channel (orange solid) and (-1) -th channel (blue dashed).

In addition to the impact of noise, multiple channel light interaction can also affect the energy distribution among channels. We note that to a pulse in one of the

channel of a DSML state, only the leading or trailing edge of the pulse is affected by the pulse in the other channel. In a multi-channel cavity, there are multiple pulse interactions. For example, in Fig. 4-8(c) both leading and trailing edges of the pulse in the 0-th channel are affected by the pulses in (± 1)-th channels. The combined effect of the pulses in (-1)-th and ($+1$)-th channel decreases the total frequency detuning of the pulse in the 0-th channel.

As a result, in Fig 4-5 we note that even the ($+1$)-th channel is first mode-locked, the 0-th channel can get a higher energy than the ($+1$)-th channel when the pump is increased. Starting from the single channel mode-locked state in ($+1$)-th channel, the 0-th and (-1)-th channel start to grow, but the latter at a much slower rate. The frequency pull from the pulse in the (-1)-th channel on that in the 0-th channel is opposite to the frequency pull by the ($+1$)-th channel on the 0-th channel. Thus the 0-th channel suffers a smaller filter loss when compared to the ($+1$)-th channel, eventually, the 0-th channel has a higher energy, as shown in Fig. 4-5(b).

Summary

We studied multi-channel laser cavity using the extended heuristic model. The frequency detuning and gain loss dynamics determine the steady state output. We found that the FWM and XPM induced frequency shift and the spectral filtering lead to different energy in different channels even when a flat gain profile is assumed.

Multi-channel mode-locked laser has also been found in other works with distributed models [59, 64]. The gain bandwidth and the nature of the gain, a combination of homogenous and inhomogeneous gain, were included. These works

focused on the impact of different parameters on the mode-locked solutions. In our work, besides the impact of parameters, we aim to delineate the working mechanisms and different balances among different dynamic states in the cavity.

Chapter 5

Conclusions and Future

Works

We proposed an extended heuristic model by including the pulse shaping effects to study the nonlinear dynamics of different mode-locked lasers. We studied mode-locking in single-, dual- and multi-channel laser cavities with the extended model.

For single-channel mode-locking, we investigated the impact of spectral filtering in a laser cavity. With the pulse shaping effects, the nonlinear loss is not caused by the SA only. The filter also introduces loss to the pulse. Thus multi-pulsing will be triggered even if a monotonic transmission of SA is used. In addition to multi-pulsing and chaos, we also observed a high energy mode-locked pulse if the filter bandwidth is increased. The evolution of this pulse spectrum in the gain fiber plays a critical role in the laser dynamics. If TOD is included in the model, the multi-pulse state may also be obtained owing to pulse splitting.

We also studied the laser dynamics in multi-channel mode-locked laser cavity. We started from a dual-channel cavity and found the state that both channels are mode-locked and the phases of these channels are also locked. Light interaction between the channels determines the final output. We found that the SA can balance the walk-off of the pulse caused by GVD, hence pulses with different central frequencies move together in the time domain. We also found that the FWM induced frequency shift and the spectral filtering introduced an additional loss mechanism which leads to the energy difference between the two channels. The same mechanisms are found to determine the output of multi-channel lasers. The interaction is more complex as more pulses are involved.

The study of laser dynamics is important for understanding the mode-locking mechanism in the laser cavity. Our work in this thesis added to the understanding of

the laser cavity and its design. There are further works to be carried out in the future:

First, there are multiple elements in different positions in a laser cavity. In our work, we placed the SA after the gain element as the gain element increases the pulse intensity. The SA will give a smaller loss to the higher intensity light. As the pulse spectrum varies along the laser cavity, different arrangement of the filter, SA and fiber will lead to different pulse evolution in one roundtrip. The distributed model averages the effect of the elements over one roundtrip thus washing out the impact of the element locations. Differently, our model can easily study the impact of the element position, which was not carried out in the current study. In future work, the impact of element positions should be carried out.

Second, the work presented here assumed the fiber lasers have net anomalous dispersion. The heuristic model can also be applied to other lasers such as the ANDi lasers, where the cavities are in the normal dispersion region. In our work, the high energy pulse requires wider filter bandwidth, but Andy Chong [52] pointed out that decreasing the filter bandwidth would give a higher energy pulse. Also, the position of spectral filter is believed to significantly influence the mode-locking performance. In future work, we would study the mode-locking in ANDi laser and dispersion management (DM) laser cavity.

Another direction worth investigating is whether the filter profile can be engineered to increase the pulse energy. The impact of the filter profile on the mode-locked pulse energy should be studied. In addition, in a multi-channel mode-locked laser cavity, the comb filter profile can be designed to give a uniform laser output or any desired output.

We are also interested in extending the proposed model to other types of lasers, e.g. solid-state lasers or semiconductor lasers. We note that distributed models such as those based on the Ginsburg–Landau equation have been used to model Ti:Sapphire lasers. Thus, the proposed model can be applied to solid-state lasers as well. For semiconductor lasers, the gain dynamics are different from that of optical fiber and solid-state lasers. In semiconductor lasers, the lifetime of the upper-state is in the order of nanoseconds, which is much shorter than that of the gain medium in fiber lasers (~microseconds) or in Ti: Sapphire lasers (~milliseconds) [102]. As a result, the leading and trailing edges of the mode-locked pulse will experience different gain in a semiconductor laser. In order to extend the proposed model to semiconductor lasers, the gain relaxation time should be taken into account. We might use the gain model in [103] as $\dot{g} = -\frac{g - g_0}{\tau} - \frac{gP}{E_{\text{sat}}}$ where g_0 is small-signal gain, τ the relaxation time of the gain medium, P the power of the light in the cavity, and E_{sat} the saturation energy.

Appendix A: Acronyms

ANDi	all normal dispersion
AOM	acousto-optic modulator
CQGLE	cubic-quintic Ginzburg–Landau equation
cSHE	complex Swift-Hohenberg equation
diff-TFM	difference time frequency map
DM	dispersion managed
DS	dissipative soliton
DSML	dual-channel simultaneously mode-locked
EDFA	erbium-doped optical fiber amplifier
FWM	four wave mixing
FWHM	full width at half maximum
FFT	fast Fourier transform
GVD	group velocity dispersion
IFFT	inverse fast Fourier transform
IST	inverse scattering transform
LED	light-emitting diode
MBE	molecular beam epitaxy
MOCVD	metal organic chemical vapor deposition
MOPVE	metal organic phase vapor epitaxy
MSML	multi-channel simultaneously mode-locked

NALM	nonlinear amplifying loop mirror
NLS	nonlinear Schrödinger equation
NPR	nonlinear polarization rotation
ODE	ordinary differential equation
PC	polarization controller
PDE	partial differential equation
PI	polarization isolator
SA	saturable absorber
SAM	self-amplitude modulation
SESAM	semiconductor saturable absorber mirror
SMF	single mode fiber
SPM	self-phase modulation
SWNT	single-wall carbon nanotube
SSFM	split-step Fourier method
TFM	time frequency map
TOD	third order dispersion
WDM	wavelength division-multiplexing
XPM	cross-phase modulation

Appendix B: Split-step Fourier

Method

The light propagating in the fiber is modeled by the NLS equation which is written as

$$\frac{\partial A}{\partial z} = -\frac{i}{2}\beta_2 \frac{\partial^2 A}{\partial t^2} + i\gamma |A|^2 A, \quad (\text{B-1})$$

where β_2 and γ are the second order dispersion and nonlinear coefficients, respectively.

The NLS equation is a nonlinear PDE and it generally does not have analytic solutions except for some specific cases, e.g. inverse scattering transform (IST) method [104]. A numerical approach is hence often needed. Split-step Fourier method (SSFM) can be used to solve NLS numerically. Thanks to the fast Fourier transform (FFT) [105], SSFM can be a fast method for solving the NSL numerically.

SSFM splits the NLS into two equations

$$\frac{\partial A}{\partial z} = -\frac{i}{2}\beta_2 \frac{\partial^2 A}{\partial t^2}, \quad (\text{B-2})$$

$$\frac{\partial A}{\partial z} = i\gamma |A|^2 A. \quad (\text{B-3})$$

Eq. (B-2) and Eq. (B-3) contain the effect of dispersion and nonlinearity only, respectively. In general, dispersion and nonlinearity are modifying the light together along the fiber. The SSFM gets an approximate solution by assuming that the dispersive and nonlinear effects are acting independently over a sufficiently small distance Δz in the fiber. For each propagation step Δz , the light is calculated as

$$A(z + \Delta z, t) \simeq \exp(\Delta z \hat{D}) \exp(\Delta z \hat{N}) A(z, t), \quad (\text{B-4})$$

where $\hat{D} = -\frac{i}{2} \beta_2 \frac{\partial^2}{\partial t^2}$, and $\hat{N} = i\gamma |A|^2$ are dispersion and nonlinearity operator.

Appendix C: Convergence of Split-step Fourier Method

The SSFM is an approximation as mentioned above. It causes a numerical error and requires a careful selection of the Δz [106-110].

We should note that in SSFM, the noncommuting operators \hat{D} and \hat{N} ($\hat{D}\hat{N} - \hat{N}\hat{D} \neq 0$) cause the calculation error. Here the operators $\hat{D} = -\frac{i}{2}\beta_2 \frac{\partial^2}{\partial t^2}$ and $\hat{N} = i\gamma |A|^2$.

The exact solution of Eq. (B-1) is

$$A(z + \Delta z, t) = \exp\left[\Delta z(\hat{D} + \hat{N})\right]A(z, t). \quad (\text{C-1})$$

Using Baker-Hausdorff theorem [111], we have

$$\exp(\Delta z\hat{D})\exp(\Delta z\hat{N}) = \exp\left[\Delta z\left(\hat{D} + \hat{N} + \frac{1}{2}[\hat{D}, \hat{N}] + \dots\right)\right]. \quad (\text{C-2})$$

Comparing both Eqs. (C-1) and (C-2), one can note that the approximation in Eq. (B-4) only get the first order accuracy.

In our work, the SSFM in Eq. (B-4) is replaced by a symmetrizing the algorithm.

The approximation becomes

$$A(z + \Delta z, t) \simeq \exp(\Delta z\hat{D}/2)\exp(\Delta z\hat{N})\exp(\Delta z\hat{D}/2)A(z, t). \quad (\text{C-3})$$

Based on the calculation in [112], Eq. (C-3) contributes a second order accuracy. This means the numerical error is on $C(\Delta z)^3$ in each step of Δz , and the total error after the propagation in the fiber is $C(\Delta z)^2$.

As a result, a correct SSFM calculation should return a result that converges to

the true value. This means if we decrease Δz , the obtained numerical results should be closer to the true value.

This can be shown with the comparison of both the numerical results and the true analytical results for a fundamental soliton: $A_{\text{ana}} = \text{sech}(t)\exp(iz/2)$. Using the Eq. (C-3) with different values of Δz and start with $A_{\text{ana}}(0,t)$, we found the numerical error (calculated as $error = \left[\sum |A_{\text{num}}(z,t) - A_{\text{ann}}(z,t)|^2 / N \right]^{1/2}$, where N stands for the sample points) of the numerical results $A_{\text{num}}(z,t)$ decreases with Δz . As we use the symmetrizing algorithm form of SSFM, the total error after the fiber is $C(\Delta z)^2$. Hence as shown in Fig. C-1, when the Δz decreases by half, the error decreases to its quarter.

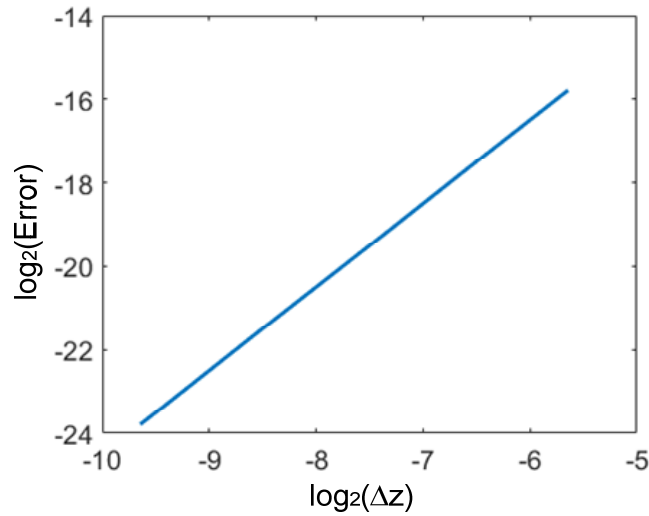


Fig. C-1. The convergence of the numerical results to the true analytical value of a fundamental soliton. The error decreases with Δz at its second order.

Appendix D: Haus's Master Equation

The mode-locking can be modeled by Haus's Master equation as

$$iU_z + U_{tt} + \gamma|U|^2 U = i(g-l)U + i\tau U_{tt} + i\mu|U|^2 U. \quad (\text{D-1})$$

It contains the action of gain, SA and spectral filter. The impact of the filter term can be shown in the following way. We drop other terms and only remain the filter term as

$$iU_z = i\tau U_{tt}. \quad (\text{D-2})$$

We solve it in the frequency domain, and the equation above becomes an ordinary differential equation (ODE)

$$\tilde{U}_z = -\tau\omega^2 \tilde{U}. \quad (\text{D-3})$$

The solution is $\tilde{U}(z, \omega) = \tilde{U}(0, \omega) \exp(-\tau\omega^2 z)$. Physically, this represents the Gaussian filter action on the light.

The mode-locking in the laser requires the action of SA. In Haus's master equation, this is modeled by the SAM term $i\mu|U|^2 U$. Its impact can be shown as

$$U_z = \mu|U|^2 U. \quad (\text{D-4})$$

We have

$$U^* U_z = \mu|U|^2 U^* U, \quad (\text{D-5})$$

$$U U_z^* = \mu|U|^2 U U^*, \quad (\text{D-6})$$

Adding these two equations, we have

$$U_z U^* + U U_z^* = 2\mu|U|^4. \quad (\text{D-7})$$

Since the intensity is $I=|U|^2$, the Eq. (D-7) can be written as

$$I_z = 2\mu I^2, \quad (\text{D-8})$$

we can know that the intensity after Δz is

$$I(\Delta z, t) - I(0, t) \simeq 2\mu I^2(0, t) \Delta z, \quad (\text{D-9})$$

and the transmission of SA is

$$T = \frac{I(\Delta z, t)}{I(0, t)} = 1 + 2\mu I(0, t) \Delta z. \quad (\text{D-10})$$

The transmission increases with the pulse intensity when μ is positive, which can be used to model the SA in the laser cavity.

The transmission increases monotonically with the light intensity when μ is positive. This might induce the blow up of the mode-locked pulse if the intensity is too high, as mentioned in Chapter 2.

Appendix E: Cubic-quintic Ginzburg-Landau Equation

The pulse might blow up in Haus's Master equation. This can be prevented by adding a saturation term to the model. The model becomes the cubic-quintic Ginzburg-Landau equation

$$iU_z + U_{tt} + \gamma |U|^2 U = i(g-l)U + i\tau U_{tt} + i\mu |U|^2 U + i\sigma |U|^4 U. \quad (\text{E-1})$$

Now, the SA action can be shown as

$$U_z = \mu |U|^2 U + \sigma |U|^4 U. \quad (\text{E-2})$$

Similarly, we have

$$I_z = 2\mu I^2 + 2\sigma I^3. \quad (\text{E-3})$$

We assume $\mu = 0.5$, the intensity after propagating Δz is

$$\frac{I(\Delta z) - I(0)}{\Delta z} \simeq I^2(0) + 2\sigma I^3(0). \quad (\text{E-4})$$

The transmission of SA now is

$$T = 1 + \Delta z [I(0) + 2\sigma I^2(0)]. \quad (\text{E-5})$$

Different from the transmission in Eq. (D-10), the transmission of SA does not monotonically increase with the intensity if σ is negative. When the intensity become high, the negative term in Eq. (E-5) becomes obvious and decreases the transmission. This could prevent the pulse blow up.

Appendix F: Logistic Map

Logistic map is a polynomial mapping and mathematically written as

$$x_{n+1} = rx_n(1 - x_n), \quad (\text{F-1})$$

where r is a positive constant. Eq. F-1 is a formula that is famous for approximating the evolution of an animal population over time.

Take x_0 as the initial value, Eq. F-1 can generate the sequence of values of x_n as

$$\begin{aligned} x_1 &= rx_0(1 - x_0), \\ x_2 &= rx_1(1 - x_1), \\ &\vdots \\ x_k &= rx_{k-1}(1 - x_{k-1}). \end{aligned} \quad (\text{F-2})$$

As the result, we can get the sequence of values $x_1, x_2 \dots x_k$.

The logistic map can be computed using a graphical procedure as shown in Fig. F-1. One first sets the initial value of x_0 , and uses the function curve (black solid curve) to get x_1 . Then find the value of x_1 on the horizontal axis through the gray dashed line ($x_{n+1} = x_n$). We can get the value of x_2 using the black solid curve again. Iteratively the sequence of x_k is obtained.

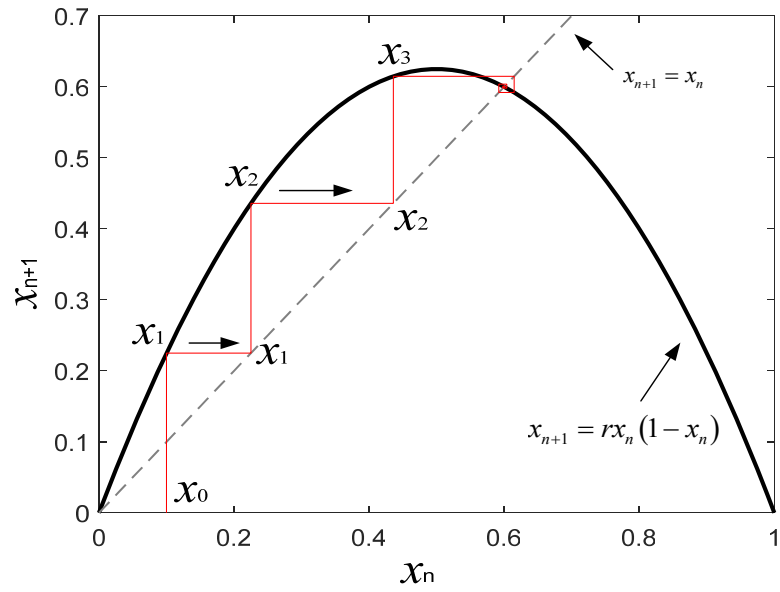


Fig. F-1. Computing the Eq. F-1 via graphical procedure

Appendix G: Chaos and Lyapunov Exponent

Chaos means the unpredictable results obtained in the systems that are sensitive to small changes in the initial conditions. It is known as the “Butterfly Effect” which states that the butterfly flapping its wings in Brazil can cause a hurricane in Texas [113].

Here we take the Eq. F-1 in Appendix F as an example. The value r in the equation is $r = 4$. Then the equation is

$$x_{n+1} = 4x_n(1 - x_n). \quad (\text{G-1})$$

Fig. G-1 give an example of the sequence computed using a graphical procedure when, for example, initial value is $x_0 = 0.2$. The result is different from last section where the iteration finally converges to the intersection.

In fact, Eq. G-1 performs the chaotic behavior. It is sensitive to small changes in its initial condition. For example, we plot two sequences where $x_0 = 0.2$ and $x_0 = 0.2 \cdot 10^{-14}$. The difference between the two trajectories is growing and when n is larger than ~ 50 the two sequences become obviously different as shown in Fig. G-2.

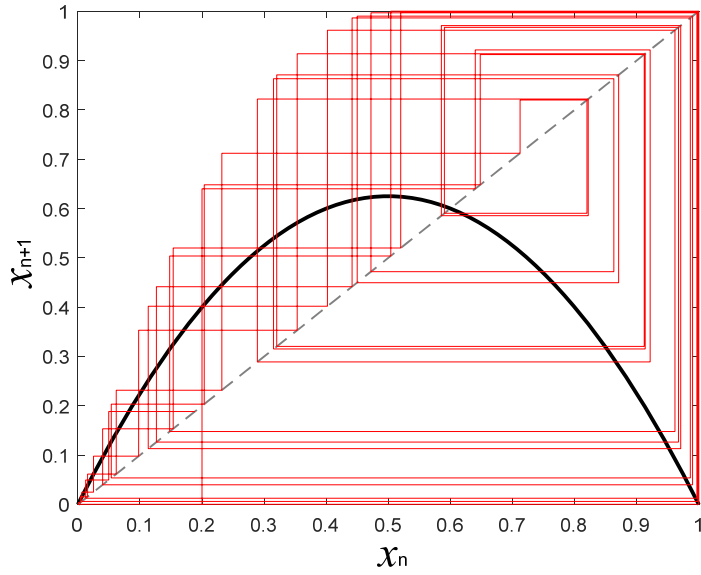


Fig. G-1. The Computing of Eq. G-1 where $r = 4$, $x_0=0.2$.

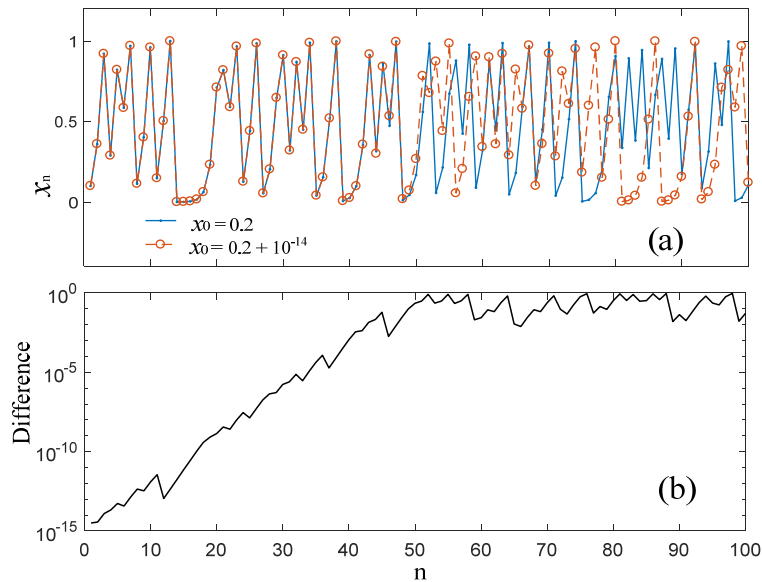


Fig. G-2. Obtained sequences from Eq. G-1 where $r = 4$, $x_0=0.2$ (blue) and $x_0=0.2+10^{-14}$ (orange circle). The difference of the two trajectories is given below.

The sensitivity to initial conditions is quantified by the Lyapunov exponents. It describes the rate of separation of close trajectories as

$$|\delta d(N)| = e^{\lambda N} |\delta d(0)|, \quad (\text{G-2})$$

where $|\delta d(0)|$ is the initial distance between the two trajectories and $|\delta d(N)|$ is the distance of N_{th} data between the two trajectories. Here λ is the Lyapunov exponent, and a positive λ indicates chaos.

Appendix H: FWM Induced Frequency Detuning

In addition to the XPM effect, the energy transfer caused by FWM process can also cause the frequency detuning. We can drop the effect of FWM by using a couple-mode equation to replace Eq. (3-7). Hence when comparing with the results got from both the coupled-mode equation and full NLS in Eq. (3-7), we can know the impact of both XPM and FWM on the mode-locked pulses.

The used couple-mode equation is obtained by substituting $U = A + B$ to Eq. (3-7) and dropping the FWM terms. The Eq. (3-7) becomes

$$\frac{\partial A}{\partial \xi} = \frac{iD}{2} \frac{\partial^2 A}{\partial \tau^2} + i\Gamma |A|^2 A + 2i\Gamma |B|^2 A, \quad (\text{H-1-a})$$

$$\frac{\partial B}{\partial \xi} = \frac{iD}{2} \frac{\partial^2 B}{\partial \tau^2} + i\Gamma |B|^2 B + 2i\Gamma |A|^2 B. \quad (\text{H-1-b})$$

The spectra got from the Eqs. (H-1-a) and (H-1-b) are shown in Fig. H-1 with the blue-dashed line. Fig. H-1(a) shows the spectra of the unequal energy mode-locking state shown in Fig. 3-8. The XPM individually can cause the asymmetrically spectral broadening. As the XPM effect is more obvious to the weak pulse, the asymmetrically broadening is stronger in weak pulse than that of the strong pulse. The frequency detuning of the pulse in the weak channel is larger than that in the strong channel.

FWM transfers the energy between the pulses in two channels and we believe it can also cause frequency detuning of the pulses. To compare the detuning caused by

FWM and XPM, we obtained the spectra obtained with full NLS in Eq. (3-7) where the FWM and XPM are all contained. Both the spectra in the case that the energies in two channels are unequal and identical are shown in Figs. H-1(a) and (b), respectively. In Fig. H-1(a), the strong pulse transfers its energy to the weak pulse through FWM process as shown by the green solid line in Fig. H-1. The central frequencies of both strong and weak pulses are modified by FWM. Quantitatively, the frequency detuning caused by XPM alone in Fig. H-1(a) is 0.092, while the detuning induced by the combination of XPM and FWM is 0.118, which increases nearly 28 %. In Fig. H-1(b), XPM alone causes a frequency detuning of 0.019, while the combination of XPM and FWM causes a detuning of 0.021, which increases nearly 10 %. Hence in addition to XPM, the energy transfers through the FWM effect also contributes to the frequency detuning of the mode-locked pulses.

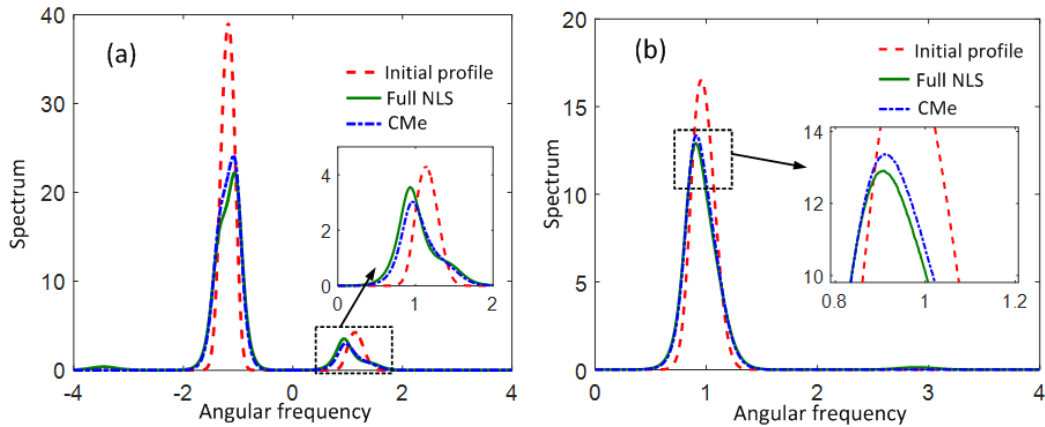


Fig. H-1. Impact of XPM and FWM on the spectral profile of the dual-channel mode-locked pulses when the energies of the two channels are (a) unequal and (b) identical. In (b), we only give the right half part of the spectrum because of its symmetry.

Appendix I: Impact of SA on energy ratio

Saturable absorber (SA) is an intensity dependent loss element. The loss is large when the light intensity is weak, and the loss is small when the light intensity is strong. In our model, we assume a fast SA the response of which depends on the instantaneous intensity of the light.

For the dual-channel simultaneous mode-locked pulse in Section 3.3.3, the two pulses move together in the time domain. When the two pulses go through the SA together, the combined pulse temporal profile suffers a larger loss where the instantaneous pulse intensity is lower, and vice versa. As a result, the modulation depth is enhanced as shown in Fig. I-1. An enhanced modulation depth indicates that the energies of the two pulses are closer. In other words, the stronger of the two pulses suffer a higher loss, while the weaker of the two pulses suffer a smaller loss. This is counter-intuitive, and the opposite will happen if two pulses go through the SA individually.

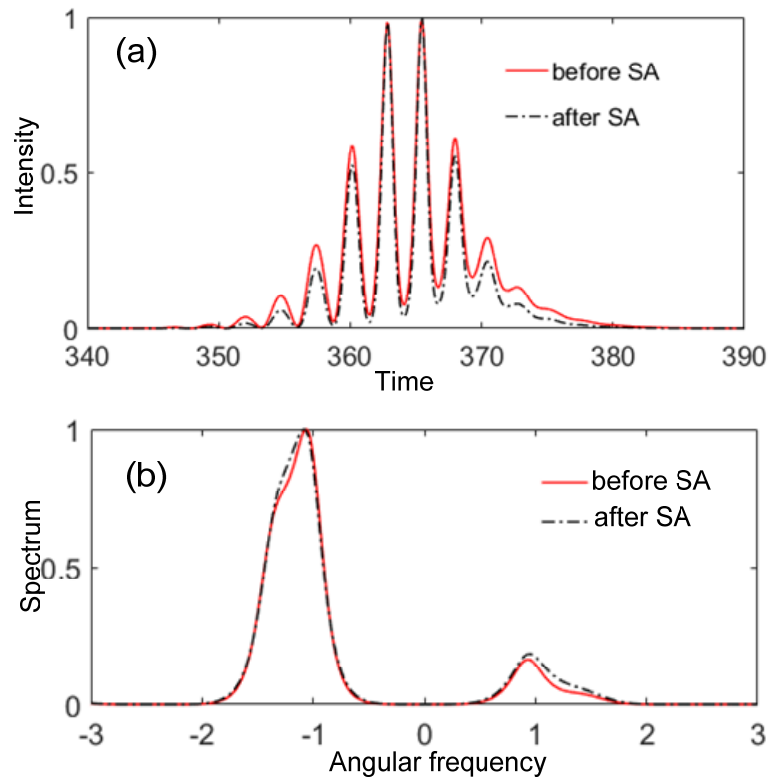


Fig. I-1. The pulse profiles of the DSML mode-locked state before and after the SA in the (a) time and (b) frequency domain. The pulse profiles are normalized by their maxima.

Appendix J: Accumulated Error in Simulations

Besides the numerical error caused by algorithms, the simulation might also accumulate errors since we are doing the float-point calculation [100, 101]. Here we show one example of the accumulated error in order to remind others to be careful about it.

One may note that in the SSFM algorithms, we have lots of FFT and IFFT calculations. However, the iteration on FFT and IFFT can accumulate the errors [100, 101]. Here is one example.

We have an array: $\mathbf{In} = [1, 2, 3, \dots, N-1, N, N, N-1, \dots, 3, 2, 1]$. Then we will do the iteration of FFT and IFFT on the array \mathbf{In} as: $\mathbf{Out} = (F^{-1}F)^m \mathbf{In}$, where F and F^{-1} represent for Fourier and inverse Fourier transforms that are done with FFT and IFFT in MATLAB, and m stands for the step of iteration.

Mathematically, the Fourier and inverse Fourier transform pairs should reproduce the input data. However, we observed that the iteration on such calculation can accumulate error as shown in Fig. J-1(a). We calculated the error as $Error = \left\{ \sum (|\mathbf{Out}| - |\mathbf{In}|)^2 / [N_{\text{sam}} \max(|\mathbf{In}|)] \right\}^{1/2}$ where N_{sam} represents the number of the elements in the array. We found that the error increases with m . The output data hence becomes different. At first, the 128-th and 129-th data are both exactly 128 in

the array **In**, but after 10^5 steps of iteration, as shown in Fig. J-1(b), these two data becomes 127.999999999999860 and 127.999999999999948.

Generally, the accumulated error in FFT increases with the sample points N_{sam} and the steps of iteration m as pointed out in [100, 101]. Hence one should note that if there are too much iteration on the FFT and IFFT, the error will be accumulated to a higher level.

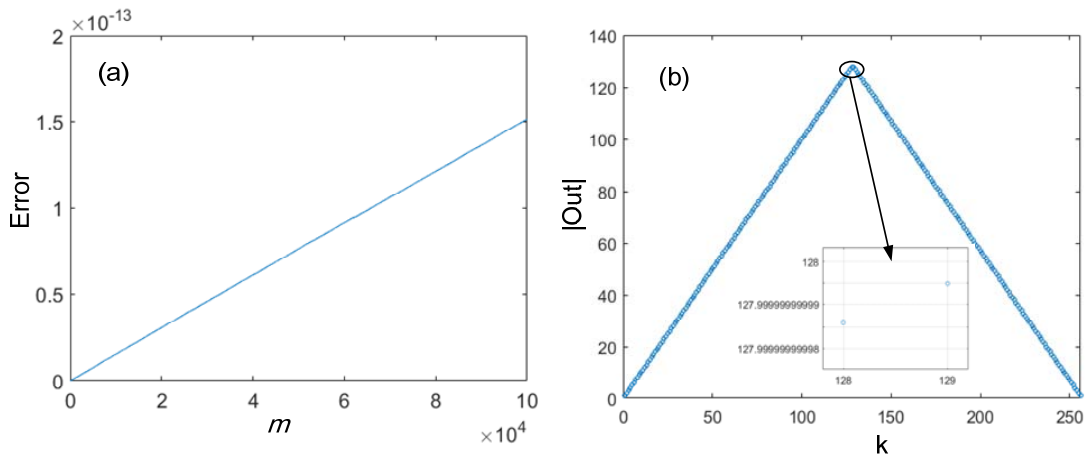


Fig. J-1. (a)The error v.s. steps of iteration on Fourier and invers Fourier transform pairs. (b) The amplitude of the array after 10^5 steps of iteration.

Bibliography

- [1] R. G. Gould, "The LASER, light amplification by stimulated emission of radiation," in *The Ann Arbor conference on optical pumping, the University of Michigan, 1959*, p. 128.
- [2] P. A. Dirac, "The quantum theory of the emission and absorption of radiation," *Proc. R. Soc. Lond. A*, vol. 114, pp. 243-265, 1927.
- [3] B. Fain and P. W. Milonni, "Classical stimulated emission," *JOSA B*, vol. 4, pp. 78-85, 1987.
- [4] O. Kamatani, S. Kawanishi, and M. Saruwatari, "Prescaled 6.3 GHz clock recovery from 50 Gbit/s TDM optical signal with 50 GHz PLL using four-wave mixing in a travelling-wave laser diode optical amplifier," *Electronics Letters*, vol. 30, pp. 807-809, 1994.
- [5] T. Okoshi and K. t. Kikuchi, "Frequency stabilisation of semiconductor lasers for heterodyne-type optical communication systems," *Electronics Letters*, vol. 16, pp. 179-181, 1980.
- [6] S. B. Alexander, *Optical communication receiver design*: SPIE Optical engineering press Bellingham, Washington, USA, 1997.
- [7] X. Zhu and J. M. Kahn, "Free-space optical communication through atmospheric turbulence channels," *IEEE Transactions on communications*, vol. 50, pp. 1293-1300, 2002.
- [8] B. Mukherjee, "WDM optical communication networks: progress and challenges," *IEEE Journal on Selected Areas in communications*, vol. 18, pp. 1810-1824, 2000.
- [9] https://en.wikipedia.org/wiki/Laser#cite_note-Gould1959-1.
- [10] T. H. Maiman, "Stimulated optical radiation in ruby," 1960.
- [11] L. Hargrove, R. L. Fork, and M. Pollack, "Locking of He-Ne laser modes induced by synchronous intracavity modulation," *Applied Physics Letters*, vol. 5, pp. 4-5, 1964.
- [12] E. Snitzer, "Optical maser action of Nd³⁺ in a barium crown glass," *Physical Review Letters*, vol. 7, p. 444, 1961.
- [13] K. Kao and G. A. Hockham, "Dielectric-fibre surface waveguides for optical frequencies," in *Proceedings of the Institution of Electrical Engineers*, 1966, pp. 1151-1158.
- [14] F. Kapron, D. B. Keck, and R. D. Maurer, "Radiation losses in glass optical waveguides," *Applied Physics Letters*, vol. 17, pp. 423-425, 1970.

- [15] ["https://www.fiberoptics4sale.com/blogs/archive-posts/95048006-optical-fiber-loss-and-attenuation."](https://www.fiberoptics4sale.com/blogs/archive-posts/95048006-optical-fiber-loss-and-attenuation.)
- [16] S. T. Cundiff and J. Ye, "Colloquium: Femtosecond optical frequency combs," *Reviews of Modern Physics*, vol. 75, p. 325, 2003.
- [17] S. A. Diddams, "The evolving optical frequency comb," *JOSA B*, vol. 27, pp. B51-B62, 2010.
- [18] J. M. Dudley, G. Genty, and S. Coen, "Supercontinuum generation in photonic crystal fiber," *Reviews of modern physics*, vol. 78, p. 1135, 2006.
- [19] J. Mazumder and W. Steen, "Heat transfer model for CW laser material processing," *Journal of Applied Physics*, vol. 51, pp. 941-947, 1980.
- [20] S. Yun, C. Boudoux, M. Pierce, J. De Boer, G. Tearney, and B. Bouma, "Extended-cavity semiconductor wavelength-swept laser for biomedical imaging," *Ieee Photonics Technology Letters*, vol. 16, pp. 293-295, 2004.
- [21] A. Husakou and J. Herrmann, "Supercontinuum generation of higher-order solitons by fission in photonic crystal fibers," *Physical Review Letters*, vol. 87, p. 203901, 2001.
- [22] W. J. Wadsworth, A. Ortigosa-Blanch, J. C. Knight, T. A. Birks, T.-P. M. Man, and P. S. J. Russell, "Supercontinuum generation in photonic crystal fibers and optical fiber tapers: a novel light source," *JOSA B*, vol. 19, pp. 2148-2155, 2002.
- [23] T. Birks, W. Wadsworth, and P. S. J. Russell, "Supercontinuum generation in tapered fibers," *Optics letters*, vol. 25, pp. 1415-1417, 2000.
- [24] J. Herrmann, U. Griebner, N. Zhavoronkov, A. Husakou, D. Nickel, J. Knight, *et al.*, "Experimental evidence for supercontinuum generation by fission of higher-order solitons in photonic fibers," *Physical Review Letters*, vol. 88, p. 173901, 2002.
- [25] O. Svelto, "Ray and wave propagation through optical media," in *Principles of Lasers*, ed: Springer, 2010, pp. 131-161.
- [26] G. Huggett, "MODE-LOCKING OF CW LASERS BY REGENERATIVE RF FEEDBACK," *Applied Physics Letters*, vol. 13, pp. 186-187, 1968.
- [27] ["http://www.rp-photonics.com/semiconductor_saturable_absorber_mirrors.html."](http://www.rp-photonics.com/semiconductor_saturable_absorber_mirrors.html)
- [28] D. H. Sutter, G. Steinmeyer, L. Gallmann, N. Matuschek, F. Morier-Genoud, U. Keller, *et al.*, "Semiconductor saturable-absorber mirror-assisted Kerr-lens mode-locked Ti: sapphire laser producing pulses in the two-cycle regime," *Optics letters*, vol. 24, pp. 631-633, 1999.
- [29] F. Kartner, I. Jung, and U. Keller, "Soliton mode-locking with saturable absorbers,"

- IEEE Journal of Selected Topics in Quantum Electronics*, vol. 2, pp. 540-556, 1996.
- [30] G. Spühler, K. Weingarten, R. Grange, L. Krainer, M. Haiml, V. Liverini, *et al.*, "Semiconductor saturable absorber mirror structures with low saturation fluence," *Applied Physics B*, vol. 81, pp. 27-32, 2005.
- [31] H. H. Tan, C. Jagadish, M. Lederer, B. Luther-Davies, J. Zou, D. J. H. Cockayne, *et al.*, "Role of implantation-induced defects on the response time of semiconductor saturable absorbers," *Applied physics letters*, vol. 75, pp. 1437-1439, 1999.
- [32] A. Schmidt, S. Rivier, W. B. Cho, J. H. Yim, S. Y. Choi, S. Lee, *et al.*, "Sub-100 fs single-walled carbon nanotube saturable absorber mode-locked Yb-laser operation near 1 μm ," *Optics express*, vol. 17, pp. 20109-20116, 2009.
- [33] T. Hasan, Z. Sun, F. Wang, F. Bonaccorso, P. H. Tan, A. G. Rozhin, *et al.*, "Nanotube-polymer composites for ultrafast photonics," *Advanced Materials*, vol. 21, pp. 3874-3899, 2009.
- [34] I. H. Baek, H. W. Lee, S. Bae, B. H. Hong, Y. H. Ahn, D.-I. Yeom, *et al.*, "Efficient mode-locking of sub-70-fs Ti: sapphire laser by graphene saturable absorber," *Applied Physics Express*, vol. 5, p. 032701, 2012.
- [35] G. Zhu, X. Zhu, K. Balakrishnan, R. A. Norwood, and N. Peyghambarian, "Fe 2+: ZnSe and graphene Q-switched singly Ho 3+-doped ZBLAN fiber lasers at 3 μm ," *Optical Materials Express*, vol. 3, pp. 1365-1377, 2013.
- [36] Z. Luo, M. Zhou, J. Weng, G. Huang, H. Xu, C. Ye, *et al.*, "Graphene-based passively Q-switched dual-wavelength erbium-doped fiber laser," *Optics letters*, vol. 35, pp. 3709-3711, 2010.
- [37] H. Liu, A.-P. Luo, F.-Z. Wang, R. Tang, M. Liu, Z.-C. Luo, *et al.*, "Femtosecond pulse erbium-doped fiber laser by a few-layer MoS₂ saturable absorber," *Optics letters*, vol. 39, pp. 4591-4594, 2014.
- [38] S. Wang, H. Yu, H. Zhang, A. Wang, M. Zhao, Y. Chen, *et al.*, "Broadband few-layer MoS₂ saturable absorbers," *Advanced materials*, vol. 26, pp. 3538-3544, 2014.
- [39] Y. Chen, G. Jiang, S. Chen, Z. Guo, X. Yu, C. Zhao, *et al.*, "Mechanically exfoliated black phosphorus as a new saturable absorber for both Q-switching and mode-locking laser operation," *Optics express*, vol. 23, pp. 12823-12833, 2015.
- [40] Z.-C. Luo, M. Liu, Z.-N. Guo, X.-F. Jiang, A.-P. Luo, C.-J. Zhao, *et al.*, "Microfiber-based few-layer black phosphorus saturable absorber for ultra-fast fiber laser," *Optics express*, vol. 23, pp. 20030-20039, 2015.
- [41] D. Richardson, R. Laming, D. Payne, M. Phillips, and V. Matsas, "320 fs soliton

- generation with passively mode-locked erbium fibre laser," *Electronics Letters*, vol. 27, pp. 730-732, 1991.
- [42] E. Kuzin, B. I. Escamilla, D. Garcia-Gomez, and J. Haus, "Fiber laser mode locked by a Sagnac interferometer with nonlinear polarization rotation," *Optics letters*, vol. 26, pp. 1559-1561, 2001.
- [43] A. Komarov, H. Leblond, and F. Sanchez, "Multistability and hysteresis phenomena in passively mode-locked fiber lasers," *Physical review A*, vol. 71, p. 053809, 2005.
- [44] M. Hofer, M. Ober, F. Haberl, and M. Fermann, "Characterization of ultrashort pulse formation in passively mode-locked fiber lasers," *IEEE journal of quantum electronics*, vol. 28, pp. 720-728, 1992.
- [45] M. Fermann, M. Andrejco, Y. Silberberg, and M. Stock, "Passive mode locking by using nonlinear polarization evolution in a polarization-maintaining erbium-doped fiber," *Optics letters*, vol. 18, pp. 894-896, 1993.
- [46] V. Matsas, T. Newson, D. Richardson, and D. Payne, "Selfstarting passively mode-locked fibre ring soliton laser exploiting nonlinear polarisation rotation," *Electronics Letters*, vol. 28, pp. 1391-1393, 1992.
- [47] K. Tamura, H. Haus, and E. Ippen, "Self-starting additive pulse mode-locked erbium fibre ring laser," *Electronics Letters*, vol. 28, pp. 2226-2228, 1992.
- [48] H. Dorren, D. Lenstra, Y. Liu, M. T. Hill, and G.-D. Khoe, "Nonlinear polarization rotation in semiconductor optical amplifiers: Theory and application to all-optical flip-flop memories," *IEEE Journal of Quantum Electronics*, vol. 39, pp. 141-148, 2003.
- [49] F. Li, P. Wai, and J. N. Kutz, "Geometrical description of the onset of multi-pulsing in mode-locked laser cavities," *JOSA B*, vol. 27, pp. 2068-2077, 2010.
- [50] H. A. Haus, J. G. Fujimoto, and E. P. Ippen, "Structures for additive pulse mode locking," *JOSA B*, vol. 8, pp. 2068-2076, 1991.
- [51] H. A. Haus, J. G. Fujimoto, and E. P. Ippen, "Analytic theory of additive pulse and Kerr lens mode locking," *IEEE Journal of quantum electronics*, vol. 28, pp. 2086-2096, 1992.
- [52] H. A. Haus, "Mode-locking of lasers," *IEEE Journal of Selected Topics in Quantum Electronics*, vol. 6, pp. 1173-1185, 2000.
- [53] O. Svelto and D. C. Hanna, "Principles of lasers," 1998.
- [54] F. Li, J. Yuan, Z. Kang, Q. Li, and P. Wai, "Modeling frequency comb sources," *Nanophotonics*, vol. 5, pp. 292-315, 2016.

- [55] J. N. Kutz, "Mode-locked soliton lasers," *SIAM review*, vol. 48, pp. 629-678, 2006.
- [56] X.-M. Tan, H.-J. Chen, H. Cui, Y.-K. Lv, G.-K. Zhao, Z.-C. Luo, *et al.*, "Tunable and switchable dual-waveband ultrafast fiber laser with 100 GHz repetition-rate," *Optics Express*, vol. 25, pp. 16291-16299, 2017.
- [57] Z.-C. Luo, A.-P. Luo, W.-C. Xu, H.-S. Yin, J.-R. Liu, Q. Ye, *et al.*, "Tunable multiwavelength passively mode-locked fiber ring laser using intracavity birefringence-induced comb filter," *IEEE Photonics Journal*, vol. 2, pp. 571-577, 2010.
- [58] H. Zhang, D. Tang, X. Wu, and L. Zhao, "Multi-wavelength dissipative soliton operation of an erbium-doped fiber laser," *Optics express*, vol. 17, pp. 12692-12697, 2009.
- [59] E. D. Farnum and J. N. Kutz, "Multifrequency mode-locked lasers," *JOSA B*, vol. 25, pp. 1002-1010, 2008.
- [60] G. Wei, S. Shalei, Z. Bo, S. Shuo, L. Faquan, and C. Xuewu, "Multi-wavelength canopy LiDAR for remote sensing of vegetation: Design and system performance," *ISPRS Journal of Photogrammetry and Remote Sensing*, vol. 69, pp. 1-9, 2012.
- [61] G. Hu, Y. Pan, X. Zhao, S. Yin, M. Zhang, and Z. Zheng, "Asynchronous and synchronous dual-wavelength pulse generation in a passively mode-locked fiber laser with a mode-locker," *Optics letters*, vol. 42, pp. 4942-4945, 2017.
- [62] J. M. Soto-Crespo and N. Akhmediev, "Composite solitons and two-pulse generation in passively mode-locked lasers modeled by the complex quintic Swift-Hohenberg equation," *Physical Review E*, vol. 66, p. 066610, 2002.
- [63] B. G. Bale, J. N. Kutz, and E. D. Farnum, "Dynamics of multifrequency mode-locking driven by homogenous and inhomogenous gain broadening effects," *JOSA B*, vol. 25, pp. 1479-1487, 2008.
- [64] B. G. Bale, E. Farnum, and J. N. Kutz, "Theory and simulation of passive multifrequency mode-locking with waveguide arrays," *IEEE Journal of Quantum Electronics*, vol. 44, pp. 976-983, 2008.
- [65] G. Walker, "Gain and noise characterisation of erbium doped fibre amplifiers," *Electronics letters*, vol. 27, pp. 744-745, 1991.
- [66] E. Ding, E. Shlizerman, and J. N. Kutz, "Generalized master equation for high-energy passive mode-locking: the sinusoidal Ginzburg–Landau equation," *IEEE journal of quantum electronics*, vol. 47, pp. 705-714, 2011.
- [67] A. Grudinin, D. Richardson, and D. Payne, "Energy quantisation in figure eight fibre

- laser," *Electronics Letters*, vol. 28, pp. 67-68, 1992.
- [68] F. Kurtner, J. A. Der Au, and U. Keller, "Mode-locking with slow and fast saturable absorbers-what's the difference?," *IEEE Journal of Selected Topics in Quantum Electronics*, vol. 4, pp. 159-168, 1998.
- [69] M. Lederer, B. Luther-Davies, H. H. Tan, C. Jagadish, N. Akhmediev, and J. M. Soto-Crespo, "Multipulse operation of a Ti: sapphire laser mode locked by an ion-implanted semiconductor saturable-absorber mirror," *JOSA B*, vol. 16, pp. 895-904, 1999.
- [70] D. Li, D. Tang, L. Zhao, and D. Shen, "Mechanism of dissipative-soliton-resonance generation in passively mode-locked all-normal-dispersion fiber lasers," *Journal of Lightwave Technology*, vol. 33, pp. 3781-3787, 2015.
- [71] F. Li, E. Ding, J. N. Kutz, and P. Wai, "Dual transmission filters for enhanced energy in mode-locked fiber lasers," *Optics express*, vol. 19, pp. 23408-23419, 2011.
- [72] F. Li, X. Feng, H. Zheng, C. Lu, H. Tam, J. N. Kutz, *et al.*, "Multiwavelength lasers with homogeneous gain and intensity-dependent loss," *Optics Communications*, vol. 284, pp. 2327-2336, 2011.
- [73] X. Zhang, F. Li, K. Nakkeeran, J. Yuan, Z. Kang, J. N. Kutz, *et al.*, "Impact of Spectral Filtering on Multipulsing Instability in Mode-Locked Fiber Lasers," *IEEE Journal of Selected Topics in Quantum Electronics*, vol. 24, pp. 1-9, 2018.
- [74] E. Ding, W. H. Renninger, F. W. Wise, P. Grellu, E. Shlizerman, and J. N. Kutz, "High-energy passive mode-locking of fiber lasers," *International journal of optics*, vol. 2012, 2012.
- [75] X. Zhang, F. Li, Z. Kang, J. Yuan, and P. K. A. Wai, "Spectral filtering induced multipulsing in mode-locked soliton lasers," in *Australian Conference on Optical Fibre Technology*, 2016, p. JT4A. 7.
- [76] G. P. Agrawal, "Nonlinear fiber optics," in *Nonlinear Science at the Dawn of the 21st Century*, ed: Springer, 2000, pp. 195-211.
- [77] M. Zhang, E. Kelleher, A. Pozharov, E. Obratsova, S. Popov, and J. Taylor, "Passive synchronization of all-fiber lasers through a common saturable absorber," *Optics letters*, vol. 36, pp. 3984-3986, 2011.
- [78] K. Tamura, E. Ippen, and H. Haus, "Optimization of filtering in soliton fiber lasers," *IEEE photonics technology letters*, vol. 6, pp. 1433-1435, 1994.
- [79] S. Wang, S. Droste, L. C. Sinclair, I. Coddington, N. R. Newbury, T. F. Carruthers, *et al.*, "Wake mode sidebands and instability in mode-locked lasers with slow saturable

- absorbers," *Optics letters*, vol. 42, pp. 2362-2365, 2017.
- [80] A. Chong, W. H. Renninger, and F. W. Wise, "Properties of normal-dispersion femtosecond fiber lasers," *JOSA B*, vol. 25, pp. 140-148, 2008.
- [81] J. A. Der Au, D. Kopf, F. Morier-Genoud, M. Moser, and U. Keller, "60-fs pulses from a diode-pumped Nd: glass laser," *Optics letters*, vol. 22, pp. 307-309, 1997.
- [82] B. Collings, K. Bergman, and W. Knox, "True fundamental solitons in a passively mode-locked short-cavity Cr 4+: YAG laser," *Optics letters*, vol. 22, pp. 1098-1100, 1997.
- [83] V. L. Kalashnikov, E. Sorokin, and I. T. Sorokina, "Multipulse operation and limits of the Kerr-lens mode-locking stability," *IEEE journal of quantum electronics*, vol. 39, pp. 323-336, 2003.
- [84] B. G. Bale, K. Kieu, J. N. Kutz, and F. Wise, "Transition dynamics for multi-pulsing in mode-locked lasers," *Optics express*, vol. 17, pp. 23137-23146, 2009.
- [85] J. M. Soto-Crespo, M. Grapinet, P. Grelu, and N. Akhmediev, "Bifurcations and multiple-period soliton pulsations in a passively mode-locked fiber laser," *Physical Review E*, vol. 70, p. 066612, 2004.
- [86] A. Bednyakova and S. K. Turitsyn, "Adiabatic soliton laser," *Physical review letters*, vol. 114, p. 113901, 2015.
- [87] K. Blow, N. Doran, and D. Wood, "Trapping of energy into solitary waves in amplified nonlinear dispersive systems," *Optics letters*, vol. 12, pp. 1011-1013, 1987.
- [88] K. Blow, N. Doran, and D. Wood, "Generation and stabilization of short soliton pulses in the amplified nonlinear Schrödinger equation," *JOSA B*, vol. 5, pp. 381-391, 1988.
- [89] P. Wai, C. R. Menyuk, Y. Lee, and H. Chen, "Nonlinear pulse propagation in the neighborhood of the zero-dispersion wavelength of monomode optical fibers," *Optics letters*, vol. 11, pp. 464-466, 1986.
- [90] J. N. Kutz, C. Lyngå, and B. Eggleton, "Enhanced supercontinuum generation through dispersion-management," *Optics Express*, vol. 13, pp. 3989-3998, 2005.
- [91] K. Ohkuma, Y. H. Ichikawa, and Y. Abe, "Soliton propagation along optical fibers," *Optics letters*, vol. 12, pp. 516-518, 1987.
- [92] X. Zhang, F. Li, J. Yuan, Z. Kang, and P. Wai, "Dynamics of Dual Frequency Mode-Locked Fiber Lasers," in *Conference on Lasers and Electro-Optics/Pacific Rim*, 2018, p. W3A. 49.
- [93] X. Zhang, S. Wang, F. Li, C. R. Menyuk, and P. Wai, "Design of a Dual-Channel

- Modelocked Fiber Laser that Avoids Multi-Pulsing," in *CLEO: Applications and Technology*, 2018, p. JTh2A. 125.
- [94] N. Akhmediev and A. Ankiewicz, "Dissipative Solitons in the Complex Ginzburg-Landau and Swift-Hohenberg Equations," in *Dissipative Solitons*. vol. 661, N. Akhmediev and A. Ankiewicz, Eds., ed: Springer Berlin / Heidelberg, 2005, pp. 17-34.
- [95] R. Stolen and J. Bjorkholm, "Parametric amplification and frequency conversion in optical fibers," *IEEE Journal of Quantum Electronics*, vol. 18, pp. 1062-1072, 1982.
- [96] C. Furst, A. Leitenstorfer, and A. Laubereau, "Mechanism for self-synchronization of femtosecond pulses in a two-color Ti: sapphire laser," *IEEE Journal of Selected Topics in Quantum Electronics*, vol. 2, pp. 473-479, 1996.
- [97] X. Liu, D. Han, Z. Sun, C. Zeng, H. Lu, D. Mao, *et al.*, "Versatile multi-wavelength ultrafast fiber laser mode-locked by carbon nanotubes," *Scientific reports*, vol. 3, p. 2718, 2013.
- [98] X. Liu, L. Zhan, S. Luo, Z. Gu, J. Liu, Y. Wang, *et al.*, "Multiwavelength erbium-doped fiber laser based on a nonlinear amplifying loop mirror assisted by un-pumped EDF," *Optics express*, vol. 20, pp. 7088-7094, 2012.
- [99] X. Feng, H.-Y. Tam, H. Liu, and P. Wai, "Multiwavelength erbium-doped fiber laser employing a nonlinear optical loop mirror," *Optics communications*, vol. 268, pp. 278-281, 2006.
- [100] J. C. Schatzman, "Accuracy of the discrete Fourier transform and the fast Fourier transform," *SIAM Journal on Scientific Computing*, vol. 17, pp. 1150-1166, 1996.
- [101] T. Kaneko and B. Liu, "Accumulation of round-off error in fast Fourier transforms," *Journal of the ACM (JACM)*, vol. 17, pp. 637-654, 1970.
- [102] "https://www.rp-photonics.com/upper_state_lifetime.html."
- [103] "https://www.rp-photonics.com/gain_saturation.html."
- [104] V. E. e. Zakharov and S. V. Manakov, "On the complete integrability of a nonlinear Schrödinger equation," *Theoretical and Mathematical Physics*, vol. 19, pp. 551-559, 1974.
- [105] C. Van Loan, *Computational frameworks for the fast Fourier transform* vol. 10: Siam, 1992.
- [106] O. V. Sinkin, R. Holzlöhner, J. Zweck, and C. R. Menyuk, "Optimization of the split-step Fourier method in modeling optical-fiber communications systems," *Journal of lightwave technology*, vol. 21, p. 61, 2003.

- [107] J. Van Roey, J. Van der Donk, and P. Lagasse, "Beam-propagation method: analysis and assessment," *Josa*, vol. 71, pp. 803-810, 1981.
- [108] L. Thylen, "The beam propagation method: an analysis of its applicability," *Optical and quantum electronics*, vol. 15, pp. 433-439, 1983.
- [109] J. Saijonmaa and D. Yevick, "Beam-propagation analysis of loss in bent optical waveguides and fibers," *JOSA*, vol. 73, pp. 1785-1791, 1983.
- [110] D. Yevick and B. Hermansson, "New fast Fourier transform and finite-element approaches to the calculation of multiple-stripe-geometry laser modes," *Journal of applied physics*, vol. 59, pp. 1769-1771, 1986.
- [111] G. H. Weiss and A. A. Maradudin, "The Baker-Hausdorff Formula and a Problem in Crystal Physics," *Journal of Mathematical Physics*, vol. 3, pp. 771-777, 1962.
- [112] Q. Li, *Pedestal-free pulse compression in nonlinear fibers and nonlinear fiber Bragg gratings*, 2009.
- [113] G. Boeing, "Chaos theory and the logistic map," *at UC Berkeley*, 2015.